1
Polymeric and Small-Molecule Semiconductors for Organic Field-Effect Transistors

Hakan Usta and Antonio Facchetti

1.1
Introduction

π-Conjugated small-molecule and polymer semiconductors are of interest because of their unique optical and electrical properties which will enable the fabrication of new optoelectronic devices having unique functionalities [1–3]. Besides the discovery of new materials, the development of organic-semiconductor-based optoelectronics requires a much better understanding of the electronic structure, charge-transport properties, as well as light–molecule/polymer and charge–charge interactions in the corresponding thin films [4]. Although these aspects are fundamental for the optimization of these materials, the goal in this chapter is to review the very recent achievements in the development of molecular and polymeric semiconductors for charge transport in thin-film transistors (TFTs). In particular, we will first introduce the basic concepts of organic semiconductor structure and organic thin-film transistor (OTFT) operation and then focus on initial studies and very recent works. Excellent review articles are available in the literature for the intermediate period [5, 6].

1.2
Organic Semiconductor Structural Design

Organic semiconductors for OTFTs must possess two essential structural features for their successful implementation in printed electronics (Figure 1.1) [7]. The first is a π-conjugated core/chain composed of linked unsaturated units. The extended π orbitals enable achieving the characteristic charge-transport and optical properties [8]. The second is core functionalization with solubilizing substituents, which is essential for inexpensive manufacture by solution methods as well as for enhancing solid-state core interactions [9]. This latter feature was not met in the

Large Area and Flexible Electronics, First Edition. Edited by Mario Caironi and Yong-Young Noh.

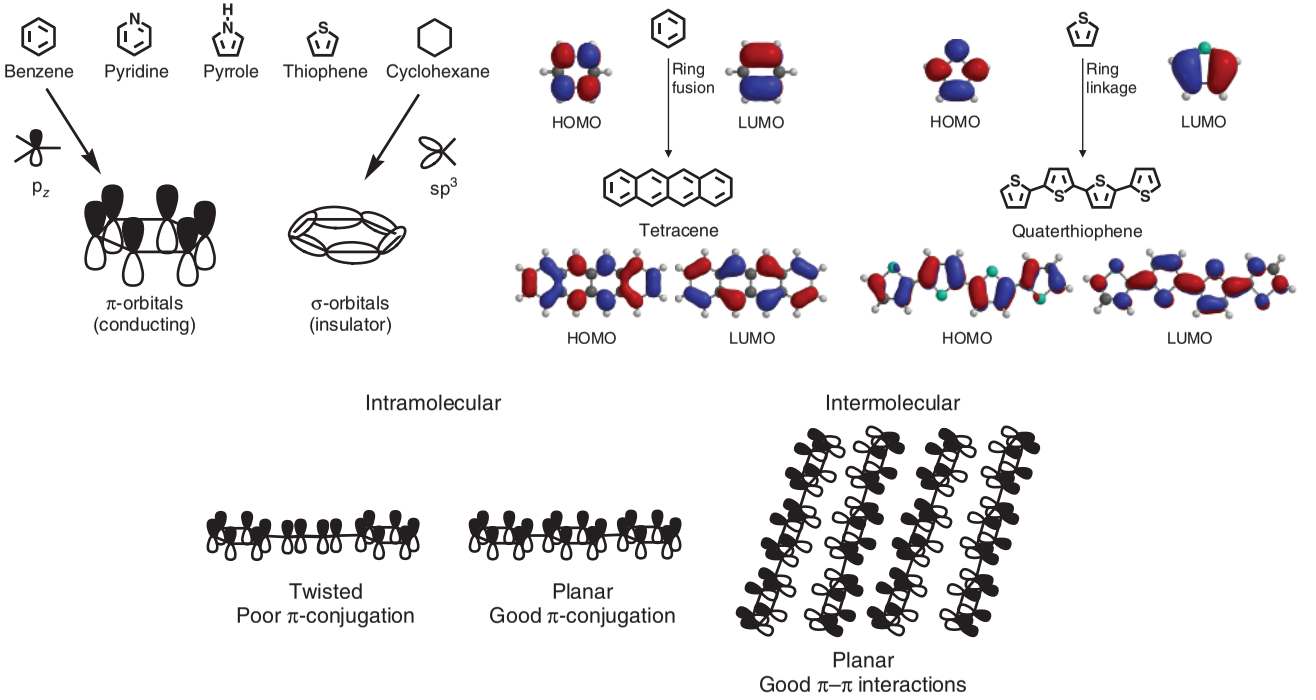

Figure 1.1 Schematic representation of a π-conjugated unit, molecular topologies of the Frontier molecular orbital (FMO), and structural connectivity affording conducting/motifs, twisted/planar connections, and intermolecular interactions.

initial studies, as most of the OTFTs were fabricated with the semiconductor film deposited by vacuum sublimation. Among the most common unsaturated units used for core construction, there are mono(poly)cyclic aromatic hydrocarbons, heterocycles, benzofused systems, and simple olefinic and acetylenic groups. The extent of conjugation/interaction between these units determines the semiconductor solution/solid state electronic structure, which in turn controls the key molecular/polymeric properties such as optical absorption/emission, redox characteristics, and frontier molecular orbital energy levels. Other important architecture parameters relevant to polymers are the molecular weight (M_w) and the polydispersity (PD) index because they influence the solubility, solution aggregation, formulation rheology, and thin-film formation and morphology for both pristine and blended materials. Because when going from low (oligomers) to high (polymer) molecular weights the electronic structure, thermal properties, and microstructure of polymers generally vary considerably, it is important to achieve an M_w/PD regime where a certain property stabilizes so that greater reproducibility of that polymer property can be achieved from batch to batch. This value is likely to be strongly dependent on the polymer structure, but for most soluble thiophene-based polymers, a number-averaged molecular weight value of about 20–30 kDa and a PD of 1.2–1.8 are reasonable for these threshold values [10].

There are several advantages in using polymeric versus molecular π-conjugated semiconductors. Thin films of polymeric materials are generally very smooth and uniform, enabling a great control over a large range of the film structural and morphological characteristics. Printing requires great control of the solution rheological properties, which can be tuned efficiently for polymeric materials. Polymer crystalline domains are typically much smaller than the length scale of several optoelectronic devices, resulting in isotropic transport characteristics. This results in low device-to-device performance variability, which is particularly important for TFT integration into circuits. Furthermore, the fabrication of multilayers from solution deposition processes requires that each stacked layer is inert to the solvents and processing temperatures that it is subsequently exposed to during device manufacture. The reduced solubility parameter window of polymers and their large bulk viscosity typically increase the options to find orthogonal solvents for solution deposition on top of polymer layers, thus expanding the choice of materials that can be used in devices. Finally, because polymers do not vaporize before decomposition and thus have negligible vapor pressure, they are not susceptible to interlayer diffusion during the typical thermal cycles during device fabrication, and typically exhibit robust mechanical properties, making nanometer-thick semiconductor films potentially compatible with roll-to-roll fabrication on flexible substrates. However, during recent years, several new approaches have been developed to improve small-molecule processability from solutions, including the use of spin coating, slot dye coating, and blade coating.

1.3 Thin-Film Transistor Applications

OTFTs are a low-cost technology alternative to amorphous hydrogenated silicon transistors for applications in large-area OTFT-based arrays, for example, backplane/driver circuits for active matrix displays, where high transistor density and switching speeds are not necessary. They may also be attractive for applications in low-end microelectronics (e.g., radio frequency identification tags and sensors), where the high cost of packaging conventional Si circuits is prohibitive for everyday items [11]. The advantages of OTFTs stems from the potential lower manufacturing costs and reduced capital investments thanks to device fabrication using common solution-based deposition and patterning techniques such as offset, gravure, screen/stencil, and inkjet printing, to cite just a few. Furthermore, OTFT-based circuits based on conjugated polymers are compatible with plastic substrates so that compact, lightweight, and structurally robust and flexible electronic devices can be fabricated.

Figure 1.2 shows a schematic structure of a bottom-gate top-contact OTFT. Note that several other device architectures can be fabricated depending on the relative position of the contacts and the dielectric/semiconductor layers (not shown). An OTFT is composed of three electrodes (source, drain, and gate), a gate dielectric layer, and an organic or polymer semiconductor layer. In this device, negligible source–drain current ($I_{SD} = 0$ A) flows when the gate voltage

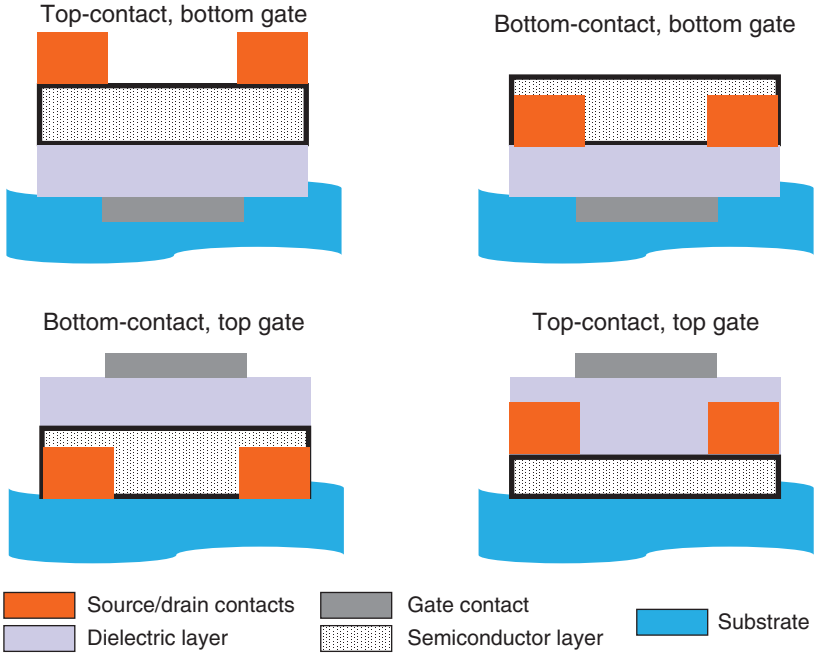

Figure 1.2 Structure and materials of four thin-film transistor architectures.

is zero ($V_G = 0$ V) independent of the bias applied between the source and the drain contacts (V_{SD}). The device turns on ($I_{SD} \neq 0$ A) when a gate field is applied ($V_G \neq 0$ V), which induces charge carriers in the semiconductor at the interface with the dielectric layer. The transistor's performance is evaluated from the output and transfer current–voltage plots, from which critical parameters such as the field-effect mobility (μ), current on/off ratio (I_{on}/I_{off}), threshold voltage (V_T), and subthreshold swing (S) are measured (Figure 1.3).

Within the metal–oxide–semiconductor field-effect transistor (MOSFET) gradual channel model approximation, the carrier mobility in the linear and saturation regimes can be extracted from the following standard MOSFET equations:

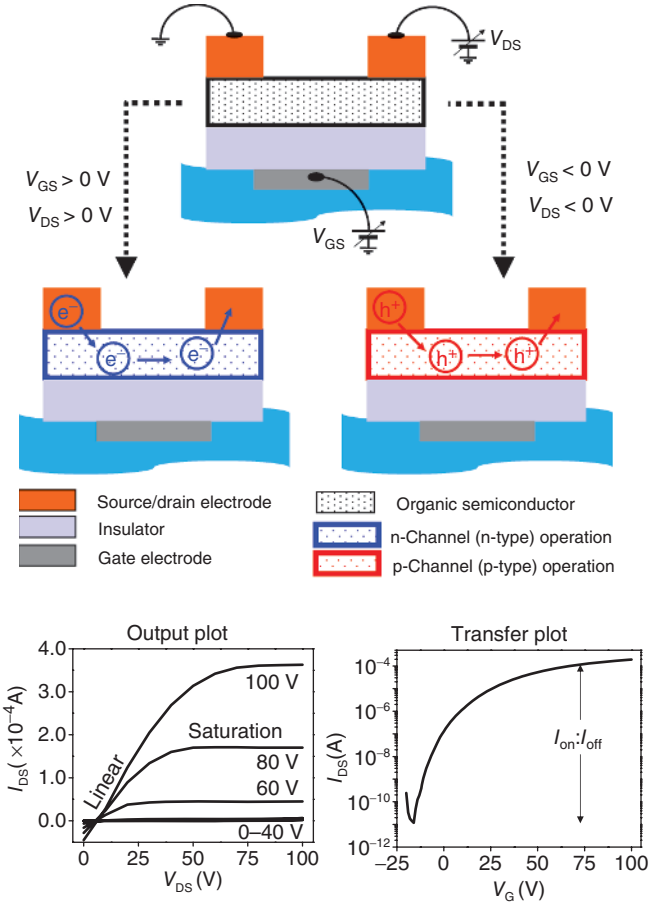

Figure 1.3 (a) Top: Schematic representation of electron and hole transport in bottom-gate top-contact TFTs. Bottom: Output plot of the source–drain current versus the source–drain voltage at a given V_G and (b) transfer plot of the source–drain current versus the gate voltage at different V_{SD}'s.

$$\left(I_{SD}\right)_{lin} = \left(\frac{W}{L}\right)\mu_{FET}C_i\left(\frac{V_{SG} - V_T - V_{SD}}{2}\right)V_{SD} \tag{1.1}$$

$$\left(I_{SD}\right)_{sat} = \left(\frac{W}{2L}\right)\mu_{FET}C_i(V_{SG} - V_T)^2 \tag{1.2}$$

where V_{SD} is the drain voltage with the source electrode grounded. W and L are the transistor channel width and length, respectively, and C_i is the capacitance per unit area of the dielectric layer. Polymeric semiconductors for TFTs can be divided into three classes depending on whether the majority charge carriers are holes (p-channel), electrons (n-channel), or both (ambipolar) under different gate bias conditions. Until recently, polymeric semiconductors for TFTs were particularly challenging because most of them were difficult to synthesize/reproduce in optimal batches, poorly soluble, or very sensitive to ambient conditions, and/or exhibited poor charge-carrier mobility. Insoluble polymers preclude their use with solution deposition techniques, while air sensitivity requires manufacturing in cost-prohibitive inert atmosphere. However, during the last 3 years, a few polymeric semiconductors have been found to exhibit the combination of all required properties, enabling the realization of OTFT meeting first-generation market products.

1.4 p-Channel Semiconductors

The most performing semiconductors for OFETs (organic field-effect transistors) are p-channel devices. Besides the basic structural requirements discussed previously, the common strategy to obtain good hole-transporting semiconductors for TFTs is via a delicate balance of the HOMO (highest occupied molecular orbital) energy level which should lie somewhere around −5 to −5.5 eV. When E_{HOMO} is too high (low ionization potential (IP)), easy oxidation by air and acceptor sites dramatically compromises the TFT's ambient stability and current on–off ratio. For $E_{HOMO} \ll -5.5$ eV (high IP), very large I_{on}:I_{off} and good mobilities can be achieved, but these devices typically exhibit unacceptably large threshold voltages. In this section, we will first summarize very briefly the key historical p-channel semiconductors (Figure 1.4), and then move to more recent studies regarding the development of polymers and small molecules.

1.4.1 Polymers

Poly(3-substitutedthiophene)s are one of the most studied polymer families for (semi)conductor/optical applications [8b, 12]. These systems have the advantage that the presence of the 3-substituent strongly enhances solution processability and thin-film-forming capacities. The performance of poly(3-alkylthiophene)-based OFETs, particularly Poly(3-hexylthiophene) (P3HT) (**P1**), has been

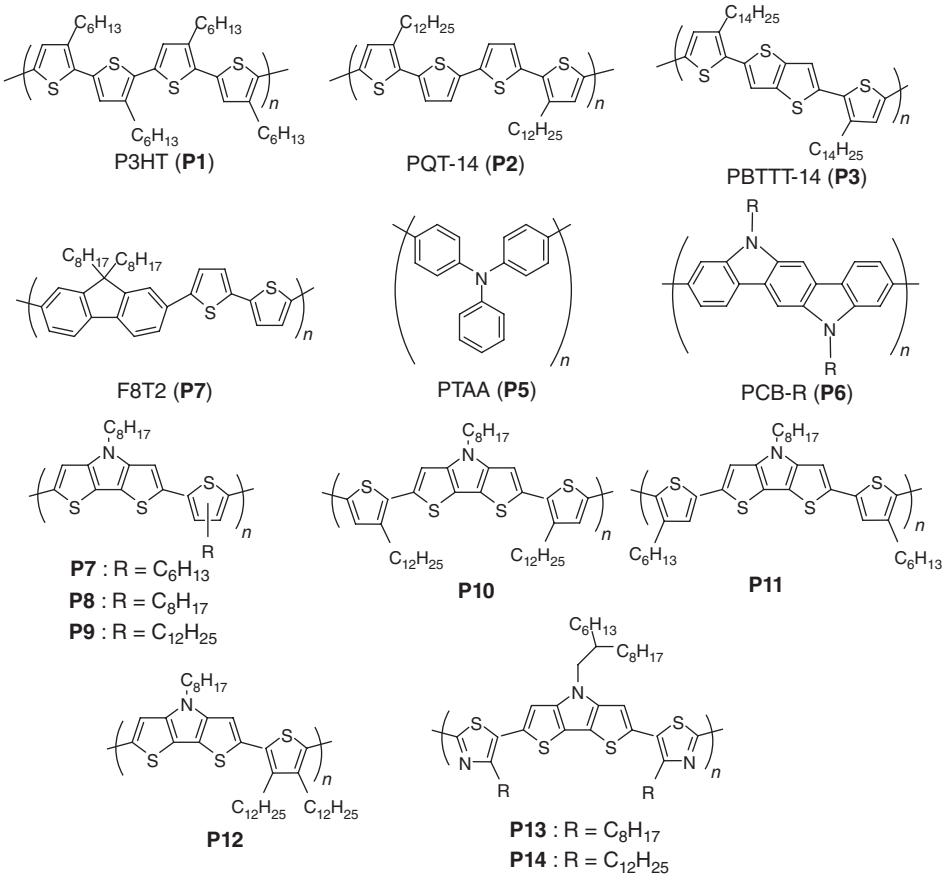

Figure 1.4 Chemical structure of the p-channel semiconductors **P1–P14**.

investigated by various groups considering the effects of the molecular weight of Poly(3-alkylthiophene) (P3AT) [13–15], film deposition solvent [16], film morphology [17, 18], film thickness [19], and fabrication process [20], as well as humidity [21] and length of the core substituent (alkyl chain) [22]. These studies have deepened our understandings of the charge-transport properties of polymeric semiconductors as a whole. However, it was challenging to achieve good control over the regioregularity in several poly(3-alkylthiophene) synthesis, and exposure of P3AT films to air usually caused an increase in the carrier density, thus degrading the transistor's I_{on}/I_{off} ratio. Therefore, high I_{on}:I_{off} ratios for P3AT are consistently achieved by preparing and testing the devices in dry N_2 [23]. To address these problems, new polythiophenes have been developed. Ong *et al.* reported a class of solution-processable regioregular polyquaterthiophenes (PQTs) that affords excellent FET performance under ambient conditions. This class of polythiophenes was designed on the basis of the following structural

considerations: (i) presence long alkyl side chains for solution processability; (ii) structural regularity to induce and facilitate molecular self-assembly; and (iii) control of the π-conjugation extension to achieve a delicate balance between transistor functionality and oxidative doping stability. These semiconductors exhibit unique self-assembly ability and form highly structured thin films when deposited from solution under appropriate conditions. FETs fabricated in air with PQT-12 (**P2**, Figure 1.4) channel layers have provided high field-effect mobility of up to 0.14 $cm^2 V^{-1} s^{-1}$ and high I_{on}/I_{off} ratios of $>10^7$ [24]. Chabinyc *et al.* investigated the effects of humidity on unencapsulated **P2**-based OFETs. The field-effect mobility of **P2** TFTs decreases and the rate of trapping of charge carriers increases under increasing humidity [25], pointing out that not only n-channel semiconductors are H_2O sensitive.

Instead of increasing the IP of polythiophene by sterically twisting the repeat units in the backbone, McCulloch *et al.* [26, 27] synthesized polymers incorporating thieno[3,2-*b*]thiophene (**P3**) as co-monomers. The delocalization of electrons from the fused aromatic units into the backbone is less favorable than from a single thiophene ring, which is due to the larger resonance stabilization energy of the fused ring over the single thiophene ring. The decreased delocalization along the backbone lowers the polymer HOMO level. The charge-carrier mobilities of **P3** are high, with values of 0.2–0.6 $cm^2 V^{-1} s^{-1}$ obtained on annealed devices in a nitrogen atmosphere and up to 0.7 $cm^2 V^{-1} s^{-1}$ for devices of 5 μm channel length. DeLongchamp *et al.* [28] investigated in detail the origin of the enhanced crystallinity of this polymer. From first-principles energy minimization using density functional theory (DFT), the authors predicted that the conjugated polymeric planes of **P3** are substantially tilted within their crystalline lamellae. This prediction was confirmed experimentally using a combination of polarized photon spectroscopies including near edge X-ray absorption fine structure (NEXAFS) and IR. Other important first-generation polymeric semiconductor families are those based on 9,9-dialkylfluorene-*alt*-bithiophene (e.g., F8T2, **P4**) [29, 30], triarylamine (**P5**) [31], and carbazole (e.g., Polycarbazole (PCB), **P6**) [32, 33] units (Figure 1.4).

During the last 3 years, several new structures, particularly based on fused units, have been developed, resulting in even greater p-channel TFT performances (Figure 1.5). Rasmussen and coworkers [34] pioneered the use of *N*-alkyldithieno[3,2-*b*:2′,3′-*d*]pyrrole (DTP) as a very promising fused aromatic building block for electronic materials. This core exhibits a completely flat crystal structure, indicating good π conjugation across the fused rings. Upon polymerization, poly(*N*-alkyl dithieno[3,2-*b*:2′,3′-*d*]pyrrole)s exhibit excellent stability in their oxidized state, have low band gaps, and show efficient red fluorescence in solution [35]. However, some Poly(dithieno[3,2-b:2′,3′-d]pyrrole) (PDTPs) have low solubilities and low molecular weights, which greatly limit their use in devices. To improve the solubility of PDTPs and to create a number of DTP-based copolymers, McCullough *et al.* [36] described the synthesis, characterization, electrical conductivity, and field-effect mobility of a series of novel soluble *N*-alkyl DTP–thiophene copolymers (**P7–P12**, Figure 1.5) and

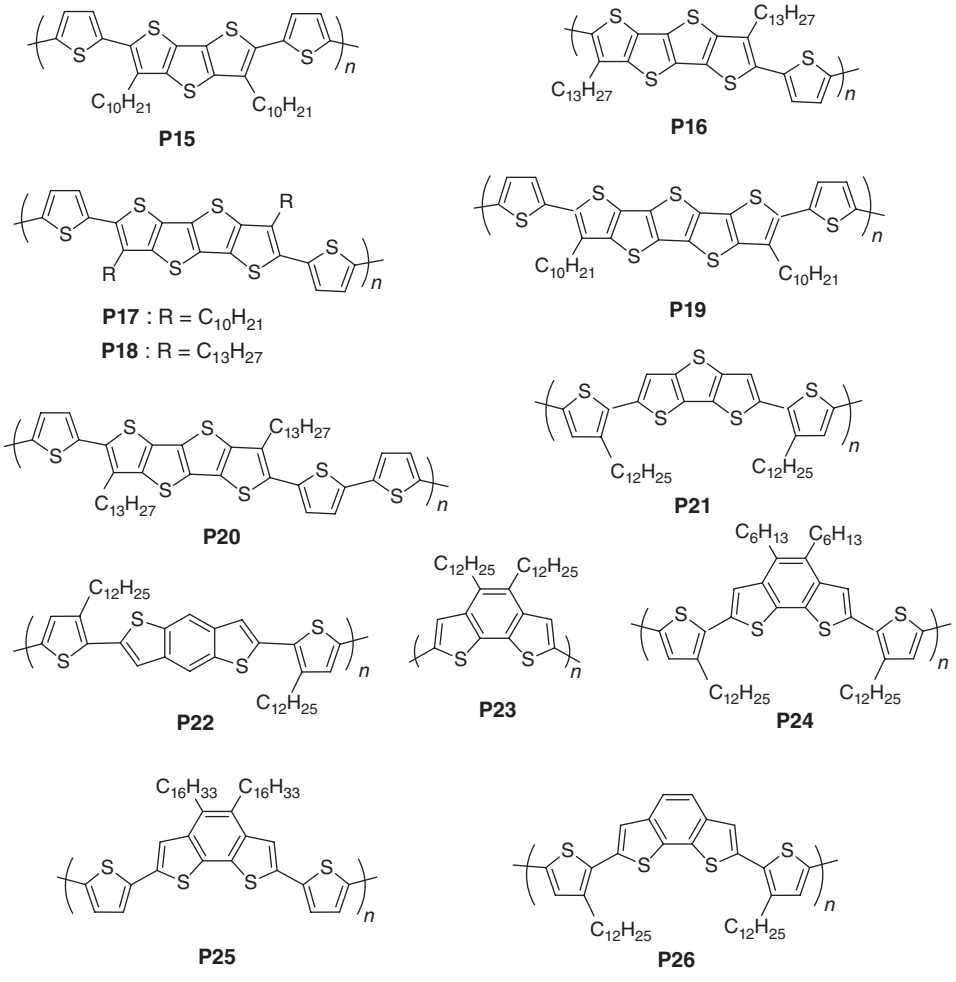

Figure 1.5 Chemical structure of fused thiophene-based p-channel semiconductors **P15**–**P26**.

compared them with the well-studied regioregular P3HT. These polymers were synthesized using a Stille coupling reaction, and exhibited molecular weights of 10–50 kDa. The incorporation of planar DTP units extends the π conjugation, and the introduction of thiophene subunits imparts good solubility, high conductivity, and high charge-carrier mobility. Optical characterization revealed that the bandgaps of **P7**–**P12** were between 1.74 and 2.00 eV, which is lower than the value for regioregular poly(3-alkylthiophenes), and the HOMO energy levels were between −4.68 and −4.96 eV. When doped, these polymers exhibited high conductivities up to 230 S cm^{-1} with excellent stability. The microstructure and surface morphologies of, for instance, poly(2-(4,4′-didodecyl-2,2′-bithiophen-5-yl)-4-octyl-4*H*-bisthieno[3,2-*b*:2′,3′-*d*]pyrrole) (**P10**) thin films were studied

by X-ray diffraction and atomic force microscopy (AFM). The as-cast **P10** thin films exhibited poorly defined, randomly ordered lamellar structures, which improved significantly after thermal annealing (Figure 1.6). FET devices showed typical p-channel transistor behavior. Interestingly, the mobilities of the as-cast, less ordered samples were much higher than those observed after annealing. The highest values of the maximum and average mobilities were observed for as-cast **P10** (0.21 and 0.13 $cm^2 V^{-1} s^{-1}$, respectively). The authors' goals were to test the idea that high mobility and excellent electrical and structural reproducibility could be achieved in amorphous π-conjugated materials that could possess long-range π connectivity on the microscopic scale.

To improve the air stability of these materials, the authors included electron-deficient units into the polymer backbone to increase the IP [37]. To this end, the same group used the electron-deficient bithiazole (Tz) unit, which is known to increase IP [38]. The new polymers **P13** and **P14** (Figure 1.4), defined as "transistor paints," achieved excellent FET performance with hole mobilities as high as 0.14 and 0.10 $cm^2 V^{-1} s^{-1}$ and current on/off ratios up to 10^6 without post-deposition thermal annealing. Furthermore, these devices exhibited excellent air stability, showing no significant degradation over 60 days.

He, Malliaras, and coworkers [39] recently reported a family of fused-ring thiophene copolymers (**P15–P20**) as materials of interest for TFT applications. In an initial study, a comparison of the properties of **P15** to **P17** showed that the polymer with the even-numbered fused-thiophene core exhibited a much smaller lamellar spacing than the polymers featuring odd-numbered fused-thiophene cores. As a result, transistors fabricated from the polymer with the even-numbered fused-thiophene core (**P16**) yielded a much higher field-effect mobility than the other two (**P15** and **P17**). To obtain further insight into the structure–property relationships in these polymeric semiconductors, more recently they included additional polymers, which were used to elucidate the role of symmetry of the polymer repeat unit on structure and device performance (Figure 1.7). Devices made from the polymer with four fused rings (**P17**) showed a hole mobility of 0.087 $cm^2 V^{-1} s^{-1}$, whereas devices made from the polymers with three (**P15**) and five fused rings (**P19**) showed hole mobilities of 0.0017 and 0.0023 $cm^2 V^{-1} s^{-1}$, respectively. Devices made from **P16** and **P20** showed a hole mobility of 0.042 and 0.022 $cm^2 V^{-1} s^{-1}$, respectively, which is ~10 times lower than that achieved with **P18** (0.33 $cm^2 V^{-1} s^{-1}$) [40].

These results strongly suggest a correlation between a repeat unit that possesses a C_2 axis perpendicular to the conjugation plane, a minimum attainable lamellar spacing, and high field-effect mobility. Ong and coworkers [41] reported a new dithienothiophene-based copolymer, **P21**, which is structurally similar to **P15** and shows mobilities of ~0.01 $cm^2 V^{-1} s^{-1}$, corroborating these symmetry-driven trends.

Mullen *et al.* developed benzo[2,1-*b*;3,4-*b*0]dithiophene-containing homo- and copolymers (**P23–P26**) having solubilizing alkyl chains attached to the benzo unit [42] as an alternative to the classic Benzo[1,2-b:4,5-b']dithiophene (TBT)-based copolymer **P22** [43]. The homopolymer **P23** is very soluble in dichlorobenzene,

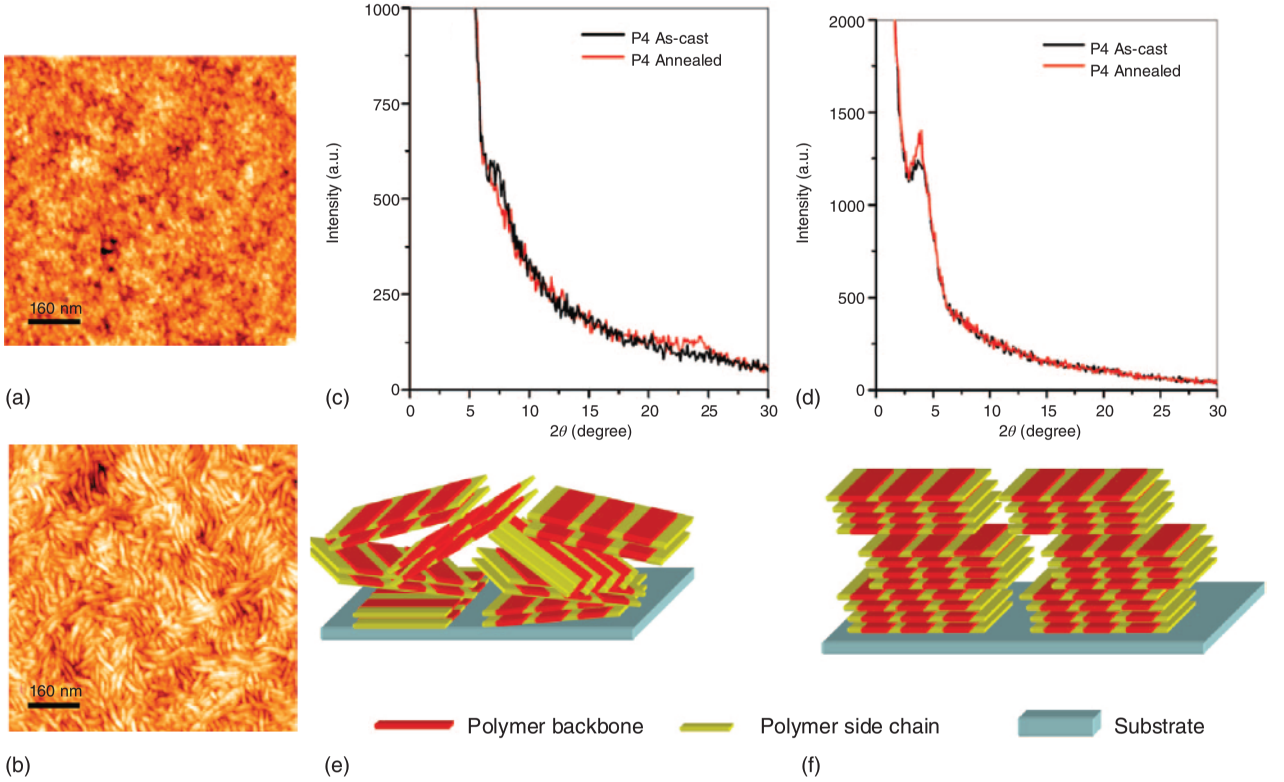

Figure 1.6 Tapping-mode AFM height images of **P10** drop-cast on octadecyltrichlorosilane (OTS)-treated SiO_2/Si surfaces (a) as-cast and (b) annealed at 120 °C for 30 min and then cooled to room temperature in a vacuum. X-ray Diffraction (XRD) profile of **P10** thin films on an OTS-treated SiO_2/Si substrate as cast (black trace) and after annealing at 120 °C for 30 min (red trace). (c) Out-of-plane XRD profile. (d) In-plane XRD profile. Scheme of molecular packing of **P10** (e) as cast and (f) after annealing at 120 °C for 30 min [36]. (Reproduced with permission. Copyright © 2008 American Chemical Society.)

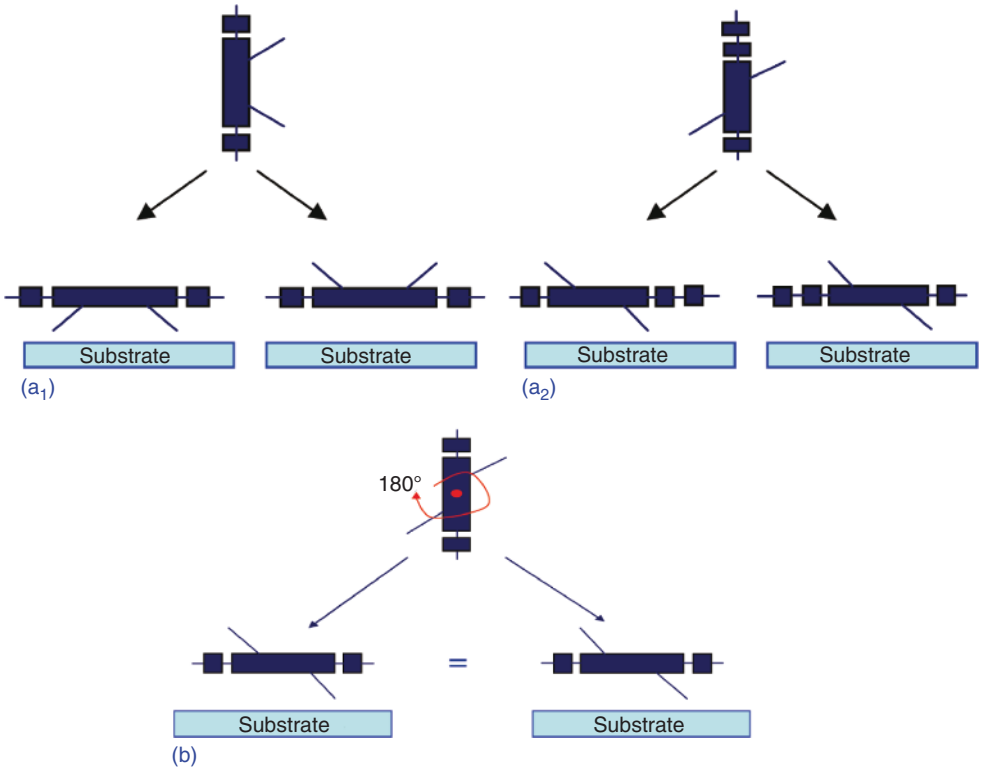

Figure 1.7 Possible configurations of the repeat unit with respect to the substrate, for repeat units (a_1 and a_2) without and (b) with C_2 symmetry. Judging from the family of closely related conjugated polymers that we have investigated, C_2 symmetry seems to enable a very small lamellar period and promote high mobility [40]. (Reproduced with permission. Copyright © 2010 American Chemical Society.)

and top-contact TFTs exhibit low charge-carrier mobility of $\sim 10^{-4}$ cm^2 V^{-1} s^{-1}, probably because the polymer backbone is too stiff. The other copolymers exhibit greater performance ranging from 0.001 to >0.1 cm^2 V^{-1} s^{-1} for bottom-gate top-contact transistors. Top-gate devices based on **P26** on a poly(ethylene terephthalate) (PET) film were also fabricated, which exhibited exceptionally large carrier mobility of >0.5 cm^2 V^{-1} s^{-1}.

Among the many approaches to increasing air stability, the incorporation of unsubstituted conjugated moieties in poly(alkylthiophene) backbones resulted in much better oxidative stability and hole mobility, as demonstrated in PQT (**P2**) and Poly(2,5p-bis(thiophenp-2yl)thieno(3,2p-b)thiophene) (PBTTT) (**P3**). These unsubstituted conjugated moieties possess rotational freedom, which curtails the effective conjugation length, lowers the HOMO level, and consequently increases oxidative stability. Unsubstituted thiophene moieties, along with lengthened alkyl side chains, play also another important role by promoting favorable interdigitation of the side chains. This leads to well-organized intermolecular

3D ordering and large crystalline domains, and consequently high mobility. Thienylenevinylene derivatives, a combination of thiophene and vinyl groups, are known to have an extended conjugated system, which is a crucial component for building organic electronic devices [44]. In addition, the incorporation of vinylene bonds in an aromatic polymer backbone leads to an increase in the degree of coplanarity of the polymer backbone, as the vinylene bond reduces steric hindrance on successive aromatic rings [45]. Recently Kim *et al.* reported high-performance OTFTs with a new thienylenevinylene polymer **P27** (Figure 1.8). An unsubstituted dithienylethylene unit is symmetrically inserted between dodecylthiophenes, thereby allowing some rotational freedom between the alkyl thiophene and unsubstituted dithienylethylene units, which lowered the HOMO level. **P27**-based OTFTs showed unoptimized charge-carrier mobility of 0.15 $cm^2 V^{-1} s^{-1}$ with a relatively high oxidative stability.

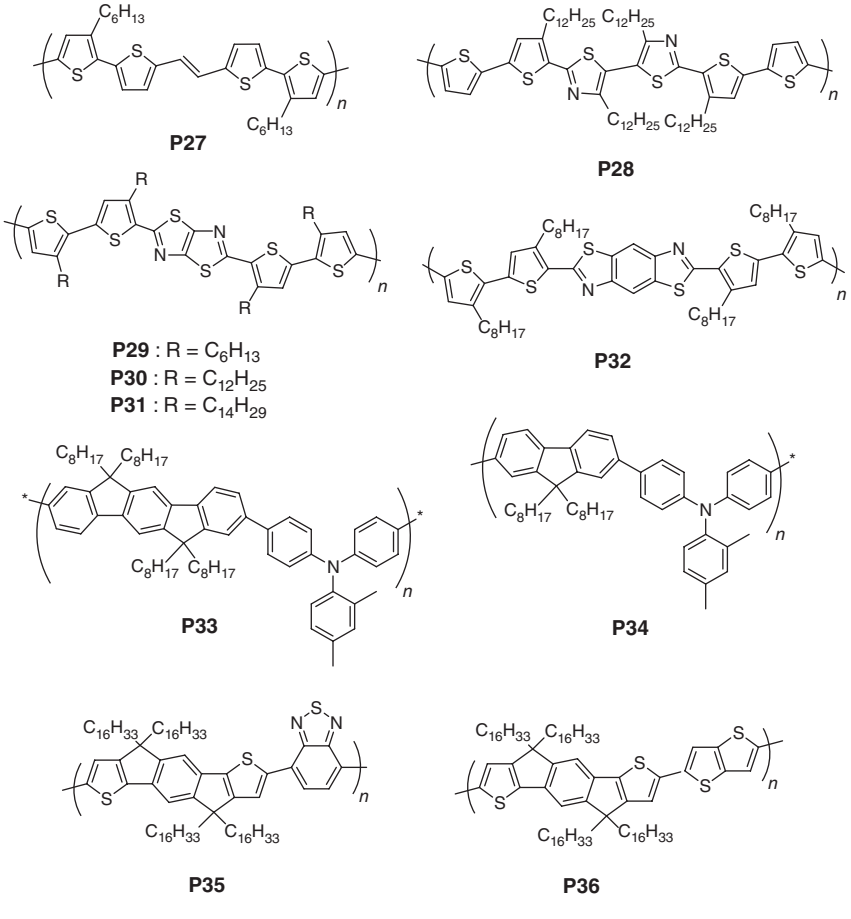

Figure 1.8 Chemical structure of p-channel semiconductors **P27–P36**.

Some interesting structures incorporating the thiazole ring have been reported, mainly with the goal to increase the oxidative stability. Another common problem with OFETs is the electrical instability under external bias stress, likely due to charge traps created through partial disorder in the structure of the thin films and the chemical characteristics of the semiconductor/insulator interface. Bias-stress instability and environmental instability can be significant challenges for semiconducting polymers [46]. To be usable in conventional electronics, OTFTs should exhibit similar characteristics with respect to electrical bias stress [47]. Although there have been a few studies aimed at enhancing the electrical stability of π-conjugated polymers under external bias stress, an adequate understanding of the relationship between the crystalline nanostructure and the bias-stress-driven electrical instability on the microscopic scale is still needed. Lee and coworkers [48] have initiated an in-depth and systematic study addressing the bias stress in polymers using highly ordered π-conjugated copolymer thin films with minimal concentration of charge traps. They used a new thiazole polymer, **P28** (Figure 1.8), having alkyl chain-substituted thiophene/thiazole blocks along the polymer backbone to increase the IP because of the enhanced rotational freedom along the backbone [27] and the electron-accepting nature of the 5,5′-bithiazole units [37b, 49, 49a,b]. In particular, **P28** presents a liquid-crystalline nature with a clear mesophase region, resulting in highly crystalline thin films forming spontaneously through the self-assembly of individual chains after thermal annealing. Most importantly, this novel polymer exhibits high field-effect mobilities of 0.33 $cm^2 V^{-1} s^{-1}$, good environmental stability, and unprecedented bias-stress stability comparable to that of amorphous silicon.

McCullough *et al.* [50] reported copolymers (**P29–P31**, Figure 1.8) incorporating a fused thiazolothiazole ring in the backbone. Despite the low molecular weights of this family ($M_n = 4-9$ kDa), they exhibit field-effect mobilities from 0.02 to 0.3 $cm^2 V^{-1} s^{-1}$ with high current on/off ratios of $\sim 10^6$. The use of thiazolothiazole-fused ring ensures a very rigid and coplanar backbone and thereby highly extended π-electron conjugation and strong π stacking. The electron-deficient nature of the thiazolothiazole affords high oxidative stability. However, the uneven placement of the alkyl side chains along the backbone reduced interdigitation and promoted amorphous-like π stacking and π connectivity along the chain while enhancing solubility. With regard to the side-chain arrangement, the key difference between the **P29–P31** family and PBTTT/PQT polymers is that, while the side chains in the former polymers are still arranged regiosymmetrically, they are not equally spaced along the backbone. Thus, as a consequence, the side chains are apparently disordered and do not interdigitate as seen in PBTTT or PQT (Figure 1.9). Most interestingly, despite all these factors, X-ray diffraction patterns of **P29** indicate very strong lamellar ordering, and FETs fabricated from these materials show high field-effect mobilities. All these results appear quite surprising in view of the previously mentioned findings on the role of side-chain interdigitation/ordering and indicate that strong interdigitation and formation of extended regular terrace-like structures are not necessary for high carrier mobility in polythiophene-like materials.

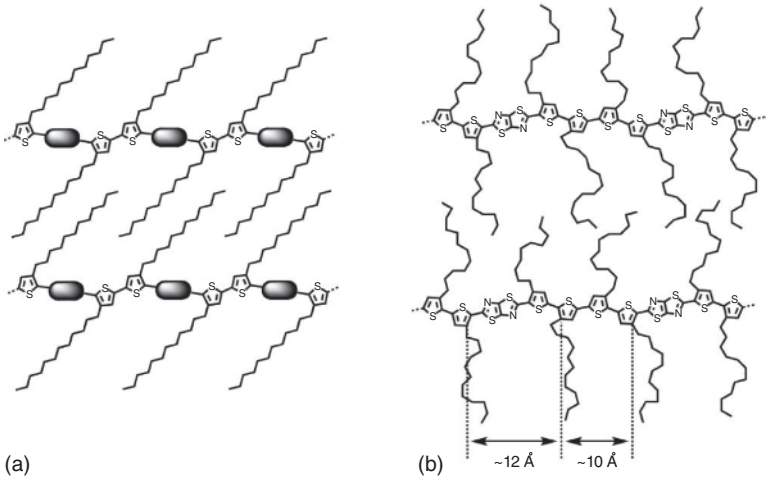

Figure 1.9 Schematic illustrations for (a) the packing structure of PQT (**P2**) and PBTTT (**P3**) with dodecyl side chain with uniform side-chain interdigitation and (b) proposed packing structure for **P30** with disordered side chains [50]. (Reproduced with permission. Copyright © 2009 American Chemical Society.)

Jenekhe and coworkers have reported an interesting polymer, **P32** (Figure 1.8), designed with the knowledge that benzobisthiazole and benzobisoxazole polymers and small molecules exhibit efficient π stacking and strong intermolecular interactions in the solid state [51] leading to high-temperature resistance with glass-transition temperatures that can exceed 300–400 °C and relatively high electron affinity [52]. Earlier studies of a benzobisthiazole polymer as an n-channel semiconductor in FETs had found a low mobility of electrons, requiring a high-electron-affinity polymer in a blend to achieve electron injection [53]. Recently, TFTs based on benzobisthiazole small molecules were shown to exhibit high field-effect mobilities for both holes and electrons (see below) [54]. The authors reported a new soluble benzobisthiazole-thiophene copolymer based on alternating benzobisthiazole and oligo-3-octylthiophene units in the backbone (**P32**), resulting in improved oxidative stability, thermal stability, interchain interactions, and thus enhanced charge-transport properties of the polymers. The highly crystalline **P32** thin films exhibit a field-effect carrier mobility of up to 0.01 $cm^2\ V^{-1}\ s^{-1}$.

Zhang and coworkers reported two classes of polymers based on fluorene and indenofluorene copolymerized with triarylamine (**P33** and **P34**, Figure 1.8) [55] and indacenodithiophene copolymerized with benzothiadiazole and thienothiophene (**P35** and **P36**) [56]. Bottom-contact, top-gate (BC–TG) (and bottom-gate) architecture FET devices based on **P33** and **P34** were fabricated with the polymer semiconductors deposited from solution. Compared to the best triarylamine homopolymers [46c] (mobility of $\sim 4 \times 10^{-3}\ cm^2\ V^{-1}\ s^{-1}$) the new polymers exhibited improved mobility by a factor of 5–0.02 $cm^2\ V^{-1}\ s^{-1}$ by the introduction of the fluorene unit, which further increased to 0.04 $cm^2\ V^{-1}\ s^{-1}$ for

the indenofluorene copolymer and current on/off ratios of $>10^6$. It is speculated that the increase in the polymer backbone planarity and persistence length in the copolymers improved the intramolecular π-orbital overlap and enhanced the local structural organization, resulting in the large measured mobilities. No evidence of thin-film crystallinity could be observed for **P33** and **P34** polymer semiconductors. For polymers **P35** and **P36** (Figure 1.8), the strategy for further improvement in charge-carrier mobility in comparison to **P33** and **P34** was to enhance the planarity of the backbone and further reduce the energetic disorder of the polymer. The aryl amine unit was replaced with more planar Benzothiadiazole (BTD) and Thienothiophene (TT) units. Grazing incidence X-ray scattering (GIXS) experiments were carried out on annealed thin films of both polymers on Si substrates to explore the microstructure, and **P35** polymer was observed to be semicrystalline while **P36** thin film was amorphous. BC–TG) architecture FET devices were fabricated with the polymer semiconductors spin-cast from a 10 mg ml^{-1} chlorobenzene solution at 2000 rpm followed by an annealing step at 100 °C for 5 min in nitrogen. **P35** transistors yield maximum hole mobilities in the range 0.8–1.2 cm^2 V^{-1} s^{-1}, with a current on/off ratio of $\sim 10^4$ and a threshold voltage of ~ -30 V. Despite the very high mobility values, FET operation is heavily injection-limited. The **P36** copolymer exhibits a lower mobility ($\sim$0.2 cm^2 V^{-1} s^{-1}), which is attributed to the more amorphous nature of the thin-film microstructure.

Inspired by the work of Marks *et al.* [57] on silole-based copolymers for TFTs, Reynolds reported copolymers of dithienosilole with BTD, following the donor–acceptor concept to broaden the optical absorption (Figure 1.10) [58]. Dithienosilole (DTS)-BTD copolymers **P37–P40**, differing by the concentration of electron-donating and electron-withdrawing substituents along the backbone, were synthesized and characterized by 2D WAXS and in bottom-contact TFTs. While all copolymers self-assembled into lamellar morphologies, only **P38** and **P40** showed a propensity to form π stacks. The highest hole mobility of 0.02 cm^2 V^{-1} s^{-1} was observed for **P40**, in agreement with the close π stacking and lamellar distances found by structural analysis (0.36 and 1.84 nm, respectively). Following a similar strategy but by using different building blocks, Bao and coworkers [59] synthesized dithiophene and fluorene copolymers (**P41** and **P42**, Figure 1.10) containing fused aromatic thieno[3,4-*b*]pyrazine moieties. Suzuki and Stille polycondensation reactions were used for the polymerization. The bandgap (E_g) of the polymers was tuned in the range 1.15–1.6 eV. These polymers showed a field-effect mobility as high as 0.2 cm^2 V^{-1} s^{-1} with current on/off ratios as high as 10^6 in OTFT devices.

Takimiya and coworkers reported several advanced molecular and polymeric semiconductors for TFTs with heteroarenes (Figure 1.10). The design rationale is that fusion of thiophene rings is necessary to avoid the twist between the adjacent thiophene rings, which would reduce the π stacking. A preliminarily synthesized [1]Benzothieno[3,2-b][1]benzothiophene (BTBT)-thiophene copolymer (PBTBT, **P43**) resulted in a highly twisted backbone ($\lambda_{max} < 400$ nm), and TFTs based on this polymer did not function despite the fact that BTBT had been successful in

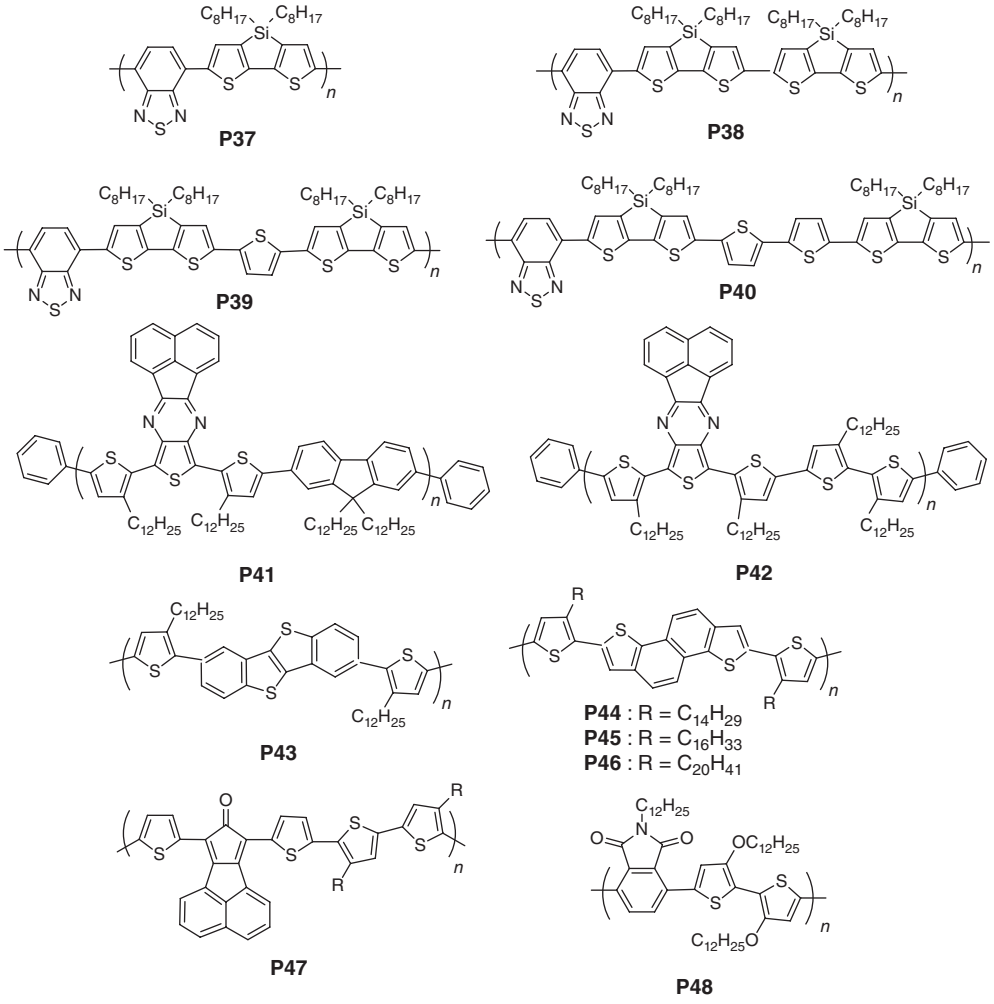

Figure 1.10 Chemical structure of p-channel semiconductors **P37–P48**.

small-molecule systems [60]. Thus, this group recently presented a new design strategy based on **P44–P46**, which incorporates naphthodithiophene (NDT) into a regiosymmetric polythiophene system [61, 62]. These polymers showed high M_n of 24–33 kDa and sufficient solubility in warm chlorinated solvents. TFTs based on **P44–P46** exhibited among the highest field-effect mobility values observed to date for semiconducting polymers (>0.3–0.5 $cm^2 V^{-1} s^{-1}$).

Wudl *et al.* [63] reported **P47** (Figure 1.10) consisting of an electron donor (thiophene) and acceptor (cyclopentadienone) alternating copolymer. The results illustrated that, despite the low molecular weight of this polymer (~6 kDa), a substantial field-effect mobility (~0.02 $cm^2 V^{-1} s^{-1}$) could be obtained. Watson *et al.* [64] reported a copolymer of phthalimide and

3,3′-dialkoxy-2,2′-bithiophene (**P48**, Figure 1.10). In this polymer, backbone planarity is enforced by attractive intramolecular interactions between the pendant oxygens and thienyl sulfur atoms [65], as shown by the crystal structures of some building blocks, intermolecular donor–acceptor interactions, and possibly increased quinoidal backbone character due to alternating donor and acceptor units [66]. The maximum field-effect mobilities were $\sim 0.28\ cm^2\ V^{-1}\ s^{-1}$ in the saturation region and current on/off current ratios of $\sim 10^4 - 10^5$.

Isoindigo has recently become a popular conjugated moiety in polymer semiconductor design because of its strong electron-withdrawing character. Its acceptor nature results from two lactam rings, and it can be synthesized from various natural sources. This makes isoindigo an attractive building block for sustainable synthetic sources [67]. Reynolds and coworkers reported the synthesis of the first set of isoindigo-based donor–acceptor copolymers with various electron-donating moieties (**P49–P54**, Figure 1.11). These polymers, in which isoindigo serves as the acceptor unit, were found to be attractive for OFET and Organic photovoltaics (OPV) applications because of their deep HOMO and LUMO (lowest unoccupied molecular orbital) levels, and their tunable absorption extended to 800 nm in the solid state [68]. Following this initial report, several new alternating copolymers bearing isoindigo units were reported, and one of these copolymers with terthiophene unit (**P55**, Figure 1.11) reached a power conversion efficiency of 6.3% in OPV devices [69]. This efficiency is a record for a polymer solar cell based on a polymer with an optical bandgap of <1.5 eV. The first air-stable and high-performance isoindigo-based polymer (**P56**, Figure 1.11) in OFETs was reported by Pei *et al.* [70] for a copolymer of isoindigo unit with bithiophene, which showed hole mobilities of up to $0.79\ cm^2\ V^{-1}\ s^{-1}$ after thermal annealing at 150 °C. These devices showed very good ambient stability including in high humidity conditions, owing to their low-lying HOMO levels. Bao and coworkers [71] developed a novel high molecular weight ($M_n > 130$ kDa, DP ≈ 30) isoindigo-based polymer (**P57**, Figure 1.11) with siloxane-terminated solubilizing groups. This new polymer with linear alkyl chains was found to have sufficient solubility for solution processing because of its terminal siloxane groups. Record field-effect mobilities of up to $2.48\ cm^2\ V^{-1}\ s^{-1}$ were obtained for **P57**. The same research group prepared a reference polymer **P56** bearing an identical π backbone with branched alkyl side chains. This polymer showed a lower hole mobility of $0.57\ cm^2\ V^{-1}\ s^{-1}$. The enhanced mobility of **P57** was attributed to the stronger intermolecular interactions of the polymer chains in the solid state. Thin-film XRD characterizations indicated a smaller π–π stacking distance (3.58 vs 3.76 Å) for **P57** compared to the reference polymer **P56** (Figure 1.12). This was attributed to the fact that the branching point of **P57** solubilizing groups was placed further away from the polymer π backbone, which allowed the polymer chains to pack more closely together [72]. To further explore this phenomenon, four isoindigo-based copolymers with branching points at various positions were synthesized, achieving an exceptionally high hole mobility of $3.62\ cm^2\ V^{-1}\ s^{-1}$ for **P58** (Figure 1.11) [73]. This study by Pei *et al.* reveals the importance of molecular engineering of alkyl side chains, not only to manipulate polymer solubility but also to enhance charge-carrier mobilities.

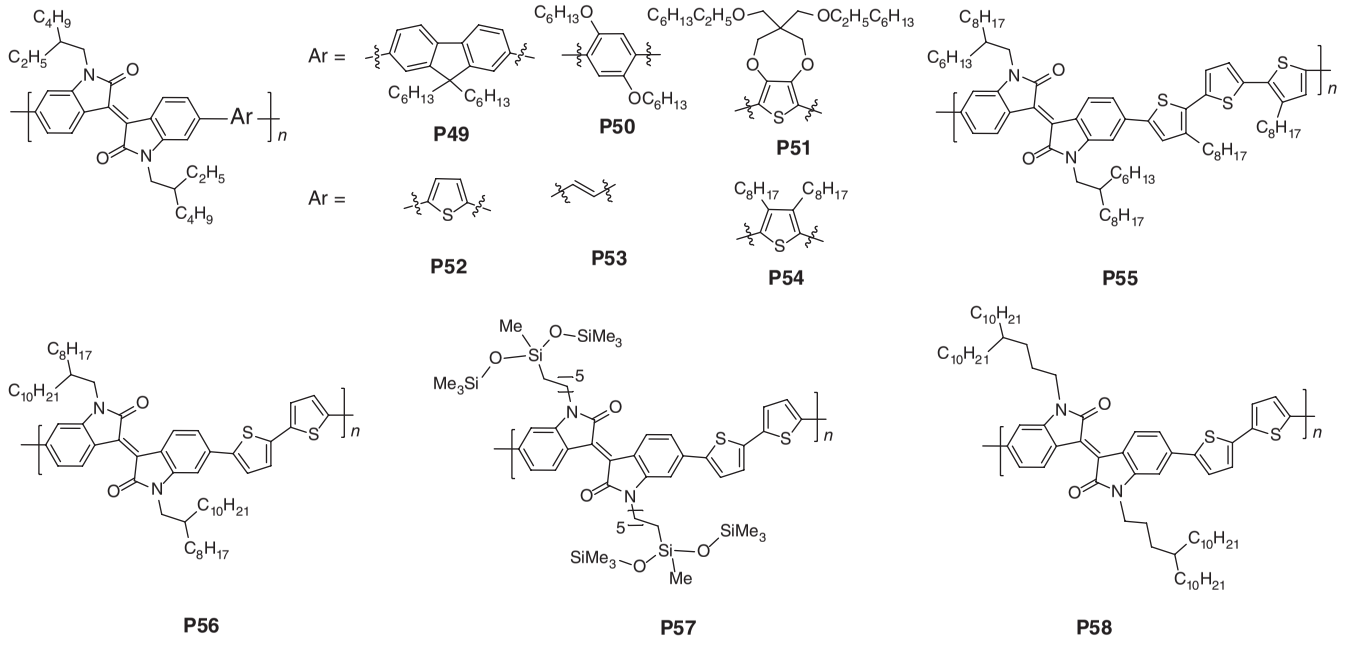

Figure 1.11 Chemical structure of p-channel semiconductors **P49**–**P58**.

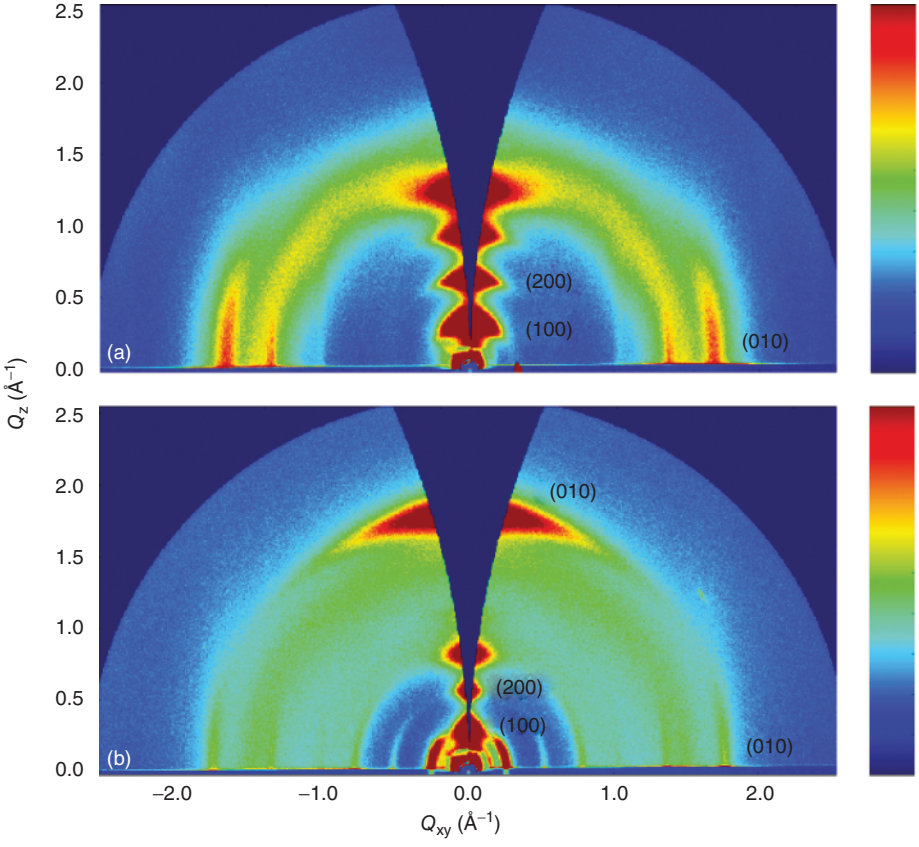

Figure 1.12 GIXD images of **P56** (a) and **P57** (b) annealed at 130 °C. **P56** displays lamellar packing common to many conjugated polymer films, with the π-stacking Bragg planes parallel to the substrate plane. In contrast, **P57** crystallites contain two kinds of textures, where the π-stacking planes are both normal and parallel to the substrate [71]. (Reproduced with permission. Copyright © 2011 American Chemical Society.)

Diketopyrrolopyrrole (DPP)-based polymers were among the first semiconducting polymers to show high charge-carrier mobilities ($\geq$1 cm^2 V^{-1} s^{-1}). As the first report of a DPP-based semiconducting polymer in 2008 [74], there have been many reports on DPP-based donor–acceptor polymer semiconductors with mobilities ranging from 0.1 to 2 cm^2 V^{-1} s^{-1}, most being around 1 cm^2 V^{-1} s^{-1} [75]. DPP-based donor–acceptor polymers exhibited extended HOMO and LUMO distributions along the polymer π backbone and optimized molecular orbital energy levels for both hole and electron injection. Therefore, most DPP-based polymers exhibited ambipolar characteristics with high hole and electron mobilities, and they will be discussed in later sections in more detail. Among these, there are some polymers that are predominantly p-channel

semiconductors. Ong and coworkers [76] recently reported an extremely high hole mobility of 10.5 $cm^2 V^{-1} s^{-1}$ for **P59** (Figure 1.13) along with long-term ambient stability. **P59** includes an unsubstituted planar thienothiophene moiety, which reduces conformational energy disorder, facilitates intermolecular packing, and promotes molecular orbital delocalization along the π backbone. High molecular weight ($M_n = 110$ kDa) was found to be the key to the high performance of this polymer, which is consistent with the earlier studies on P3HT semiconductors [13]. In another recent study, Kim *et al.* [77] developed a DPP-based polymer **P60** (Figure 1.13) with side chains having extended branching positions. Photophysical and structural studies indicated that, when the branching position of the side chain moved away from the π backbone, short π–π stacking distances (3.58–3.62 Å) were obtained, thereby enhancing intermolecular interactions. Additionally, in the polymer π backbone, incorporation of vinyl groups between the aryl units was believed to enhance the area available for intermolecular π-orbital overlaps, which leads to a long-range-ordered, edge-on lamellar crystalline microstructure. As a result, these polymer thin films showed unprecedented record-high hole mobilities of up to 5 $cm^2 V^{-1} s^{-1}$ with room-temperature processing and of up to 12 $cm^2 V^{-1} s^{-1}$ after thermal annealing. This mobility is currently the world record for a polymer semiconductor being in the mobility range of polycrystalline silicon and some other inorganic semiconductors [78]. In another study to modify aryl moieties adjacent to the DPP unit, Li and coworkers [79] synthesized a furan-containing DPP-based polymer **P61** (Figure 1.13) which showed blue shifts in UV–vis absorption characteristics and reduced HOMO energy levels compared to the thiophene analog. In furan-DPP systems, steric hindrance between lactam carbonyl and the heterocycle unit was claimed to be reduced because of the replacement of the sulfur atom with a smaller oxygen atom, which leads to enhanced backbone π coplanarity [80]. Although the polymer thin films of **P61** are found to be rather disordered in the polymer chain orientation, they showed high hole mobilities of 1.02–1.54 $cm^2 V^{-1} s^{-1}$ after thermal annealing at 200 °C. The observed good FET performance is considered to be a result of strong intermolecular interactions and the highly interconnected morphology.

In a recent study by Liu *et al.* [81], two new DPP-based copolymers **P62** and **P63** were synthesized with sextetthiophene (6T) and heptetthiophene (7T) units (Figure 1.13). The introduction of longer β-unsubstituted oliogothiophene units in DPP-based copolymers was found to have a significant effect on the molecular weight, solubility, and thin-film morphology of the DPP-oligothiophene copolymers. Although enhancing the backbone rigidity via long β-unsubstituted oliogothiophenes results in lower molecular weight polymers and poor solubility, it was found that this co-monomer strategy reduced the steric hindrance of the bulky solubilizing alkyl chains on DPP units, leading to the well-ordered lamellar structure of π–π stacking. As a result, **P62** and **P63** exhibited remarkably high hole mobilities of 3.94 and 2.82 $cm^2 V^{-1} s^{-1}$, respectively, through thermal annealing at 180–200 °C.

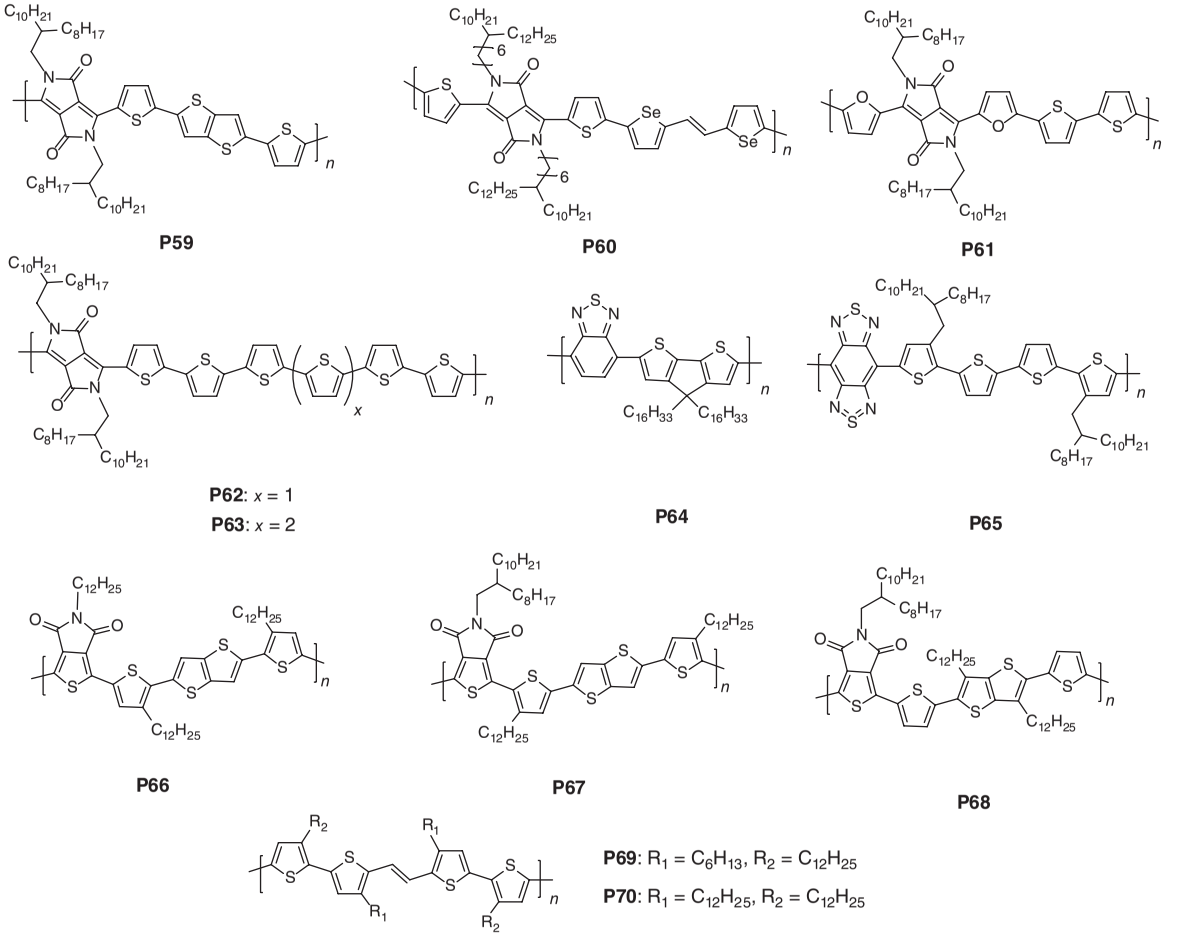

Figure 1.13 Chemical structure of p-channel semiconductors **P59**–**P70**.

Müllen and coworkers developed a copolymer **P64** (Figure 1.13) with cyclopentadithiophene and benzothiadiazole building blocks as donor acceptor units, respectively. Although earlier report on this polymer indicated a low hole mobility of 0.17 $cm^2\ V^{-1}\ s^{-1}$ [82], latest molecular weight optimizations ($M_n = 10-51$ kDa) by the same group resulted in much higher hole mobilities of up to 3.3 $cm^2\ V^{-1}\ s^{-1}$ [83]. It was shown that the molecular weight played a key role in improving hole mobilities due to the enhanced thin-film crystallinity, even though the film morphology did not change. Surprisingly, solid-state NMR analysis of **P64** did not show any overlaps between cyclopentadithiophene and benzothiadiazole building blocks, indicating that noncovalent donor–acceptor interactions are not the driving forces for the observed improvement in thin-film crystallinity with increasing M_n (Figure 1.14). Another new polymer, **P65**, with planar

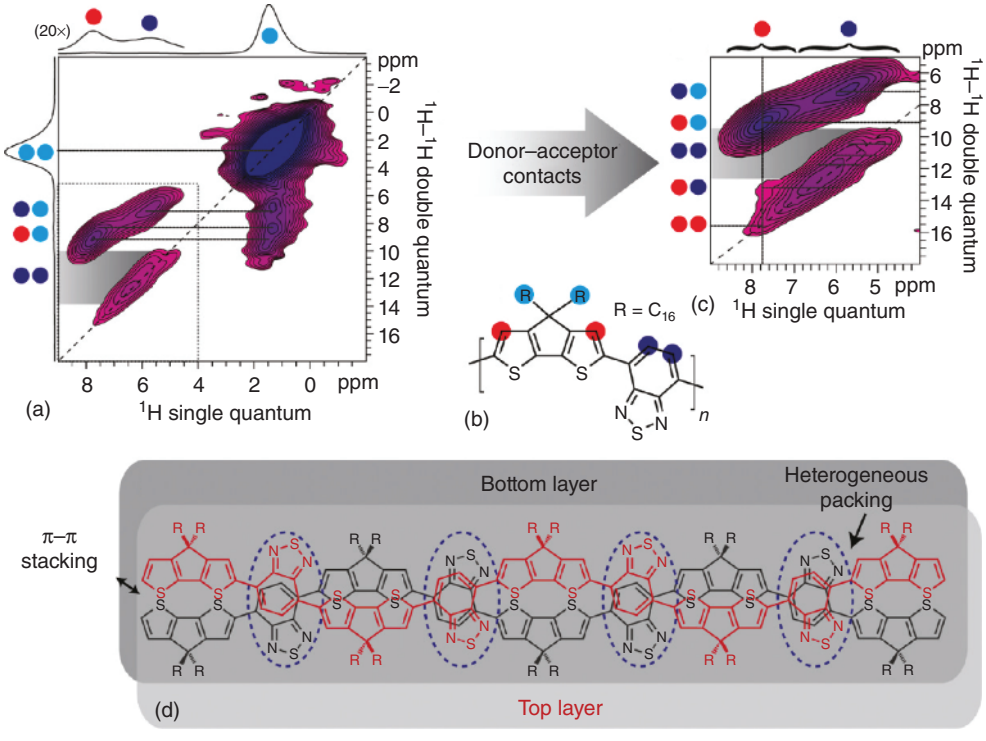

Figure 1.14 Local packing and organization of donor–acceptor groups in **P64** with $M_n = 35$ kDa. (a) 2D contour plot of the ^{1}H–^{1}H DQ–SQ correlation spectrum recorded at 20.0 T using a back-to-back recoupling/reconversion time of two rotor periods and a spinning frequency of 30.0 kHz. (b) Color scheme used for assignments. (c) Expansion of the backbone region (dashed box in panel a) showing the contacts between donor and acceptor groups. (d) Schematic drawing illustrating the local packing of donor–acceptor groups in two neighboring **P64** chains (here denoted as "layers"). The dashed circles (blue) mark the regions where the acceptor groups are heterogeneously packed on top of one another [83]. (Reproduced with permission. Copyright © 2011 American Chemical Society.)

triple-fused benzobisthiadiazole acceptor and β-alkylated quaterthiophene donor was reported by Wudl *et al.* (Figure 1.13) [84]. Through thermal annealing, the polymer chains adopt an "edge-on" orientation forming π-aligned polymer sheets which were stacked parallel to the substrate. Short π–π stacking distances of 3.5 Å were measured for these thin films. OFETs with **P65** exhibited a high carrier mobility of up to 2.5 $cm^2 V^{-1} s^{-1}$, which was attributed to high-order orientation in the crystalline state, extended π conjugation, and very tight packing in morphological pattern.

Copolymers **P66–P68** (Figure 1.13) containing thieno[3,4-*c*]pyrrole-4,6-dione (TPD) were strategically designed and synthesized by Li *et al.* [85] to study the effect of orientation of thw alkyl chain substituent on OFET device performance. While polymers **P66** and **P67** showed moderate hole mobilities (0.01–0.15 $cm^2 V^{-1} s^{-1}$), a maximum hole mobility of 1.29 $cm^2 V^{-1} s^{-1}$ was observed for **P68**-based devices. This mobility value is the highest reported to date for a TPD-containing polymer, indicating the favorable effects of the alkyl chain position on this particular polymer. This study showed that the orientation of the alkyl substituent on the π backbone dictated the polymer chain packing pattern, film morphology, and OFET device performance, which could lead to an enhancement in the charge-carrier mobilities of as high as two orders of magnitude.

Despite all the advances in donor–acceptor type polymer semiconductors in OFETs, p-channel polymers based on an electron-neutral thiophene backbone still show high mobilities. In a recent report by Kim *et al.* [86], two highly soluble polymers containing an alkyl-substituted thienylenevinylene unit **P69** and **P70** (Figure 1.13) were synthesized and characterized in top-gate/bottom-contact (TG–BC) OFET devices. These polymer thin films were found to be highly crystalline after a thermal annealing process ($T_{an.} = 200\,°C$), showing highly ordered lamellar microstructures and nanoribbon morphologies. Charge-carrier mobilities as high as 1.05 $cm^2 V^{-1} s^{-1}$ were achieved. The high solubility of **P70** enabled the fabrication of inkjet-printed complementary inverter circuits with Polyera's N2200 (see below), which exhibited a gain of ~16.

1.4.2 Small Molecules

Oligothiophenes are one of the most investigated organic semiconductor families for optoelectronic devices (Figure 1.15). The synthesis of these systems has been realized following different methodologies, and currently many α*n*Ts are commercially available. Polycrystalline films of the oligomers with four (α4T, **M1**) [87], five (α5T, **M2**) [87], six (α6T, **M3**) [88], and eight (α8T, **M4**) [89] thiophene rings have been widely examined as semiconductors for OFETs [90]. The crystal structures of α*n*Ts ($n = 2–8$) have been obtained, and they have been shown to exhibit similar features with very planar molecules packing in the characteristic herringbone (HB) motif [91].

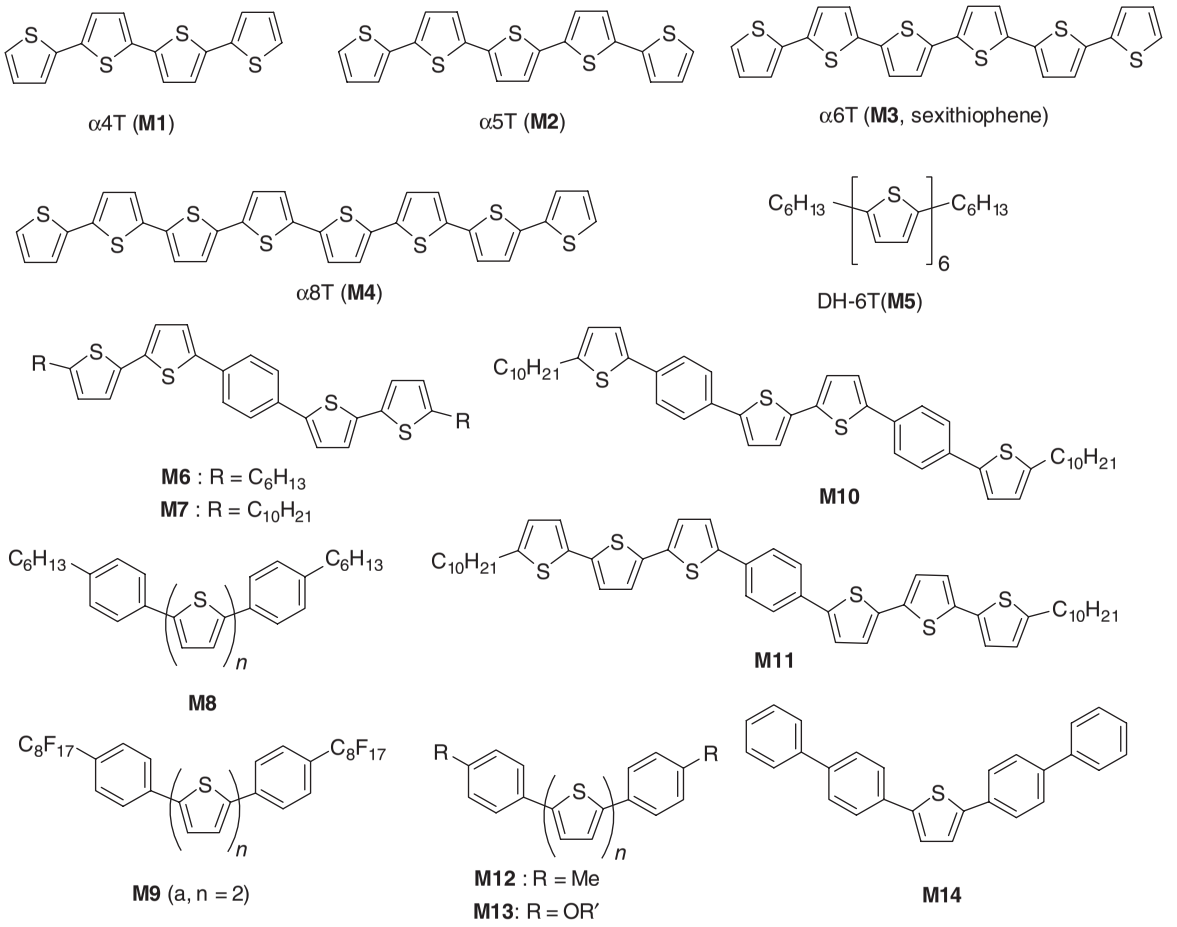

Figure 1.15 Chemical structure of p-channel small-molecule semiconductors **M1**–**M14**.

Polycrystalline films of α*n*Ts, when deposited at a relatively high temperature on SiO_2, have most of the molecules oriented with their long axis perpendicular to the substrate surface. In OFET devices, all these materials exhibit p-channel transport, and the hole mobilities are strongly dependent on the material purity, film morphology, deposition conditions, and the degree of film texturing [92]. Usually, larger cores afford greater mobilities when the devices are fabricated and measured under identical conditions [93]. The oligomers α4T and α5T exhibit mobilities of up to 0.006 and 0.08 $cm^2 V^{-1} s^{-1}$, respectively [94]. The low field-effect mobility for α4T was attributed to the poor charge injection from the contact and not to the inefficient charge transport through the material. In fact, the mobility doubles when an interfacial layer is used at the α4T source/drain contact to enhance charge injection. The highest reported mobility for α8T is 0.33 $cm^2 V^{-1} s^{-1}$ for film deposition at 120 °C [95]. This mobility value is an order of magnitude greater than previously reported for α8T and is attributed to the more favorable film morphology.

The α6T derivative is the most investigated oligomer in this series and exhibits a field-effect mobility of ~0.03 $cm^2 V^{-1} s^{-1}$ in bottom-contact Si/SiO_2 FETs [88], while single-crystalline grains of this oligomer exhibit mobilities of up to 0.075 $cm^2 V^{-1} s^{-1}$ [92c]. The film morphology and microstructure have been studied in detail. As the charge transport in OFETs occurs near the interface with the gate dielectric, Loi *et al.* have investigated the supramolecular organization of α6T ultrathin films on SiO_2 dielectric by confocal spectroscopy and microscopy. The authors demonstrated that α6T submonolayer films are composed of mixed regions where the molecules stand on and lie flat on the substrate surface. Importantly, they discovered that only after the first monolayer is completed do all the α6T molecules stand on the substrate. For films thicker than two monolayers, the photoluminescence spectra of standing molecules show a molecular H-like aggregation as in the single crystal [96].

Dinelli *et al.* have studied how the field-effect mobility of ultrathin films of α6T varies as a function of the dielectric surface coverage. FET test devices were fabricated on heavily doped n-Si wafers, with 200-nm-thick SiO_2 as dielectric which was passivated with hexamethyldisilazane. Interdigitated source and drain Ti/Au electrodes were fabricated using photolithography. Thin films of α6T were deposited by sublimation in an organic molecular beam apparatus (10^{-10} mbar base pressure). The deposition rate was monitored with a quartz oscillator. The charge-carrier mobility was found to rapidly increase with increasing surface coverage and saturated at a surface coverage of about two monolayers. For high-rate film deposition, the mobility reached a plateau with a mean value of 0.015 $cm^2 V^{-1} s^{-1}$, whereas for low-rate deposition the trend was similar but with a higher average mobility of 0.043 $cm^2 V^{-1} s^{-1}$. Therefore, the authors concluded that, for α6T films, only the two monolayers next to the dielectric interface dominated the charge transport. A quantitative analysis of spatial correlations showed that the second layer was crucial in enhancing the field-effect mobility, as it provided efficient percolation pathways for carriers generated in both the first and second layers. The upper layers do not actively contribute either because

their domains are smaller than the ones in the second layer or because the carrier density is negligible [97].

A number of synthetic strategies have been developed to functionalize the thiophene ring. In the case of oligothiophenes, core functionalization enhances the solubility and may alter the molecular packing within the crystal and, ultimately, the optoelectronic properties. Functionalization at the α,ω-positions of the oligomer typically does not affect the planarity of the π-conjugated core but enhances the solubility. Furthermore, in few cases, α,ω-functionalization with alkyl chains imparts liquid-crystalline-like properties, which dramatically modifies the solid-state ordering and enhances the field-effect mobility of the resulting films. Functionalization at the oligothiophene β,β′ positions significantly enhances compound solubility but usually disrupts the *n*T core planarity and molecular staking, leading to materials of low field-effect mobility. Among the alkyl-substituted oligothiophenes, α,ω-dimethyl [98] and α,ω-dihexyl oligomers with four [99], five [100], six (e.g., DH-6T, **M5**) [101], and eight [89] thiophene rings were among the first to be synthesized and characterized. Here again, the purity of these insoluble compounds was found to be a key factor in achieving high OFET performance [92a]. The field-effect mobilities of these oligomers are as high as 0.1 $cm^2\ V^{-1}\ s^{-1}$ [100]. The field-effect mobility of DH-6T (**M5**) is typically reported to be between 0.02 and 0.07 $cm^2\ V^{-1}\ s^{-1}$ depending on the deposition conditions and the dielectric material used for device fabrication [102]. The high mobility of DH-6T, obtained almost two decade ago, was explained by the high degree of DH-6T film self-organization thanks to the presence of the alkyl chains at the α,ω positions. More recently, the highest mobility for DH-6T was reported by Dimitrakopoulos *et al.* using molecular beam deposition of the oligomer. Values of up to 0.13 $cm^2\ V^{-1}\ s^{-1}$ were measured when parylene was used as the insulating layer [103].

Phenylene-thiophene oligomers (**M6–M14**, Figure 1.15), developed separately by Hotta and Samulski [104], attracted much attention because of their potential use as the active component in organic light-emitting diodes (OLEDs) and organic laser diodes, as well as p-type semiconductors for OTFTs [105]. Compared to simple oligo/poly phenylenes and thiophenes, molecular mixing of these two aromatic rings produces structural motifs characterized by different molecular shapes and physical properties, which in turn alter the material behavior profoundly [106]. Examples of these property changes include stronger light emission and low-threshold amplified spontaneous emission (ASE) from a liquid-crystalline polymer blend [107].

Ponomarenko *et al.* investigated the end-capped bithiophene-phenylene-bithiophene core with variable alkyl chain lengths from $-C_6H_{13}$ (**M6**) to $-C_{10}H_{21}$ (**M7**). These molecules exhibit field-effect hole mobilities of ∼0.3 $cm^2\ V^{-1}\ s^{-1}$ [108], which is more than an order of magnitude greater than those obtained by Hong *et al.* [109] for the compound **M6**. The reason for this large increase in performance was not clear, but the authors attributed it to material purity and the use of cross-linked poly(hydroxystyrene) as the gate dielectric. Other phenylene-thiophene derivatives **M10** and **M11** (Figure 1.15) were also synthesized.

It was found that **M11** had properties similar to those of **M7**, whereas **M10** had an order of magnitude lower mobility due to poor molecular ordering [110]. Electrochemical measurements of the oligomers containing a phenyl ring were shown to have better oxidative stability than the all-thiophene analogs, and FET devices operated in air without degradation. Recently, tolyl end-substituted oligothiophenes with three, four, and five thiophene rings have also been synthesized by Mohapatra *et al.* [105a]. These derivatives (**M12**) exhibit hole mobilities of ~0.03 $cm^2 V^{-1} s^{-1}$ and very high I_{on}:I_{off} ratios of ~10^9. Interestingly, despite the fact that odd- and even-numbered oligomers have different crystal structures and film microstructures, the FET characteristics are very similar. A phenylene-thiophene oligomer series (**M13**) end-substituted with various alkoxy chains were synthesized using Stille and Suzuki coupling reactions by Sung *et al.* [111]. Oligomers with two and three core thiophene rings functionalized with an octyloxy chain exhibit the largest mobilities of ~0.18 $cm^2 V^{-1} s^{-1}$ (I_{on}:$I_{off} > 10^7$) and ~0.09 $cm^2 V^{-1} s^{-1}$ (I_{on}:$I_{off} \sim 10^4$), respectively. Thin-film morphologies analyzed using AFM revealed higher nucleation densities for films of branched alkoxy side-chain molecules compared to their straight alkyl side-chain counterparts. However, field-effect mobilities were found to strongly decrease for the branched-substituted oligomers. Finally, Ichikawa *et al.* [105d] showed that the epitaxially grown thiophene-phenylene system BP2T (**M14**) on KCl single-crystal substrates exhibits a hole mobility (0.29 – 0.66 $cm^2 V^{-1} s^{-1}$) which is much larger than that of BP2T vacuum-deposited directly on SiO_2 at room temperature and close to that of high-quality oligothiophene single crystals. A number of studies have suggested that forcing oligomers to adopt a face-to-face arrangement should enhance the π–π orbital overlap, thus facilitating charge transport by maximizing the electronic coupling between adjacent molecules. This concept has been applied to a large variety of molecules including thiophene-based semiconductors. Laquindanum *et al.* explored fused thiophenes by synthesizing bis(benzodithiophene) (BDT, **M15**, Figure 1.16). FETs based on BDT exhibit field-effect mobilities of up to 0.04 $cm^2 V^{-1} s^{-1}$ for films vapor-deposited at 100 °C [112].

Heteroacenes are another promising class of fused π-conjugated p-channel semiconductors developed for OFETs over the past decade. These structures can be considered as ladder-type acenes in which one or more benzene rings in acene backbones are replaced with heterocyclic aromatic units. To this end, there have been two different design strategies followed to date: either the benzene rings are placed in the center of the semiconductor core and heterocycles are used as end-capping rings, or benzene rings are used as end-capping units while the heterocycles are in the center. Compared to their acene anologs, both of these heteroacene families have a lower degree of aromaticity, and thus they have more stabilized HOMO energy levels (<–5.2 vs –5.0 eV for pentacene) [113], which leads to good ambient stability in OFET devices. With the former strategy, the observed hole mobilities are typically in the range of those of amorphous silicon (α-Si) (0.1 – 1.0 $cm^2 V^{-1} s^{-1}$) [114].

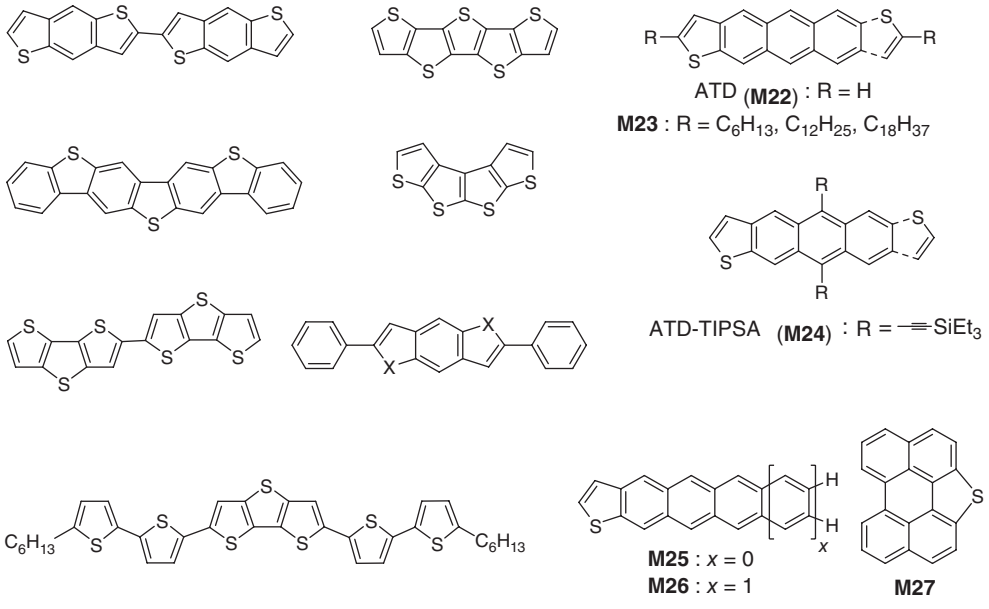

Figure 1.16 Chemical structure of p-channel small-molecule semiconductors **M15–M27**.

The fused system dibenzothienobenzothiophene (**M16**, Figure 1.16) was investigated by Sirringhaus *et al.* and coworkers [115]. As the synthesis of this compound is not regioselective, the presence of regioisomers was found to result in poor FET performance with mobilities ~0.03 $cm^2 V^{-1} s^{-1}$. However, the use of a shutter during vacuum sublimation allowed selective deposition of different fractions. The greatest field-effect mobilities were ~0.15 $cm^2 V^{-1} s^{-1}$ and $I_{on}:I_{off} > 10^6$. The same group reported the fused thiophene derivative bis(dithieno[3,2-*b*:2′,3′-*d*]thiophene) (**M17**, Figure 1.16). Crystal structures revealed that this semiconductor packs in a face-to-face stacked structure. Hole mobilities of up to ~0.05 $cm^2 V^{-1} s^{-1}$ and an $I_{on}:I_{off}$ of $>10^8$ were measured using this oligomer for both top- and bottom-contact FET structures [116]. Iosip *et al.* [117] have synthesized dithienothiophene in co-oligomers with thiophene (**M18**, Figure 1.16) and reported unoptimized FET hole mobilities of 0.02 $cm^2 V^{-1} s^{-1}$ and $I_{on}:I_{off}$ of ~10^6.

The dithienothiophene motif was extended up to seven fused rings by Zhang *et al.* [118], and it was found that these oligomers also pack in a face-to-face stacking motif. OFET devices were fabricated with the pentathienoacene (**M19**, Figure 1.16) and exhibited a mobility of 0.045 $cm^2 V^{-1} s^{-1}$ and $I_{on}:I_{off}$ up to ~10^3. These devices are very stable in air thanks to their large bandgap of 3.29 eV [119]. Finally, Nenajdenko *et al.* [120] have synthesized an annulated oligothiophene consisting of four fused thiophene rings (**M20**, Figure 1.16). X-ray crystallographic studies on single crystals of this compound confirmed that the molecule

is planar, making it attractive for semiconductor applications. Very recently, extension to other benzo[1,2-*b*:4,5-*b*′]dichalcogenophenes (**M21**, X = S, Se, Te, Figure 1.16) [121] and the utilization of larger π cores resulted in derivatives exhibiting FET mobilities of 0.17 – 2.0 $cm^2 V^{-1} s^{-1}$ [60a].

An interesting chemical approach has been to combine the molecular shape of pentacene, which leads to a favorable crystal packing geometry and orientation, with thiophene end groups, which should increase stability and also provide points of attachment for solubilizing substituents. Thus, anthradithiophene derivatives (**M22** and **M23**, Figure 1.16) were prepared and characterized for the first time by Katz *et al.* [122]. These products were obtained as a mixture of syn and anti isomers, whose separation was not possible. The field-effect mobility of Anthradithiophene (ATD) is an order of magnitude lower than that of pentacene, about 0.1 $cm^2 V^{-1} s^{-1}$, but the I_{on}:I_{off} is higher when I_{off} is recorded at zero gate bias. A highly ordered thin-film morphology is observed, which is consistent with the electrical characteristics. Hexyl-, dodecyl-, and octadecyl-disubstituted derivatives (**M23**) were also found to demonstrate modulation typical of FET devices, with the first two exhibiting higher mobilities (~0.15 $cm^2 V^{-1} s^{-1}$) than the parent compound, and with increased solubility. The third material still has significant activity (mobility ~0.06 $cm^2 V^{-1} s^{-1}$), even though it consists mostly of nonconjugated carbon atoms. Anthony *et al.* [46a] fabricated FETs based on solution-deposited films of functionalized anthradithiophene **M24** (Figure 1.16). This compound forms uniform films of excellent quality, yielding hole mobility of 1.0 $cm^2 V^{-1} s^{-1}$ with an excellent I_{on}:I_{off} of ~10^7. The high OFET performance of this material was attributed to the close π-stacked interactions in the crystal. Loo *et al.* showed that the performance of bottom-contact **M24**-based OFETs can be improved dramatically by a simple and straightforward solvent-vapor annealing process after device fabrication. Exposing the transistors to dichloroethane vapor for 2 min induces structural rearrangement and crystallization of the semiconducting film. This procedure resulted in drastic increases in I_{on} currents, and mobility increased by two orders of magnitude [123].

Very recently, thiophene-fused acenes anthra[2,3-*b*]thiophene (**M25**) and tetraceno[2,3-*b*]thiophene (**M26**) were synthesized by Valiyev *et al.* [124] (Figure 1.16). The crystal structures of **M25** and **M26** were described. The addion of the thiophene ring to the acene unit resulted in a weak dipole, and the crystal packing changes from the triclinic structure of acenes to orthorhombic. TFT devices were fabricated from these materials. Compound **M25** exhibited a field-effect mobility of ~0.1 $cm^2 V^{-1} s^{-1}$ and I_{on}:I_{off} of ~10^8 (T_D = 25 °C), whereas the compound **M26**a showed a mobility of ~0.25 $cm^2 V^{-1} s^{-1}$ and I_{on}:I_{off} of ~10^6 (T_D = 80 °C). Finally, Zhu *et al.* investigated the OFET behavior of perylo[1,12-*b*,*c*,*d*]thiophene (**M27**, Figure 1.16). Vacuum-deposited films showed moderate hole mobilities of ~0.05 $cm^2 V^{-1} s^{-1}$, I_{on}:I_{off} of ~10^5, and a low threshold voltage of −6.3 V. Interestingly, single-crystal micrometer wires were grown from solution, and OFET based on the single wire exhibited mobilities of up to ~0.8 $cm^2 V^{-1} s^{-1}$. The authors believe that the solid-state packing arrangement with the likelihood of a double-channel arrangement induced by marked S···S

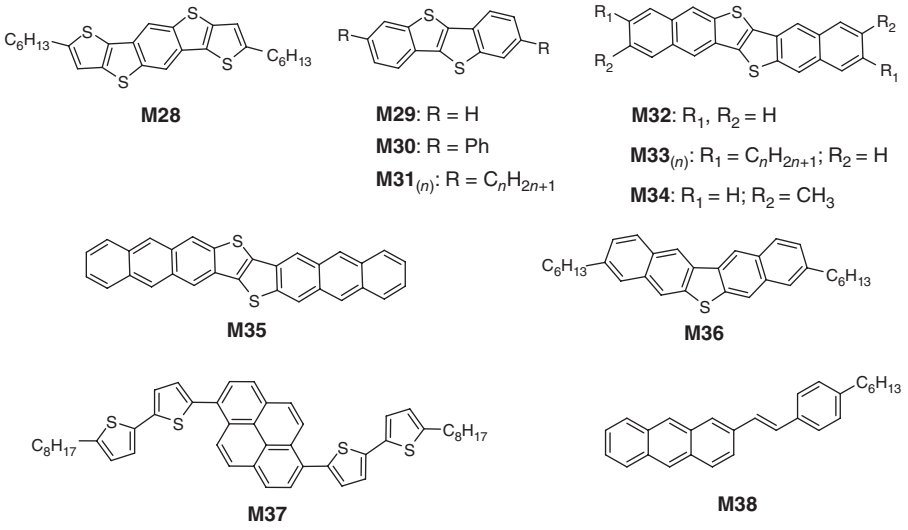

Figure 1.17 Chemical structure of p-channel small-molecule semiconductors **M28–M38**.

interactions may be the reason for the high performance. Among heteroacenes, one of the highest performances was achieved with **M28** (Figure 1.17), which was developed by Müllen *et al.* [125]. This semiconductor exhibited hole mobilities of up to 1.7 $cm^2 V^{-1} s^{-1}$ and I_{on}/I_{off} ratios of 10^7 in solution-processed OFET devices. This study was one of the early reports indicating that small heteroacene semiconductors with an extended aromatic core and solubilizing alkyl chains could be very promising for solution-processed optoelectronic devices.

A different design strategy was adopted by Takimiya and coworkers, in which the heterocycles were placed in the center of the semiconductor core and benzenes were used as end-capping rings. This approach was found to result in much higher hole mobilities compared to the earlier heteroacene-based semiconductors. In one class of such heteroacene semiconductors, a thienothiophene unit was incorporated in the center of an acene core while having benzene (BTBT, **M29–31**), naphthalene (Dinaphtho[2,3-b:2′,3′-f]thieno[3,2-b]thiophene (DNTT), **M32–34**), and anthracene (Dianthra[2,3-b:2′,3′-*f*]thieno[3,2-b]thiophene (DATT), **M35**) as end-capping moieties (Figure 1.17). The OFET devices fabricated with these semiconductors were found to be ambient-stable because of their low-lying HOMO energy levels. Among these, the BTBT (**M29**) core was developed earlier than the others via a simple thermal reaction of benzylidene dichloride with elemental sulfur or from commercially available *o*-chlorobenzaldehyde. Although the yield of **M29** synthesis is moderate (30–40%), its simplicity and fewer steps make it quite attractive for large-scale preparations. The earliest version of BTBT, **M30**, was prepared with phenyl substituents, and it showed excellent FET characteristics under ambient conditions with hole mobilities of 2.0 $cm^2 V^{-1} s^{-1}$ and I_{on}/I_{off} ratios of 10^7 [60a]. Thereafter, alkyl-substituted

BTBTs (**M31**$_{(n=5-14)}$) with various alkyl chain lengths ($n = 5-14$) were developed, which were found to be highly soluble in common organic solvents (up to ≈90 mg ml^{-1} in chloroform at room temperature). However, it is noteworthy that BTBT derivatives with alkyl chains longer than $C_{12}H_{25}$ showed reduced solubilities compared to those with shorter alkyl chains. Solution-processed OFETs fabricated with **M31**$_{(n=5-14)}$ showed typical p-channel behavior, with field-effect mobilities as high as 2.75 cm^2 V^{-1} s^{-1} and I_{on}/I_{off} ratios of 10^7 [60b]. Inspired by this initial report, several BTBT-based OFET devices were fabricated with various device configurations and solution-processing techniques, which recently yielded mobilities as high as 5 cm^2 V^{-1} s^{-1} [126]. In one of these studies, Hasegawa and coworkers [127] showed that single-crystalline thin films of **M31**$_{(n=8)}$ could be grown at the liquid–air interfaces by mixing fine droplets of an antisolvent (*N*,*N*-dimethylformamide) and semiconductor in 1,2-dichlorobenzene solution (Figure 1.18). This approach yielded inkjet-printed, patterned semiconductors with average hole mobilities of 16.4 cm^2 V^{-1} s^{-1} and a maximum value as high as 31.3cm^2 V^{-1} s^{-1}. Nonetheless, further improvements of this technique are needed to address the issues of the broad distribution of crystal orientations and mobilities and moderate single-crystal formation yields (50%).

DNTT semiconductors (**M32–34**) have lower solubilities in common organic solvents compared to their BTBT counterparts owing to their further π-extended core structures. Therefore, they were typically characterized in vapor-deposited OFET devices. Although the DNTT core itself (**M32**) shows hole mobilities of 2.9 cm^2 V^{-1} s^{-1} in vapor-deposited films [128], 2–4 times higher mobilities were achieved after attaching alkyl chains. Alkylated DNTT semiconductors (**M33**$_{(n=6-12)}$) showed very high hole mobilities close to 8 cm^2 V^{-1} s^{-1}, which is among the highest for OFETs based on polycrystalline thin films [129]. The authors claimed that the long alkyl chains attached to the DNTT core enhanced molecular ordering and resulted in tighter packing in the thin-film phase. This is attributed to the van der Waals intermolecular interactions between the alkyl groups, which is the so-called molecular fastener effect [130]. Very recently, highly crystalline OFET devices showing band-like charge transport were fabricated with decyl ($C_{10}H_{21}$)-substituted DNTT (**M33**$_{(n=10)}$) semiconductor by using a new hot-solution processing technique [131]. This new solution processing method was developed by Takeya and coworkers, and yielded devices with excellent hole mobilities of up to 11 cm^2 V^{-1} s^{-1}. The authors also showed that their method was applicable to flexible plastic substrates by fabricating top-gate devices on a flexible polyethylene naphthalate (PEN substrate with hole mobilities as high as 9 cm^2 V^{-1} s^{-1}. Another interesting DNTT derivative developed by Takimiya *et al.* [132] is **M34** with two methyl groups attached at 3 and 10 positions. Although this semiconductor did not show as high a mobility as earlier derivatives ($\mu_h = 0.8$ cm^2 V^{-1} s^{-1}), it was unique in that, different from the other DNTT-based semiconductors, it showed three-dimensional (3D) HB arrangements both in single-crystal and thin-film phases.

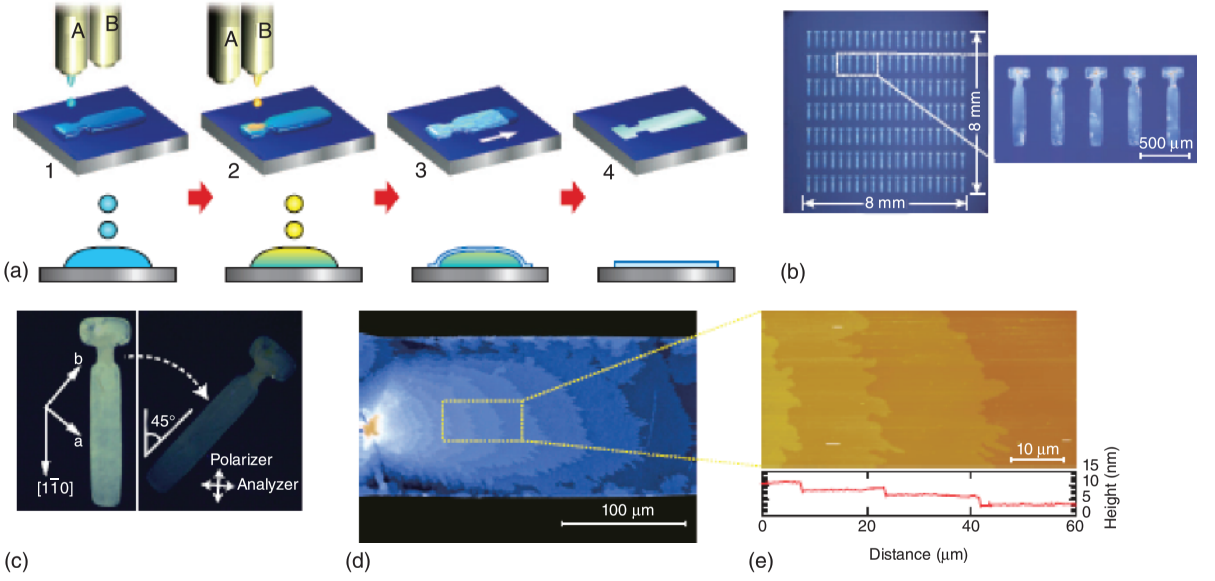

Figure 1.18 Inkjet printing of organic single-crystal thin films. (a) Schematic of the process. Antisolvent ink (A) is first inkjet-printed (step 1), and then solution ink (B) is overprinted sequentially to form intermixed droplets confined to a predefined area (step 2). Semiconducting thin films grow at liquid–air interfaces of the droplet (step 3), before the solvent fully evaporates (step 4). (b) Micrographs of a 20 × 37 array of inkjet-printed **M31**$_{(n=8)}$ single-crystal thin films. (c) Crossed-Nicols polarized micrographs of the film. (d) Expanded micrograph of the film, showing stripes caused by molecular-layer steps. (e) Atomic force microscopy image and the height profile (below) showing the step-and-terrace structure on the film surfaces [127]. (Reproduced with permission. Copyright © 2011, Nature Publishing Group.)

The longest π-extended ladder-type heteroacene compound developed by Takimiya *et al.* [133] is **M35** with eight fused aromatic rings. This semiconductor has a fairly stable device operation although it has a highly extended acene-like π system with an IP of 5.1 eV. A remarkable field-effect mobility of 3.0 $cm^2 V^{-1} s^{-1}$ was observed in vapor-deposited films, even though the thin-film microstructure was found to include both face-on and edge-on molecular orientations.

In another study, Okamoto and coworkers [134] developed a V-shaped extended heteroacene semiconductor, **M36** (Figure 1.17), which exhibited sufficient solubility in common solvents and high-mobility charge-transport characteristics (μ_h up to 9.5 $cm^2 V^{-1} s^{-1}$) in solution-crystallized OFET devices. The observed high mobility for **M36** was attributed to an almost optimized arrangement of semiconductor π backbones, which led to the maximum bandwidth and high transfer integrals (39–68 meV). It is noteworthy that these solution-crystallized films exhibit high thermal stability up to 150 °C, which is important for practical applications. It was claimed by the authors that the synthetic route followed during the synthesis of **M36** could enable mass production.

Compared to heteroacene and oligothiophene compounds, pyrene-based organic semiconductors have rarely been studied in OFETs. Only recently, a high-mobility pyrene-based liquid-crystalline semiconductor **M37** (Figure 1.17) was reported by Lee *et al.* [135]. In this semiconductor, pyrene core was disubstituted at 1 and 6 positions with 5′-octyl-2,2′-bithiophene-5-yl aromatic units. A high-performance transistor behavior with a field-effect mobility of 2.1 $cm^2 V^{-1} s^{-1}$ and I_{on}/I_{off} ratio of $\sim 10^7$ was achieved along with an improved long-term stability compared to the pentacene devices. The promising results obtained in this study indicate that pyrene-based semiconductors are good candidates for high-performance optoelectronic applications.

Finally, styrylacenes have emerged as a new promising class of p-channel semiconductors, in which the stability of an acene core is enhanced via extending the π conjugation through a styrene group. Recently, Perepichka and coworkers [136] developed a structurally simple styrylacene p-channel semiconductor **M38** (Figure 1.17), which exhibited a high field-effect hole mobility of 1.5 $cm^2 V^{-1} s^{-1}$ in thin films and 2.6 $cm^2 V^{-1} s^{-1}$ in single crystals. AFM characterizations showed that the high hole mobility of **M38**-based thin-films benefited from the perfect layer-by-layer growth at room temperature with an upright molecular orientation, which led to continuous semiconductor films at a low nominal thickness (Figure 1.19). Additionally, this semiconductor showed strong bright-blue solid-state emission with 70% photoluminescence quantum yield. This study indicates that strong π–π interactions, required for efficient charge transport in the solid-state, do not necessarily lead to quenching of the luminescence when the singlet-fission process is turned off.

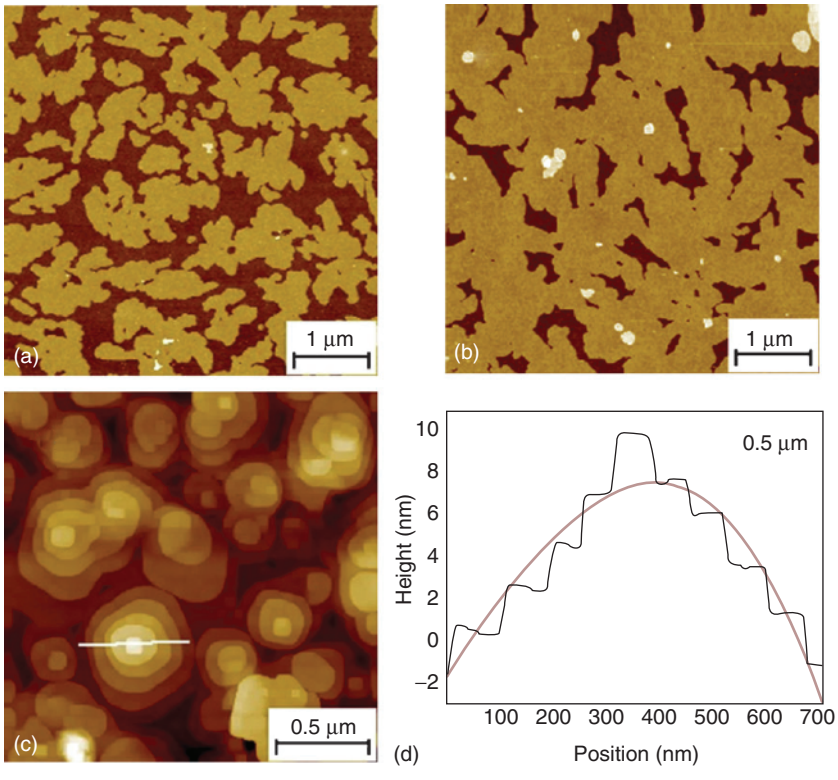

Figure 1.19 AFM images of (a) submonolayer, (b) monolayer, and (c) multilayer films of **M38** grown on Si/SiO_2. (d) Height profile of image (c) [136]. (Reproduced with permission. Copyright © 2012, John Wiley & Sons, Inc.)

1.5 n-Channel Semiconductors

1.5.1 Polymers

n-Channel polymers for TFTs, like n-channel molecular systems, have been traditionally underdeveloped compared to p-channel semiconductors. The reason of this deficiency in materials development was surprising considering that several experimental and theoretical studies suggested that organic semiconductors should transport electrons as efficiently as or even more efficiently than holes. More recently, our understanding on how to enable efficient electron transport in TFTs has improved after discovering the key role played by other factors, besides the semiconductor electronic structure, affecting electron transport. These include the following: (i) Gate dielectric surface chemistry. Most of the first-generation dielectric materials for TFTs were oxides, such as SiO_x, which efficiently trap electrons on the surface. (ii) Metal contacts [137]. This high

workfunction results in a large energy barrier for electron injection, and therefore, from an energetic perspective, low-workfunction metals such as Al or Ca should be preferable. However, air-induced oxidation of these conductor surfaces results in an insulating layer, which nullifies the benefit of having a formal lower energy barrier. (iii) Ambient atmosphere composition. At the beginning of the TFT field, very few research groups carrying out material development had the capabilities to perform measurements in an inert atmosphere or vacuum. It is known that O_2 and H_2O can efficiently inhibit electron transport, preventing several semiconductor classes to be screened for n-channel transport.

Today, several of these issues can be controlled, and, particularly, the use of dielectric surface passivation strategies and polymeric dielectric materials has resulted in impressive progress in performance. From an energetic perspective, it is now believed that a very narrow energetic window for the LUMO level, located at about −4.0 to −4.3 eV, must be achieved to enable polymeric semiconductors with good charge transport in ambient atmosphere. For higher LUMO energies (low electron affinity), the polymer performance rapidly degrades after exposure to ambient atmosphere even when using electron-trap-free dielectrics. On the other hand, for very low-lying LUMOs systems (this has been well-established for molecular semiconductors), the corresponding devices are very difficult to turn off. In this section, we will describe a few first-generation n-channel polymers, followed by more recent developments.

The first report of an n-channel TFT-active polymer was poly(benzobisimidazobenzophenanthroline) (BBL, **P71**) and the corresponding Semiladder poly (benzobisimidazobenzophenanthroline) (BBB) (**P72**) (Figure 1.20). This ladder-type polymer exhibits a high electron mobility of 0.1 $cm^2 V^{-1} s^{-1}$ as spin-coated polycrystalline film [53b] and ∼0.01 $cm^2 V^{-1} s^{-1}$ for nanobelts [138]. In a series of papers, the Northwestern University (NU) group reported polymers based on indenofluorene and bisindenofluorene cores having C≡O and $C{\equiv}C(CN)_2$ substituents (**P73** family, Figure 1.20) [57b]. A novel design approach was employed using computational modeling to identify favorable monomer properties, such as core planarity, solubilizing substituent tailorability, and appropriate electron affinity, with gratifying results. Monomeric model compounds were also synthesized to confirm these properties, and crystal structures of several cores revealed short (<3.5 Å) π−π stacking distances with favorable solubilizing substituent orientations. A family of 10 homopolymers and bithiophene **P73** copolymers was synthesized via Yamamoto and Stille polymerizations, which exhibited n-channel mobilities approaching 10^{-3} $cm^2 V^{-1} s^{-1}$ under inert conditions.

The Northwestern group have also designed new homopolymers and copolymers based on the dithenodiimide core (**P74** and **P75**, Figure 1.20) [139]. Two of these polymers are processable in common organic solvents: the homopolymer poly(*N*-(2-octyldodecyl)-2,2′-bithiophene-3,3′-dicarboximide) (P(DTI), **P74**) exhibits n-channel FET activity, and the copolymer poly(*N*-(2-octyldodecyl)-2,2′:5′,2″:5″,2‴-quaterthiophene-3,3′-dicarboximide) (P(DTI-T2), **P75**) exhibits air-stable p-channel FET operation. After annealing, **P74** films exhibit a very high degree of crystallinity and an electron mobility >0.01 $cm^2 V^{-1} s^{-1}$ with a current

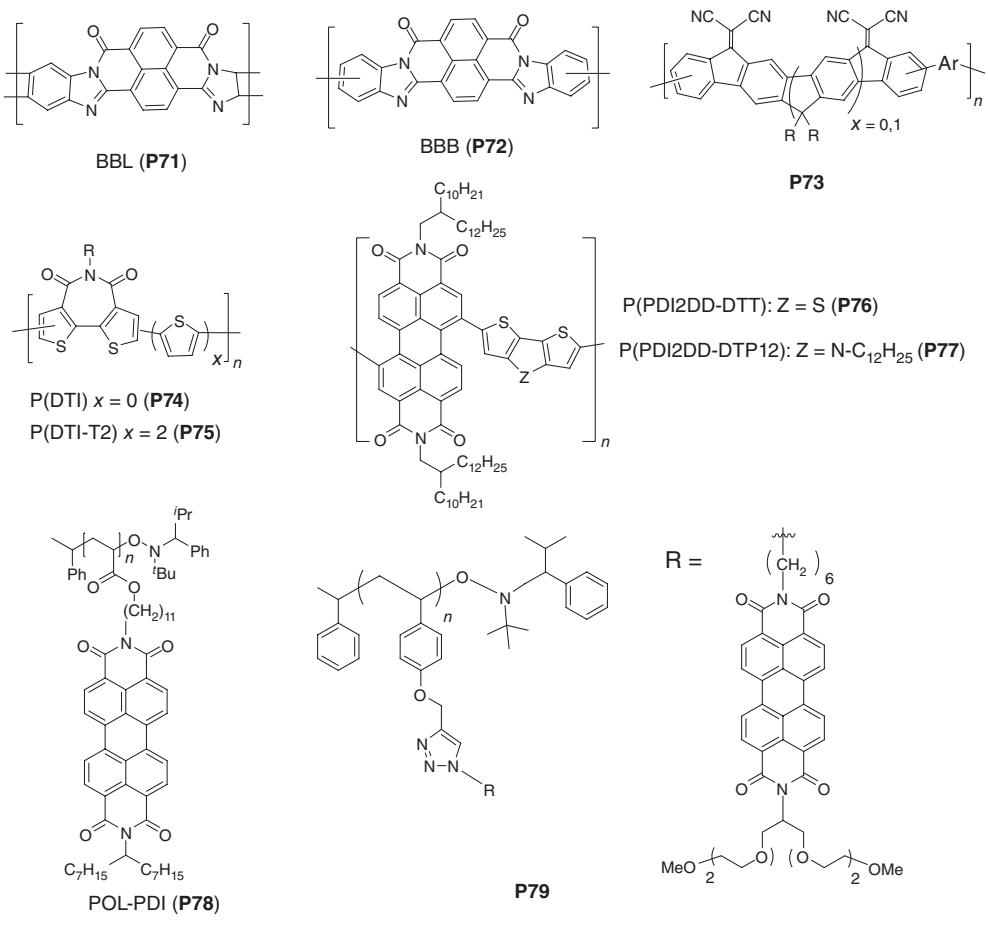

Figure 1.20 Chemical structure of n-channel polymer semiconductors **P71–P79**.

on–off ratio of 10^7, which is remarkably independent of the film deposition conditions. Extraordinarily, P(DTI) films also exhibit terracing in AFM images with a step height matching the X-ray diffraction *d* spacing, a rare phenomenon for polymeric organic semiconductors (Figure 1.21).

Relevant n-channel polymers are those based on rylene dicarboximide cores, particularly perylene and naphthalene (Figures 1.20 and 1.22). The first perylene-based polymer (P(PDI2DD-DTT), **P76**, Figure 1.20) was synthesized by Stille coupling of *N*,*N*′-dialkyl-1,7-dibromo-3,4,9,10-perylene diimide (PDI) with a distannyl derivative of dithienothiophene [140]. The M_w of P(PDI2DD-DTT) was not very high (~15 kDa using gel permeation chromatography (GPC)) and it was soluble in several solvents and could readily be processed from solution. Differential scanning calorimetry (DSC) showed a glass-transition temperature of 215 °C, while thermal gravimetric analysis (TGA) suggested excellent thermal stability with an onset decomposition temperature under nitrogen of 410 °C.

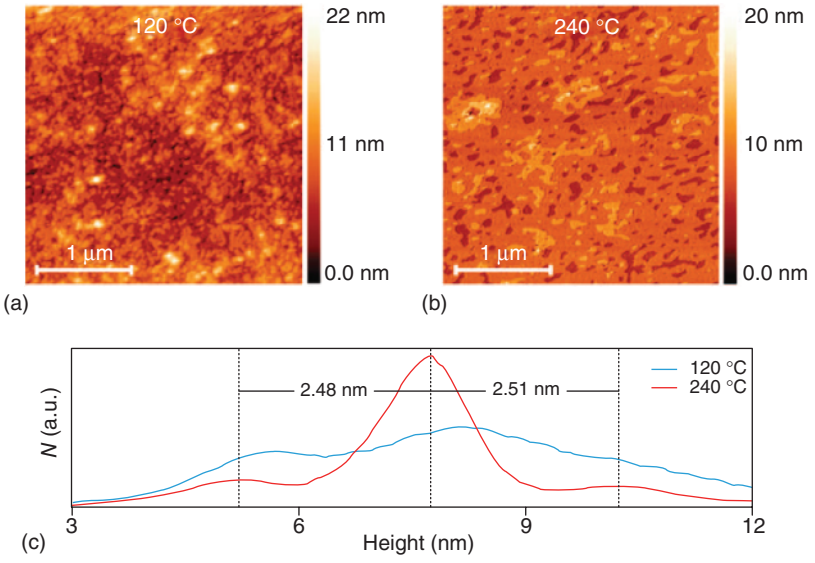

Figure 1.21 AFM images of **P74** films spin-cast from 1,2,3-TRICHLOROBENZENE (TCB) and annealed at 120 °C for 30 min (a) and 240 °C for 2 h (b), and a height histogram (c) for both images (120 °C in blue and 240 °C in red) revealing the formation of a terraced surface having a 2.50-nm step height [139]. (Reproduced with permission. Copyright © 2008 American Chemical Society.)

Polymer **P76**-based OFETs (Al source/drain electrodes, top-contact/bottom-gate geometry) were measured under nitrogen and exhibited electron mobilities as high as ~0.01 $cm^2 V^{-1} s^{-1}$ and $I_{on}:I_{off} > 10^4$. Very recently, a dithienopyrrole analog, **P77** (Figure 1.20), was reported to show an electron mobility of 7.4×10^{-4} $cm^2 V^{-1} s^{-1}$, which increased to 1.2×10^{-3} $cm^2 V^{-1} s^{-1}$ on annealing at 100 °C for 60 min under inert atmosphere [141]. The lower mobility observed for **P77** may be related to the dilution of the electron-transporting unit by the presence of the additional N-substituents of the dithienopyrrole donors. Thelakkat *et al.* [142] have reported OFETs based on polymers containing perylene unit as pendant groups, such as **P78** (Figure 1.20). For this polymer, after thermal annealing at 210 °C for 60 min, the threshold voltage dropped significantly to 7 V, while the current and charge-carrier mobility both increased by 100 times, approaching 1.2×10^{-3} $cm^2 V^{-1} s^{-1}$. Unfortunately, OFETs based on these polymers are unstable under ambient conditions. In a recent work by Thelakkat and coworkers [143], electron-deficient semiconducting side-chain polymers carrying perylenediimide pendant moieties were synthesized with a combination of "click" chemistry and nitroxide-mediated radical polymerization. Space-charge-limited current (SCLC) measurements indicated appreciable electron mobilities of up to 0.01 $cm^2 V^{-1} s^{-1}$ for **P79** (Figure 1.20), which carries oligoethyleneglycol substituents. This study demonstrated that, by varying the

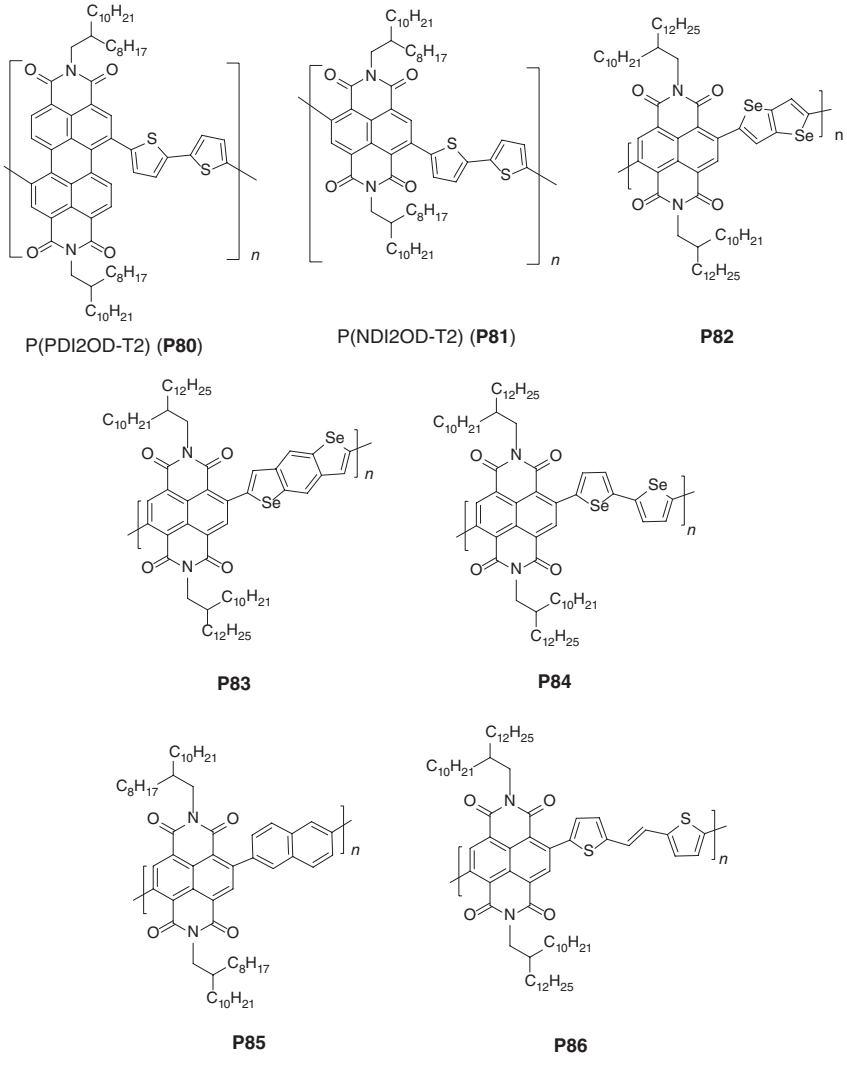

Figure 1.22 Chemical structure of n-channel polymer semiconductors **P80**–**P86**.

substituents of side-chain polymers, optical and charge-transport properties can be fine-tuned.

Recently, the Polyera Corporation team has reported the synthesis, characterization, and comparative properties of *N*,*N*′-dialkylperylenedicarboximide-dithiophene (PDIR-T2, **P80**, Figure 1.22) and *N*,*N*′-dialkylnaphthalenedicarboximide-dithiophene (NDIR-T2, **P81**, Figure 1.22) copolymers and the fabrication of the corresponding bottom-gate TFTs on Si/SiO_2 substrates [144]. Their results demonstrate that the choice of the NDIR versus PDIR co-monomer is strategic to achieving both high-performance bottom-gate n-channel TFTs and

device functioning under ambient conditions. The rylene building block and the polymer structural design rationale were as follows: (i) The electron-poor NDIR co-monomer was selected because of the large electron affinity of this core, comparable to that of the far more π-extended PDIR systems. (ii) Equally important, NDIR-Br_2 can be easily isolated as pure 2,6-diastereoisomers, enabling the synthesis of a regioregular polymeric backbone. Note that the isolation of PDIR-Br_2 regioisomers, although demonstrated, is tedious. Therefore, compared to PDIR-based polymers, it should lead to a more π-conjugated structure and, consequently, better charge-transport efficiencies. (iii) Proper alkyl (R) functionalization at the rylene nitrogen atoms, in that study 2-octyldodecyl (2OD), should result in highly soluble and processable, yet charge-transport-efficient, polymers. (iv) Finally, the dithiophene (T2) unit is utilized because of the commercial availability, stability, and known electronic structure and geometric characteristics of this core, likely providing highly conjugated, planar, and rod-like polymers. The new NDIR- and PDIR-based polymers were synthesized in high yields via a Pd-catalyzed Stille polymerization. Using the reported synthetic procedure, the polymer M_ws are larger for P(NDI2OD-T2) (**P81**) (~250 K, PD ~ 5) than for P(PDI2OD-T2) (**P80**) (~32 K PD ~ 3). The optical and electrochemical properties of these new systems reveal important aspects of the polymer electronic structures and NDIR versus PDIR co-monomer effects. Bottom-gate top-contact OTFTs were fabricated on n^{++}-Si/SiO_2/OTS substrates on which the semiconducting polymer solutions (~3–10 mg ml^{-1} in 1,2-Dichlorobenzene (DCB)-$CHCl_3$) were spin-coated to afford ~100-nm-thick films. The films were annealed at 110 °C for 4 h before the TFT structure was completed by Au source/drain vapor deposition. Electrical measurements were performed both under high vacuum and in ambient atmosphere. Electron mobilities of ~0.08–0.06 $cm^2\,V^{-1}\,s^{-1}$ for P(NDI2OD-T2) and ~0.003–0.001 $cm^2\,V^{-1}\,s^{-1}$ for P(PDI2OD-T2) were measured in vacuum. However, when the same TFT array was measured in ambient atmosphere, the P(NDI2OD-T2)-based devices continued to function also after 16 weeks from fabrication ($\mu_e \sim 0.01$ $cm^2\,V^{-1}\,s^{-1}$), while P(PDI2OD-T2) mobility dropped to ~2×10^{-4} $cm^2\,V^{-1}\,s^{-1}$ within 1 week, in agreement with previous studies on PDI-based polymers (Figure 1.23). In a very recent study, we addressed the effect of the regioregularity of these systems by synthesizing the regioregular (only 1,7-linked) P(PDI2OD-T2) as well as the regioirregular (2,6- + 2,7-linked) P(NDI2OD-T2) polymers. The TFT results showed that the regioirregular P(NDI2OD-T2)-based devices exhibited 10 times lower electron mobilities, corroborating the key role of the polymer architecture regiochemistry [145].

The same team also developed high-performance polymeric TG–BC TFTs and the first all-polymeric complementary metal–oxide–semiconductor (CMOS) circuit functioning in ambient based on P(NDI2OD-T2) (**P81**) [146]. These TG–BC TFTs were fabricated on glass or PET and had the structure substrate/Au(source–drain contacts)/P(NDI2OD-T2)/polymeric dielectric/Au(gate contact). This structure was selected because of the superior injection characteristics of typical staggered (top-gate) architectures and considering the facile channel miniaturization for bottom-contact TFTs which

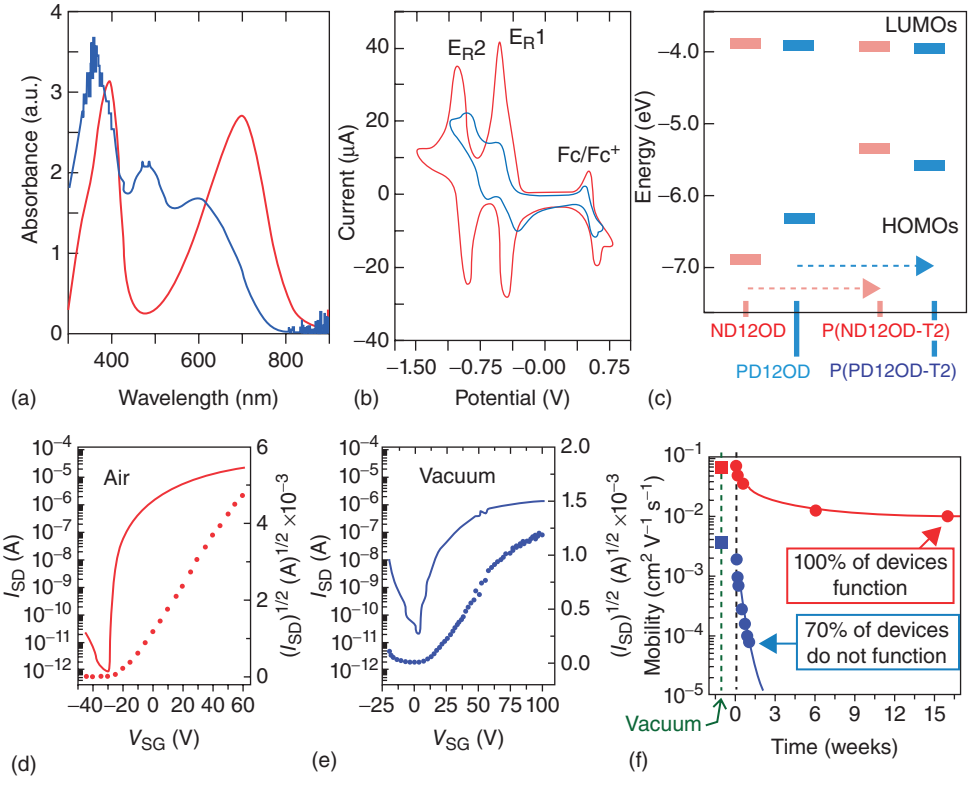

Figure 1.23 (a) Optical absorption spectra of spin-coated P(NDI2OD-T2) (red line) and P(PDI2OD-T2) (blue line) films (~30 nm thick) on glass. (b) Thin-film cyclic voltammetries (Fc (+0.54 V vs SCE (saturated calomel electrode)) internal standard) of P(NDI2OD-T2) (red line) and P(PDI2OD-T2) (blue line) thin films on a Pt electrode. The ER1 values of NDI2OD and PDI2OD (not shown) are −0.49 and 0.46 V versus SCE, respectively. (c) Energy diagram for the specified rylene monomers and polymers. (d) *I*–*V* transfer plots for P(NDI2OD-T2) TFT in air for 1 h and (e) P(PDI2OD-T2) TFT in vacuum. (f) Polymer TFT electron mobility plots in vacuum and ambient (RH) 20–40%, ($T \approx 25\,^{\circ}C$) versus time [144]. (Reproduced with permission. Copyright © 2009 American Chemical Society.)

could lead to high-frequency circuits. These devices were fabricated with the P(NDI2OD-T2) film deposited by spin-coating as well as gravure, flexographic, and inkjet printing and with the dielectric layer deposited by spin-coating. Furthermore, TFTs in which both the semiconductor and dielectric layers were gravure-printed were demonstrated. All device fabrication processes were performed under ambient conditions with the exception of the Au contact vapor-deposition and the film-drying steps (110 °C). The TG–BC TFTs based on this polymer exhibited excellent n-channel OTFT characteristics in ambient, with electron mobilities of up to ~0.45–0.85 $cm^2\,V^{-1}\,s^{-1}$, I_{on}:$I_{off} > 10^5$, and $V_{on} \sim 0$–5 V. Importantly, the carrier mobility of P(NDI2OD-T2)-based TFTs

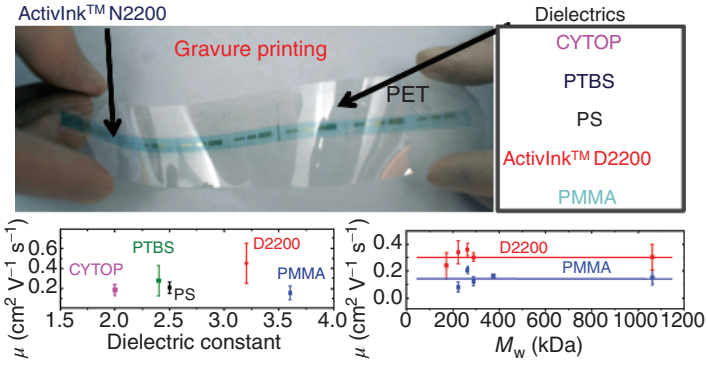

Figure 1.24 Top: Optical image of the first gravure-printed n-channel polymeric TFTs on a PET web fabricated at Polyera. Bottom: Mobility versus dielectric constant (k) of the polymeric gate dielectric (left) and molecular weight (M_w) (right) [146]. (Reproduced with permission. Copyright © 2009, Nature Publishing Group.)

was insensitive to the dielectric constant (k) of the gate dielectric material (Figure 1.24). This is of great importance to broaden the compatibility of this n-channel semiconductor family with several p-channel materials *using the same gate dielectric*. Furthermore, this polymer's TFT properties are independent of the polymer molecular weight (M_w) over a large range of values ($M_w \sim 200$ kDa to >1 MDa, Figure 1.20). The insensitivity of the device performance on the polymer chain-length extension is of extreme importance for large-scale synthesis and batch-to-batch reproducibility of the TFT characteristics. P(NDI2OD-T2)-based TFTs are also exceptionally stable in ambient up to ~70% relative humidity. Because of the stability of this n-channel polymer family, excellent TFT performance with high-work-function metal contacts, and compatibility with Polyera UV-curable dielectrics with both p- and n-channel semiconductors, they also enabled the first polymeric complementary logic. We have also fabricated printed inverters with P(NDI2OD-T2) (**P81**, n-channel), P3HT (p-channel), and ActivInk™ D2200 (gate dielectric). These inverters show remarkably small hysteresis, reflecting the transistor's threshold voltage stability. The voltage gains for the gravure-printed devices are very large ($dV_{OUT}/dV_{IN}(\text{max}) > 25-60$). More recently, Noh *et al.* fabricated monolithically integrated polymeric complementary circuits using P(NDI2OD-T2) and two p-type polymers P3HT and a new dithiophene-based polymer (Polyera ActivInk P2100). Inkjet-printed TG–BC FETs exhibited very high hole and electron mobilities (μ_{FET}) of $0.2-0.5\ \text{cm}^2\ \text{V}^{-1}\ \text{s}^{-1}$. The active regions of the FET were patterned and via holes were defined by direct inkjet printing of the conjugated polymer solutions and the polymer gate dielectric solvent, respectively, enabling high-performance CMOS inverters (gain >30) and ring oscillators (f_{osc} up to ~50 kHz) [147].

In a recent paper, Salleo *et al.* investigated the molecular packing and structure of P(NDI2OD-T2) (**P81**). The importance of molecular packing and microstructure on performance of p-type thiophene-based semiconductors is widely appreciated and has been extensively studied [28, 148]. It is generally believed that the best transport properties are attained when there is a high degree of in-plane π stacking of the thiophene rings, because this allows two-dimensional (2D) transport along the chain backbone and along the π-stacking direction in the plane of the substrate [148e, 149]. To date, similar structure–property studies are not as well established in n-type polymers because of the lack of high-performing materials. X-ray scattering experiments on P(NDI2OD-T2) films revealed that this polymer exhibits an exceptional degree of in-plane ordering and adopts a largely face-on packing (π-stacking direction normal to the substrate), which is an uncommon crystallographic texture for semiconducting polymers with high field-effect mobility (Figure 1.25). Furthermore, we employed X-ray scattering from aligned films as well as AFM characterization of the top and bottom interface, and, to support these findings, discussed the implications of this unexpected crystalline texture for charge transport [150].

Finally, recent bulk electron transport studies using both time-of-flight and electron-only current measurements suggest a bulk mobility of $\sim 5 \times 10^{-3}\ \mathrm{cm^2\ V^{-1}\ s^{-1}}$ for **P81**, which is the highest value reported for time-of-flight (TOF) electron transport in conjugated polymers (Figure 1.26) [151].

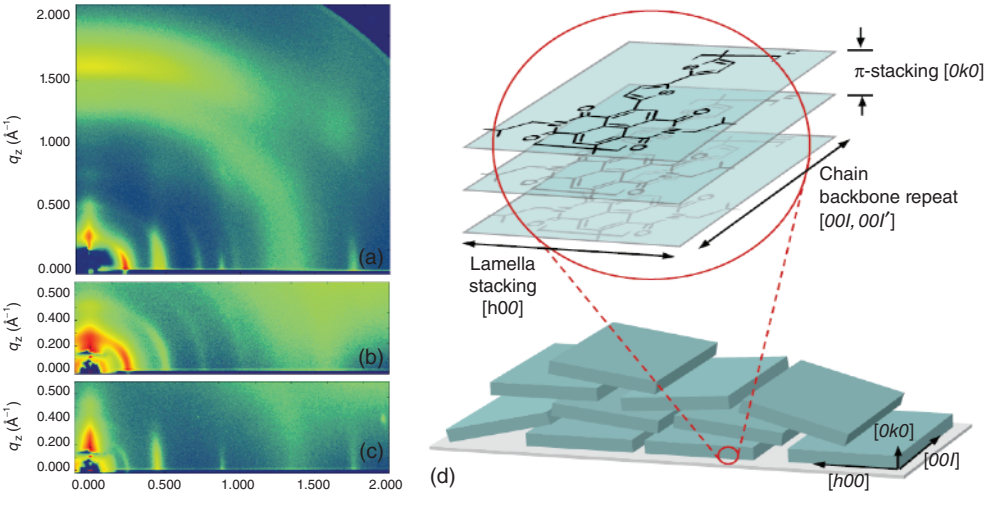

Figure 1.25 X-ray characterization of P(NDI2OD-T2) structure. (a–c) 2D grazing incidence diffraction pattern from spun-cast, isotropic film (a), dip-coated, aligned film with scattering vector *q* nominally perpendicular to the fiber direction (b), and *q* nominally parallel to the fiber direction (c). (d) Schematic of face-on molecular packing of P(NDI2OD-T2) inferred from X-ray data (top) indicating the repeat directions referenced. Proposed microstructural arrangement of the crystallites (bottom) indicating slight disorder in the π-stacking and lamella stacking directions of the flat, platelet-like crystallites [150]. (Reproduced with permission. Copyright © 2010, John Wiley & Sons, Inc.)

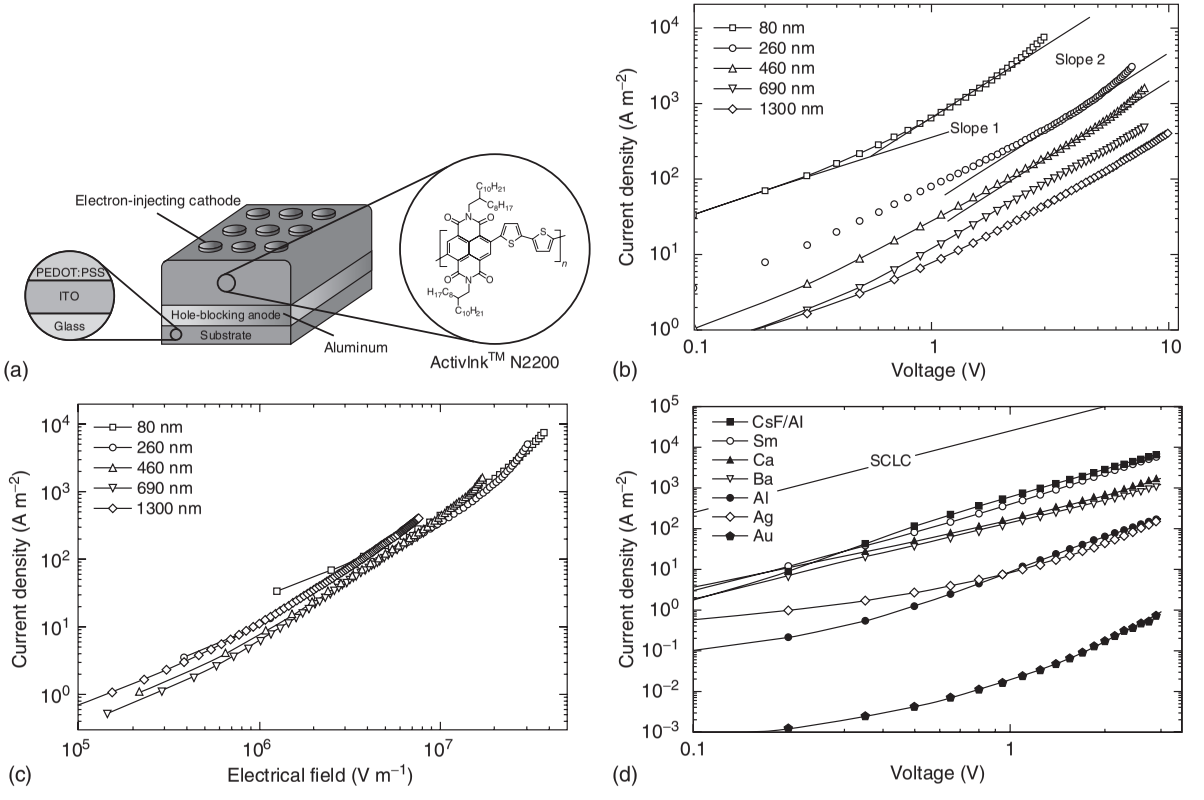

Figure 1.26 (a) Schematic illustration of an electron-only device used to investigate the charge transport of the conjugated n-type polymer **P81** used in this work. PEDOT:PSS is used as a smoothing layer for the hole-blocking bottom aluminum anode to avoid negative differential resistance effects. (b) *J–V* characteristics of **P81** electron-only devices with a barium cathode for several N2200 layer thicknesses. (c) *J–E* characteristics of **P81** electron-only devices with barium cathode for several layer thicknesses. (d) *J–V* characteristics of **P81** electron-only devices ($d = 85$ nm) with different electron-injecting top electrodes. The straight line shows the expected current according to the Mott–Gurney law using the average TOF mobility ($\mu_{TOF} = 5 \times 10^{-3}$ cm^2 V^{-1} s^{-1}) [151]. (Reproduced with permission. Copyright © 2010, John Wiley & Sons, Inc.)

Importantly, the electron-only device currents were found to be injection-limited for a wide range of electrode work functions and semiconductor layer thicknesses, despite the rather high electron affinity of this polymer. Contact-limited currents were observed even when low-work-function metals such as Sm, Ca, Ba, or Cs were employed, which are known to enable ohmic contacts with other n-type polymers [152]. However, the previously investigated polymers typically exhibit rather low bulk-transport-limited currents owing to, for example, severe electron trapping in an exponential density-of-states distribution. Thus, we believe that evaporation of reactive metals onto layers of conjugated polymers may generally cause injection barriers (through the formation of oxides and chemical defects), but that these barriers are masked by the low bulk currents in the majority of n-type polymers that have been investigated to date.

Recently, Jenekhe and coworkers reported the synthesis and physicochemical properties of new NDI (naphthalene diimide)-based polymers **P82–P84** (Figure 1.22) with selenophene-based donor units instead of the bithiophene unit used earlier [153]. Bottom-gate/top-contact OFETs gave average electron mobilities as high as 0.24 $cm^2 V^{-1} s^{-1}$ with I_{on}/I_{off} ratios of $10^4–10^6$. The authors also mentioned that in the phenyl end-capped high molecular weight **P84**, large enhancement of the field-effect mobilities were observed compared to the uncapped polymers. In a parallel study by Yang *et al.* [154], an acene-based centrosymmetric copolymer of NDI, **P85** (Figure 1.22), was synthesized and characterized in bottom-gate/top-contact OFET devices. Electron mobilities as high as 0.056 $cm^2 V^{-1} s^{-1}$ were obtained for **P85**-based devices, which indicates that, in addition to the donor strength, the geometric feature of the donor moiety also strongly affects the charge-transport characteristics. Noh and coworkers [155] recently reported another high-performance NDI-based n-channel polymer, **P86** (Figure 1.22), which is systematically designed and synthesized with alternating long alkyl (2-decyltetradecyl) substituted NDI (acceptor) and thienylene–vinylene–thienylene (donor) building blocks. Compared to the famous P(NDI2OD-T2), this new polymer has an extended π-conjugated backbone with a comparable LUMO energy level (−4.00 eV). TG–BC devices fabricated with polymer **P86** demonstrated an extremely high electron mobility of 1.8 $cm^2 V^{-1} s^{-1}$ ($I_{on}/I_{off} = 10^6$) with high air and bias-stress stability. In this device architecture, a typical polymer dielectric, poly(methyl methacrylate) (PMMA), was used. This OFET device is among the best performing polymer-based n-channel device reported to date. The high performance of **P86** was attributed to the π-extended conjugation of its polymer backbone, enhanced π–π intermolecular interactions, improved crystallinity in thin-film phase with a highly interdigitated lamellar structure, and mixed face-on/edge-on orientations.

In a recent report by Pei and coworkers [156], a novel highly electron-deficient poly(*p*-phenylenevinylene) (PPV) derivative, benzodifurandione-based PPV **P87** (Figure 1.27), was developed. This new polymer includes strong electron-withdrawing carbonyl groups on the double bonds, which extends the backbone π conjugation and forms intramolecular hydrogen bonds to afford a "locked" aromatic plane. Solubilizing alkyl groups (4-octadecyldocosyl) with distant

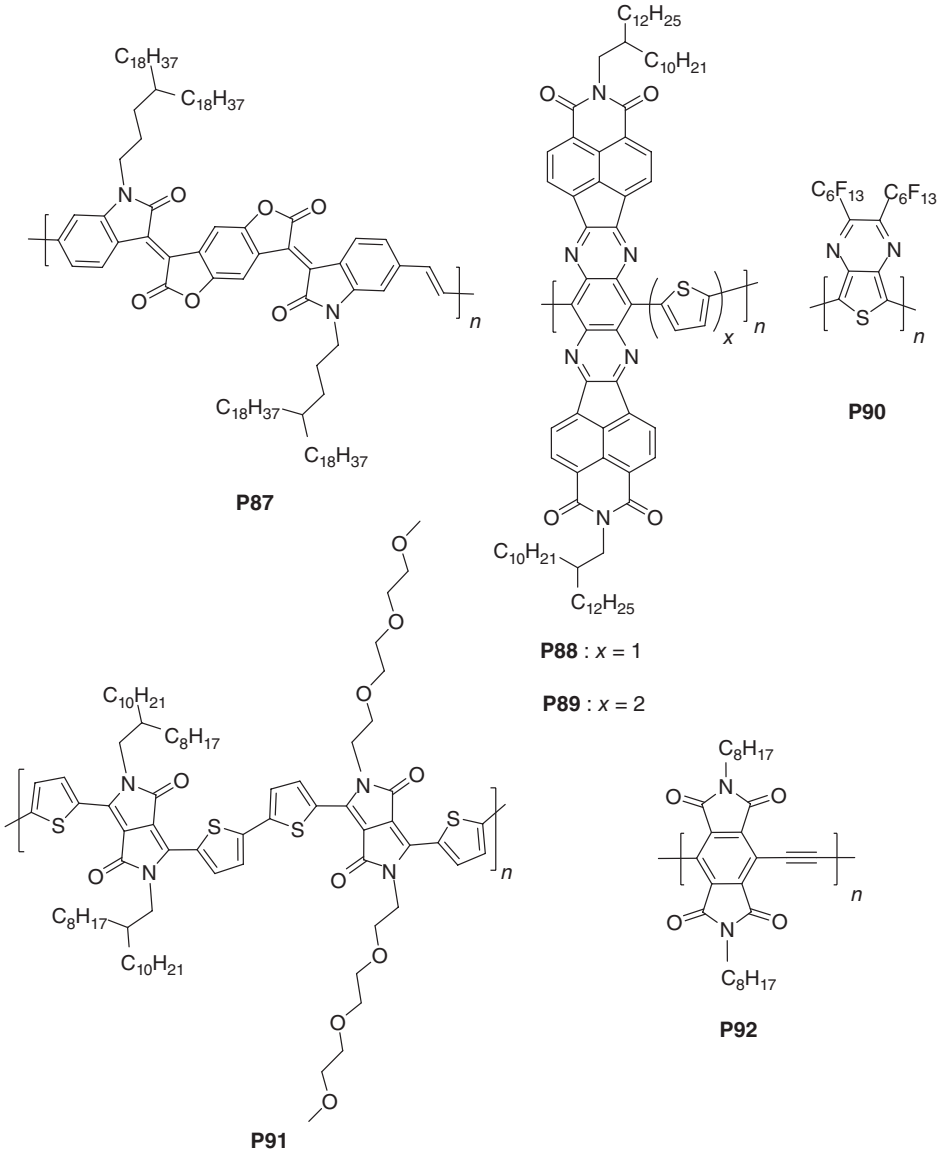

Figure 1.27 Chemical structure of n-channel polymer semiconductors **P87–P92**.

branching points are used as side chains to ensure both good solubility and interchain π–π stacking. The authors claim that this new polymer overcomes the common defects in PPVs, such as conformational disorder, weak interchain interaction, and a high LUMO level, all of which should lead to high n-channel mobilities. Grazing-incident X-ray diffraction (GIXD) and AFM characterizations indicated the formation of crystalline fiber-like intercalating networks with

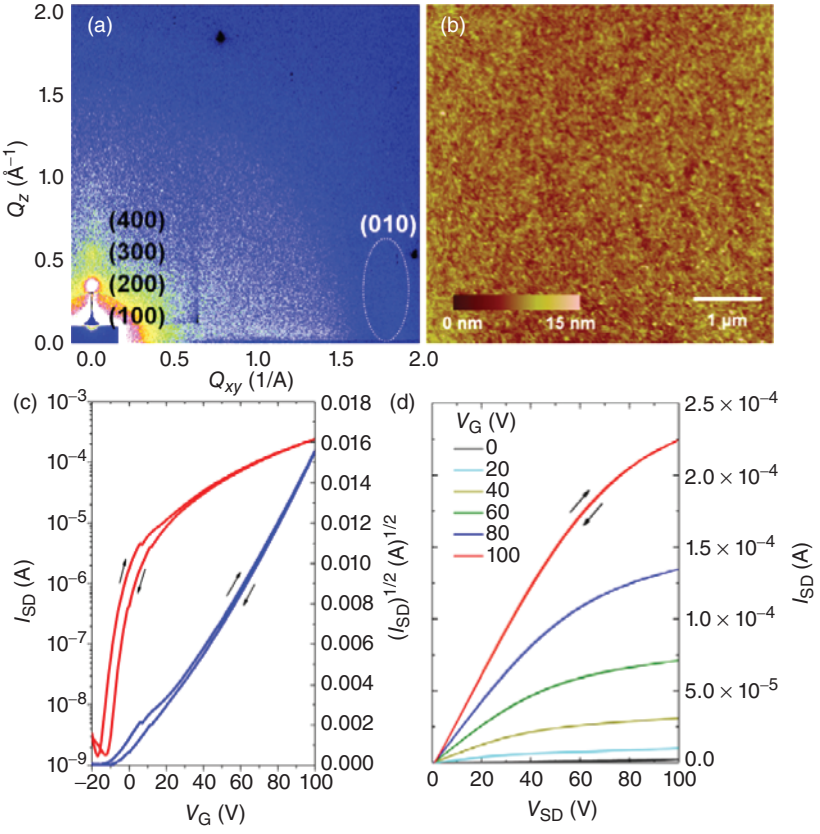

Figure 1.28 (a) 2D-GIXD pattern and (b) AFM height images of polymer **P87** film prepared by spin-coating its DCB solution (3 mg ml^{-1}). (c) Transfer and (d) output characteristics of a **P87** device under ambient conditions ($L = 10$ μm, $W = 200$ μm, $C_i = 3.7$ nF cm^{-2}), measured $V_T = 5$ V [156]. (Reproduced with permission. Copyright © 2013, American Chemical Society.)

a good lamellar edge-on packing and a short interchain π–π stacking distance of ~3.55 Å (Figure 1.28a,b). Unlike other PPV derivatives, **P87** clearly exhibited a much stronger aggregation tendency and more ordered packing. Using **P87** as the semiconductor layer in a TG–BC OFET device, electron mobilities as high as 1.1 cm^2 V^{-1} s^{-1} were achieved under ambient conditions (Figure 1.28c,d). This is one of the highest mobilities achieved to date in n-channel polymer OFETs.

The first example of a heterocyclic diimide building block, tetraazabenzodifluoranthenediimide (BFI), was recently synthesized by Jenekhe *et al.* [157] via fusion of a synthetically tunable tetraazaanthracene core and two naphthalene imide units. This new core forms a large, rigid, ladder-type macromolecular structure with 11 aromatic rings (2.0-nm-long π-conjugated framework) and shows high electron affinity (3.6–4.3 eV) and tunable optoelectronic properties. In a later report by the same group, two copolymers, **P88** and **P89** (Figure 1.27), were

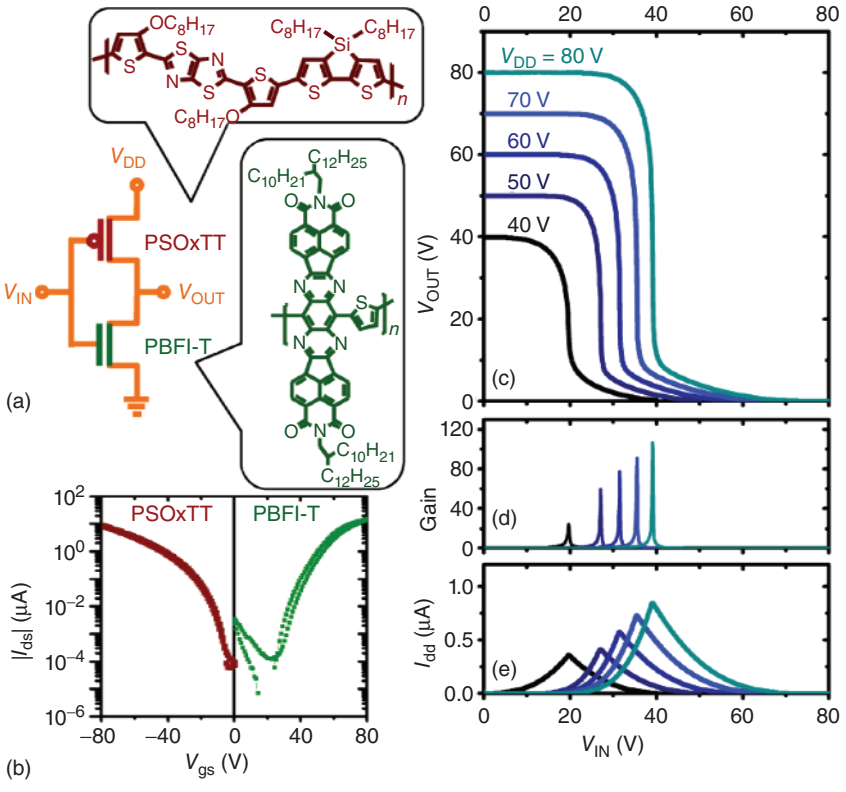

Figure 1.29 (a) Schematic of a complementary p/n polymer inverter and molecular structures of p-channel polymer PSOxTT and n-channel polymer Poly(tetraazabenzodifluoranthenediimide-thiophene) (PBFI-T) (**P88**). (b) Transfer curves of the p-channel and n-channel polymer transistors. Static switching characteristics of the inverter. (c) Output voltage, (d) gain, and (e) current as a function of input voltage (V_{IN}) with various power supply voltages (V_{DD}) [158]. (Reproduced with permission. Copyright © 2013, American Chemical Society.)

prepared by incorporating BFI as the key building block along with thiophene and bithiophene monomers, respectively [158]. These polymers exhibit a novel two-dimensional (2D) π conjugation both along the main chain and in the lateral direction, leading to efficient n-channel transport in OFETs with electron mobilities of 0.3 $cm^2 V^{-1} s^{-1}$. Complementary inverters with **P88**-based transistors showed nearly ideal switching characteristics with a high gain of 107 (Figure 1.29).

Although the fluorination of π-conjugated small molecules has shown great promise in designing high-performance n-channel semiconductors, there have been only limited reports on fluorinated n-channel polymers. Swager and coworkers [159] recently reported the synthesis of a highly fluorinated, low-bandgap (E_g^{opt} = 0.87 eV), π-conjugated polymer, poly-(2,3-bis(perfluorohexyl)thieno[3,4-*b*]pyrazine) **P90** (Figure 1.27). This new polymer exhibits exclusive solubility

in perfluorinated solvents such as perfluorooctane and perfluoro(methylcyclohexane). Additionally, it has high air- and thermal stability, high electron affinity (4.12 eV), and good electrochemical n-doping characteristics. TG–BC OFET devices with **P90** showed low electron mobilities of $\sim 10^{-5}\,cm^2\,V^{-1}\,s^{-1}$, which was attributed to the unfavorable thin-film morphology. Although the carrier mobilities obtained for this polymer is low, the authors believe that their design approach is important for the realization of orthogonally processed organic photovoltaic devices.

DPP is an attractive building block for n-channel polymer semiconductors owing to its several favorable characteristics including high electron-deficiency, enhanced backbone coplanarity, and good intermolecular $\pi-\pi$ interactions. However, to date, DPP-based polymers have been used only in p-channel and ambipolar OFET devices. In a recent study by Patil *et al.* [160], a novel DPP–DPP-based conjugated copolymer **P91** was reported with alternating alkyl and triethylene glycol side chains (Figure 1.27). It was found that this side-chain architecture provides good solubility and high molecular weight, and induces spontaneous chain crystallization. After a careful device engineering, strictly unipolar n-channel OFET devices (TG–BC) were fabricated with electron mobilities of up to $3\,cm^2\,V^{-1}\,s^{-1}$. The authors mentioned that this unipolar behavior of **P91** with high electron mobility is crucial to printed, low-power, large-scale complementary logic circuitry.

A new class of n-channel semiconducting polymer based on the smallest rylenediimide building block pyromellitic diimide (PyDI) was recently developed by Katz and coworkers [161]. Prior to this report, the same group also developed small-molecule n-channel semiconductors based on PyDI core [162]. **P92** is an example of this new semiconductor family with ethynyl linkages and octyl (C_8H_{17}) side chains (Figure 1.27). Unipolar n-channel transfer characteristics with moderate electron mobility of $2\times 10^{-4}\,cm^2\,V^{-1}\,s^{-1}$ were observed after ambient processing. The authors claimed that, to the best of their knowledge, **P92** was the first example of a PyDI semionducting polymer, and it was the simplest n-channel polymer reported up to that time. Further chemical structure and device optimizations with this polymer are in progress.

1.5.2 Small Molecules

To the best of our knowledge, the first n-channel OFET was fabricated by Guillaud *et al.* [163] using vapor-deposited films of lutetiumphthalocyanine ($LuPc_2$, **M39**, Figure 1.30). These devices exhibit electron mobilities of $10^{-4}\,cm^2\,V^{-1}\,s^{-1}$ in vacuum. Bao *et al.* [164] demonstrated the first air-stable n-channel OTFTs using a semiconductor layer vacuum-deposited by perfluorinated phthalocyanines ($F_{16}CuPc$, **M40**, Figure 1.30). These FETs exhibited maximum electron mobilities of $\sim 0.03\,cm^2\,V^{-1}\,s^{-1}$ in air for sublimed films deposited at a gate-dielectric substrate temperature of 130 °C. This is one of the first contributions where

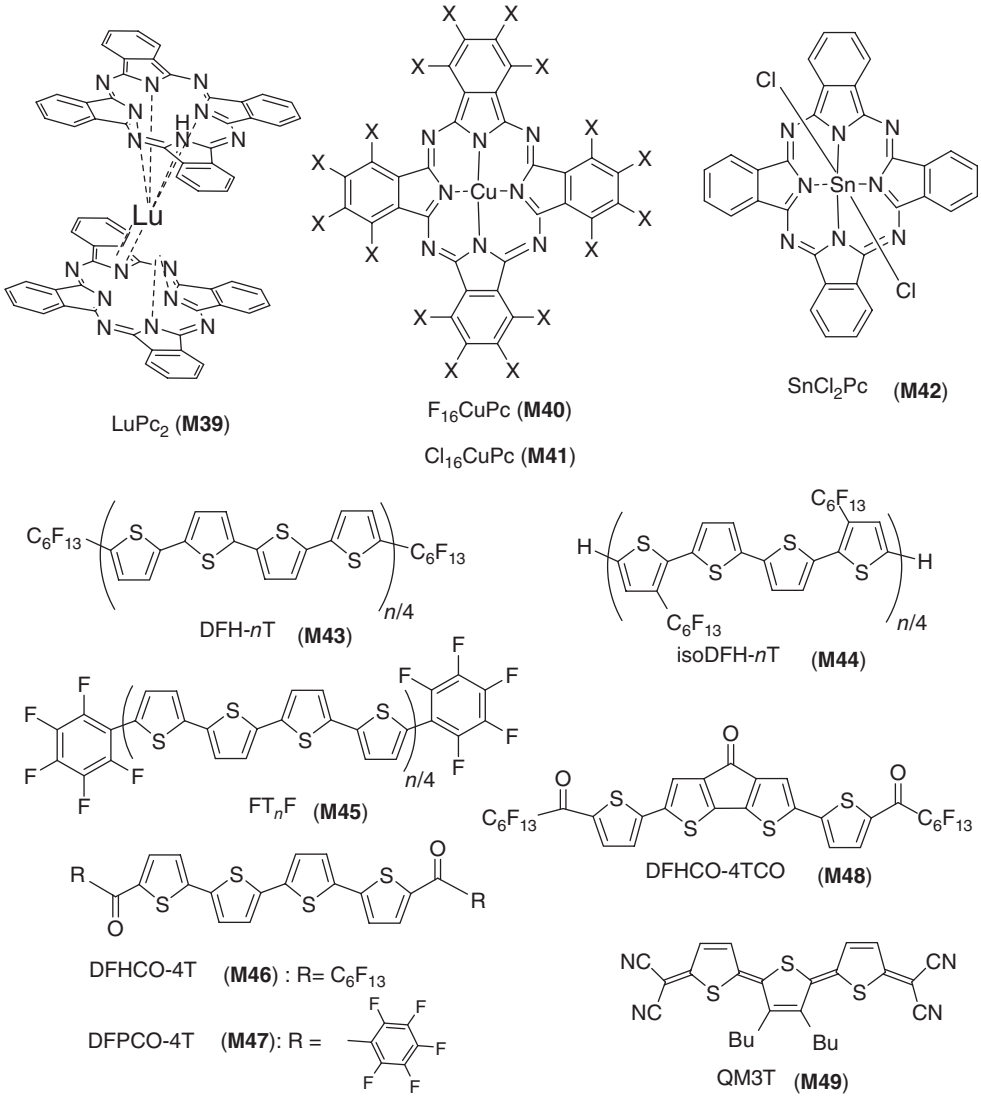

Figure 1.30 Chemical structure of n-channel small-molecule semiconductors **M39–M49**.

core functionalization of a p-channel material (CuPc) with strong electron-withdrawing F groups resulted in ambient-stable n-channel OTFTs. This material is also the most used for the fabrication of single-crystal devices [165]. A seed-induced growth by vapor processing was recently developed for *in situ* patterning of organic single-crystalline nanoribbons of F_{16}CuPc on a Si/SiO_2 surface [166]. With this method, devices based on individual F_{16}CuPc submicro/nanometer-sized ribbons were fabricated with Ag/Au asymmetrical source/drain electrodes, showing that the asymmetrical devices possessed much

higher mobilities ($0.2\,cm^2\,V^{-1}\,s^{-1}$) than the devices with Au/Au symmetrical electrodes ($0.01\,cm^2\,V^{-1}\,s^{-1}$). This is due to the asymmetrical source/drain electrode configuration which established a stepwise energy level between the electrodes and the LUMO of F_{16}CuPc, promoting electron injection and transport. Recently, Ling *et al.* [167] have used copper hexachlorophthalocyanine (Cl_{16}CuPc, **M41**, Figure 1.30) as a semiconductor for n-channel OTFTs, reporting electron mobilities of $\sim 0.01\,cm^2\,V^{-1}\,s^{-1}$. Remarkably, these devices show no performance degradation after storage in air for more than 50 days. Wang *et al.* [168] have reported n-channel FETs where the F_{16}CuPc film was epitaxy grown on *para*-hexaphenyl (*p*-6P); these devices exhibited electron mobilities as high as $0.11\,cm^2\,V^{-1}\,s^{-1}$, which approach those of the single-crystal-based devices [168]. Very recently, impressive electron mobilities of $0.30\,cm^2\,V^{-1}\,s^{-1}$ in air were reported by Song *et al.* [169] using phthalocyanato tin(IV) dichloride ($SnCl_2$Pc, **M42**, Figure 1.30) as a semiconductor.

The first n-channel oligothiophene-based transistor was fabricated at NU in 2000. In a series of papers, our group has described the synthesis, comparative physicochemical properties, and solid-state structures of several oligothiophenes substituted with perfluorohexyl chains [170]. These series include the n-channel α,ω-diperfluorohexyl-*n*Ts (DFH-*n*Ts, **M43n**, Figure 1.30) and β,β′-diperfluorohexyl-*n*Ts (isoDFH-*n*Ts, **M44n**, Figure 1.30), which were compared with the corresponding p-channel hexyl-substituted and unsubstituted oligothiophenes (α-*n*Ts, $n = 2-6$). The crystal structures of key fluorocarbon-substituted oligomers were also analyzed, which showed close π–π intermolecular interactions between the aromatic cores, whereas the fluorocarbon chains segregated into lamellar structures. X-ray structural analysis was performed for DFH-3T ($n = 3$) and DFH-4T ($n = 5$) which exhibit an all-anti, fully planar geometry, with dihedral angles between the mean plane of the rings of <2°. This value compares well with that reported for α4T but is much smaller than the 6–9° reported for α3T. The perfluorohexyl substituents exhibit a zigzag helical conformation that is characteristic of fluorocarbon chains [171] and are positioned at ∼140° with respect to the oligothiophene backbone axes in both cases. The molecular packing of DFH-4T shares the familiar "HB" motif with an angle of 50° between the mean planes of adjacent molecules. Typical HB angles for oligothiophene α*n*Ts ($n = 4-6$, 8) range between 55° and 70°. The minimum interplanar distances between neighboring molecules in DFH-4T is 3.52 Å, which is comparable to 3.5–3.9 Å in analogous oligothiophenes. The crystal structures and packing characteristics of β,β′-disubstituted systems isoDFH-5T are considerably different from those of the end-capped compounds. The effect of α,ω and β,β′ regiochemical substitution on the π core structure is dramatic, with a large torsional angle (up to 64°) forced between adjacent thiophene rings compared to the DFH-*n*Ts series. To a lesser degree, this has been observed as well for some β-alkylsubstituted oligothiophenes [172] and is due to the steric repulsion between the fluorohexyl chain CF_2 group and either the sulfur atom or the C–H moiety on the adjacent thiophene ring. It was also observed that, regardless of the differences in molecular structure and packing characteristics,

all fluorocarbon-substituted oligothiophenes exhibit similar intermolecular separations between the oligothiophene core and fluorocarbon regions.

From the electrochemical and optical data, the energy positions of the HOMOs and LUMOs of these oligothiophenes were estimated and, as expected, fluorocarbon functionalization of the oligothiophene core reduces both HOMO and LUMO energies (~0.1 – 0.5 eV depending on the core length). The shift of HOMO and LUMO energies of DFH/isoDFH-*n*Ts and the corresponding alkyl-substituted oligothiophenes is in quantitative agreement with the expected effects of fluorocarbon and hydrocarbon substituent-derived Hammett parameters. Overall, the molecular orbital energy trends within each series are determined by a balance between the nature of the substituent and density and the extension of the aromatic core. The net results from this interplay are frontier MOs where the LUMO and HOMO energies are practically independent of the conjugation length for fluorocarbon- and alkyl-substituted *n*Ts, respectively. The experimental results were confirmed by DFT computational modeling, the results of which closely paralleled the experimental trends. OFET devices were fabricated and characterized on Si/SiO_2 substrates treated with Hexamethyldisilazane (HMDS). The results clearly demonstrated the crucial importance of oligothiophene core substitution in determining the p- or n-channel activity of the semiconductor. Fluorocarbon-substituted systems are majority-carrier electron-transporting materials, while oligothiophenes (with or without $-C_6H_{13}$ chains) are majority-carrier hole-transporting semiconductors. Trends in field-effect mobilities and I_{on}/I_{off} ratios between and within these series were explained by the interplay of molecular structure and film microstructure and morphology. The films that exhibited the greatest carrier mobilities possessed the appropriate combination of large grain size and smooth, interconnected morphology, exhibit molecular orientation directed along the substrate normal, and had sufficient core conjugation/length. The second distinctive material is DFH-4T, which was shown to exhibit one of the highest n-type carrier mobility ($0.22\ cm^2\ V^{-1}\ s^{-1}$) and I_{on}/I_{off} ratio reported for an n-type transporting material. More recently, an extensive IR/electrochemical characterization of these fluorocarbon-substituted oligothiophenes has been performed by Casado and López Navarrete [170e].

The NU group also reported the comparative properties of arene-thiophene and fluoroarene-thiophene (FT_nF (**M45**), $n = 2-4$, Figure 1.30) semiconductors [173] with respect to regiochemical modifications of the core and oligothiophene core-shortening. These extensive studies included thermal analysis, optical spectroscopy, cyclic voltammetry, single-crystal XRD structural data for the majority of these compounds, film microstructure and morphology, and OTFT fabrication and characterization. For the fluoroarene-thiophene series, the majority charge-transport type and mobilities ($0.00001 - 0.5\ cm^2\ V^{-1}\ s^{-1}$) and the I_{on}/I_{off} current ratios ($10^1 - 10^8$) change dramatically with molecular regiochemistry as well as with the substrate deposition temperature. The large electron mobility of FTTTTF was attributed to the favorable interaction between the electron-rich and electron-deficient groups, thereby achieving optimum molecular $\pi-\pi$ overlap and excellent film texture. The shorter fluoroarene-thiophene oligomers ($n = 2, 3$)

are also n-type semiconductors, demonstrating that fluoroarene end-substitution promotes majority charge flip independently of the thiophene core extension. DFT band structure calculations are shedding light on the majority charge-carrier flip in this family [174].

An effective strategy to tune oligothiophene core energy levels, optical characteristics, and solid-state packing is to functionalize the oligothiophene core with strong inductive/mesomeric carbonyl (C≡O) groups. In the first systems, the investigated carbonyl chemical functionalities included perfluorohexylcarbonyl groups (e.g., 5,5″-diperfluorohexylcarbonyl-2,2′:5′,2″:5″,2‴ (DFHCO-4T), **M46**, Figure 1.30) installed at the oligothiophene α,ω positions as well as bridged carbonyl groups positioned at the center of the molecular core (e.g., DFHCO-4TCO, **M48**, Figure 1.30) [175]. OFETs were fabricated on HMDS-treated Si/SiO_2 substrates, and DFHCO-4T showed monopolar n-type activity (in vacuum) with an exceptionally high mobility of 0.32 $cm^2\,V^{-1}\,s^{-1}$ for semiconducting films deposited at a substrate temperature of 25 °C. Note that similar carbonyl group effect on n-type (electron) transport was previously demonstrated in electroactive aromatic polyketones and polyesters [176]. Upon additional carbonyl group introduction into the quaterthiophene core, DFHCO-4TCO exhibited stable n-type activity even in air, although the ambient electron mobility (0.01 $cm^2\,V^{-1}\,s^{-1}$) was somewhat lower than that recorded under vacuum (0.08 $cm^2\,V^{-1}\,s^{-1}$). After proper dielectric surface modification, n-type mobilities were substantially improved to 1.7 $cm^2\,V^{-1}\,s^{-1}$ for DFHCO-4T. More recently, Schols *et al.* [177] have improved the electron mobilities of DFHCO-4T Au top-contact transistors to 4.6 $cm^2\,V^{-1}\,s^{-1}$; the drastically reduced performance using Al/LiF as top contact was also explained as a consequence of an electron-transfer reaction occurring at the metal/DFHCO-4T interface. Another promising carbonyl-containing oligothiophene is DFPCO-4T (**M47**, Figure 1.30) [178]. DFPCO-4T, which crystallizes in an HB motif, with the shortest intercore distance being 3.50 Å and the average dihedral angle between the phenyl substituent and the adjacent thiophene subunit ∼53°. FETs of DFPCO-4T were fabricated with Au top-contact electrodes. Semiconductor films (50 nm) were deposited onto temperature-controlled HMDS-treated SiO_2/p^+-Si substrates by vapor deposition and drop-casting. A 50-nm layer of Au was then deposited through a shadow mask to define the source and drain electrodes. OFET characterization was performed under Argon. High electron mobilities of ∼0.5 $cm^2\,V^{-1}\,s^{-1}$ were observed for vapor-deposited DFPCO-4T films ($T_D = 80$ °C) with a threshold voltage of ∼30 V ($I_{on}:I_{off} > 10^8$). In solution-cast devices, electron mobilities were exceptionally high with a maximum of ∼0.25 $cm^2\,V^{-1}\,s^{-1}$ ($I_{on}:I_{off} = 10^5$; $V_T = 50-70$ V). Recently, the NU group has analyzed the temperature dependence of FET mobility for a series of n-channel oligothiophenes along with those of other p-channel and ambipolar organic semiconductors [179].

Frisbie *et al.* reported that quinomethane terthiophene (QM3T, **M49**, Figure 1.30) exhibits μ_s ∼0.002–0.5 $cm^2\,V^{-1}\,s^{-1}$ [180]. An extended series showing even greater performance and ambipolar transport has been recently reported

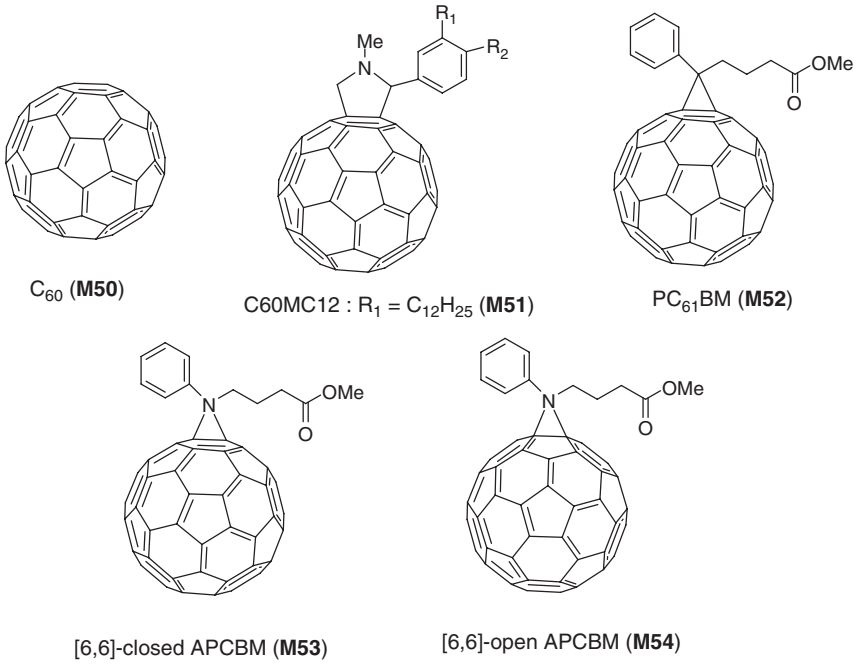

Figure 1.31 Chemical structure of n-channel small-molecule semiconductors **M50–M54**.

[181, 182]. Handa *et al.* [183] have shown a new hybrid-type dicyanomethylene-substituted terthienoquinoid compound for use as a solution-processable n-channel semiconductor; electron mobilities up to $0.16\,cm^2\,V^{-1}\,s^{-1}$ were obtained upon annealing the spin-coated films.

Figure 1.31 collects the chemical structure of several fullerene derivatives. The first report of C_{60} (**M50**)-based TFT evidenced low electron mobilities of $\sim 10^{-4}\,cm^2\,V^{-1}\,s^{-1}$ [184]. Following that report, C_{60} thin films were grown and studied in ultrahigh vacuum (UHV) [185]. TFTs were fabricated without air exposure and consisted of heavily doped n-type silicon wafers which were oxidized to leave a 3000 Å thick layer of silicon dioxide dielectric and bottom-contact Cr/Au electrodes. The authors reported electron mobilities of $0.56-0.2\,cm^2\,V^{-1}\,s^{-1}$, comparable to that obtained with time-of-flight measurements on C_{60} single crystals. n-Channel FETs based on C_{70} were first reported a few years later [186] and exhibited field effect mobilities up to $2\times10^{-3}\,cm^2\,V^{-1}\,s^{-1}$ in UHV and I_{on}/I_{off} ratios as high as 10^5. Unfortunately, the performance of C_{60}- and C_{70}-based FETs degrades quickly upon exposure to air. More recently, Itaka *et al.* [187] have enhanced the crystallinity of vapor-deposited C_{60} films by coating the dielectric with a thin layer of pentacene. These FETs exhibit electron mobilities of $\sim 2.0-5.0\,cm^2\,V^{-1}\,s^{-1}$. Jang *et al.* [188] have recently reported air-stable C_{60} TFTs with electron mobilities of $\sim 0.05\,cm^2\,V^{-1}\,s^{-1}$ by using a perfluoropolymer as the gate dielectric. Very recently, Anthopoulos *et al.* [189] have reported the greatest field-effect electron mobilities for C_{60} transistors,

which approached $\mu \sim 6\,cm^2\,V^{-1}\,s^{-1}$. They also demonstrated ring oscillators based on C_{60} films grown by hot-wall epitaxy. Low-voltage C_{60} n-channel OTFTs with high electron mobilities of $2.3\,cm^2\,V^{-1}\,s^{-1}$ were fabricated by engineering the electrode/semiconductor and dielectric/semiconductor interfaces [190].

Functionalized fullerenes are promising candidates for solution-processed n-channel OTFTs. Chikamatsu *et al.* [191] have synthesized soluble C_{60}-fused *N*-methylpyrrolidine-*meta*-C12 phenyl (C_{60}MC12, **M51**, Figure 1.31) and fabricated FETs exhibiting high electron mobilities of $\sim 0.07\,cm^2\,V^{-1}\,s^{-1}$. More recently, Wöbkenberg *et al.* developed several fluorine-containing C_{60} derivatives. Solution-processed OTFTs based on these compounds exhibit electron mobilities up to $0.15\,cm^2\,V^{-1}\,s^{-1}$ [192]. These devices show enhanced stability in ambient conditions as compared to standard methanofullerene OTFTs. Far more ambient-stable C_{60}-based FETs were developed by Chikamatsu *et al.* [193] who synthesized new soluble perfluoroalkyl-substituted C_{60} derivatives exhibiting electron mobilities as high as $0.25\,cm^2\,V^{-1}\,s^{-1}$. TFTs based on [6,6]-phenyl-C61-butyric acid methyl ester ([60]PCBM) (**M52**, Figure 1.31) and [6,6]-phenyl-C71-butyric acid methyl ester ([70]PCBM), materials widely used for the fabrication of organic photovoltaic devices, have also been recently reported [194]. Despite the fact that both derivatives form glassy films when processed from solution, their electron mobilities are high at ~0.21 and $\sim 0.1\,cm^2\,V^{-1}\,s^{-1}$ for [60]PCBM and [70]PCBM, respectively. Although the derived mobility of [60]PCBM is comparable to the best values reported in the literature, the electron mobility of [70]PCBM is the highest value reported to date for any C_{70}-based derivative. Wudl reported the one-pot preparation of two isomeric imino-PCBMs, that is, [5,6]-open azafulleroid (**M53**, Figure 1.31) and [6,6]-closed aziridinofullerene (**M54**, Figure 1.31). OFETs were fabricated on heavily doped Si wafers with a 200-nm-thick SiO_2 layer with top-contact geometry, yielding electron mobilities of ~0.04, ~0.02, and $0.03\,cm^2\,V^{-1}\,s^{-1}$ for [5,6]-open APCBM, [6,6]-closed APCBM, and PCBM, respectively. The higher electron mobility in the [5,6]-open APCBM OFET can be attributed to its 60 π-electron nature, which affords a stronger electron-acceptor strength than the [6,6] junctions [195]. Using C_{60} and pentacene CMOS NOT logic circuits were also fabricated by Kanbara *et al.* [196]. The voltage gain demonstrated was ~4. Low-voltage CMOS inverters with C_{60} (and pentacene) were reported by Kitamura and Arakawa on glass substrates [197]. The inverter operated at low voltages (1 – 5 V) and the C_{60} and pentacene TFTs had high field-effect mobilities of 0.68 and $0.59\,cm^2\,V^{-1}\,s^{-1}$ and threshold voltages of 0.80 and −0.84 V, respectively. As expected from the threshold voltages of the individual transistors, the inverter operates at supply voltages of only $V_{DD} > 1.64$ V. The signal gain calculated is in the range −50 to −150. More recently, Kippelen *et al.* demonstrated complementary inverters on PEN substrates [198].

The chemical structures of several perylenes and quaterylene derivatives are shown in Figure 1.32. Horowitz *et al.* [199] first demonstrated electron mobilities of $\sim 10^{-5}\,cm^2\,V^{-1}\,s^{-1}$ with an *N*,*N*′-diphenyl-substituted perylene, **M55-A**. In 2001, Malenfant *et al.* [200] reported n-channel OFETs based on *N*,*N*′-dioctyl PDI

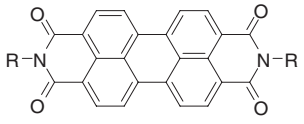

M55-A: R = C_6H_5

M55-B (PDI8): R = C_8H_{17}

M55-C: R = $C_{13}H_{27}$

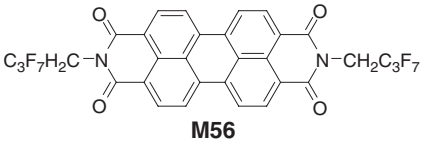

M56

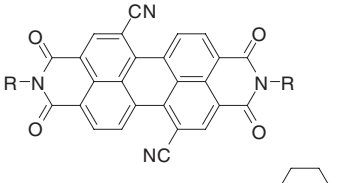

PDICy-CN_2 (**M57**-A): R =

PDIF-CN_2 (**M57**-B): R = $CH_2C_3F_7$

PDI-D (**M57**-C): R = C_8H_{17}

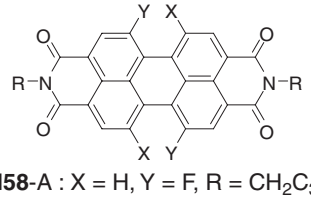

M58-A : X = H, Y = F, R = $CH_2C_3F_7$

M58-B : X = F, Y = F, R = $CH_2C_3F_7$

M58-C : X = Cl, Y = Cl, R = C_6H_5

M58-D : X = Cl, Y = Cl, R = $CH_2C_3F_7$

M58-E : X = H, Y = Br, R = $CH_2C_3F_7$

M58-F : X = Br, Y = Br, R = $CH_2C_3F_7$

M58-G : X = Cl, Y = Cl, R = H

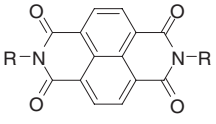

M61-A: R = H

M61-B(NDI8) : R = C_8H_{17}

M61-C: R = $CH_2C_7H_{15}$

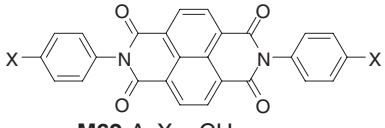

M62-A: X = CH_3

M62-B: R = CF_3

M62-C: R = $CH_2CH_2C_8F_{17}$

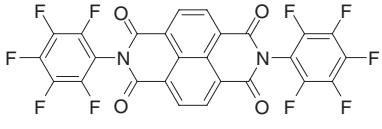

M63

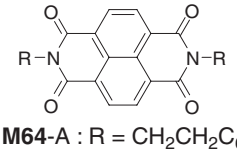

M64-A : R = $CH_2CH_2C_6F_5$

M64-B : R =

M64-C : R = C_6H_{13}

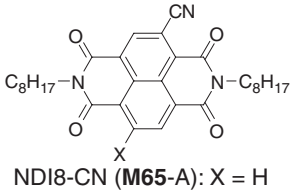

NDI8-CN (**M65**-A): X = H

NDI8-CN_2 (**M65**-B): X = CN

Figure 1.32 Chemical structure of n-channel small-molecule semiconductors **M55–M66**.

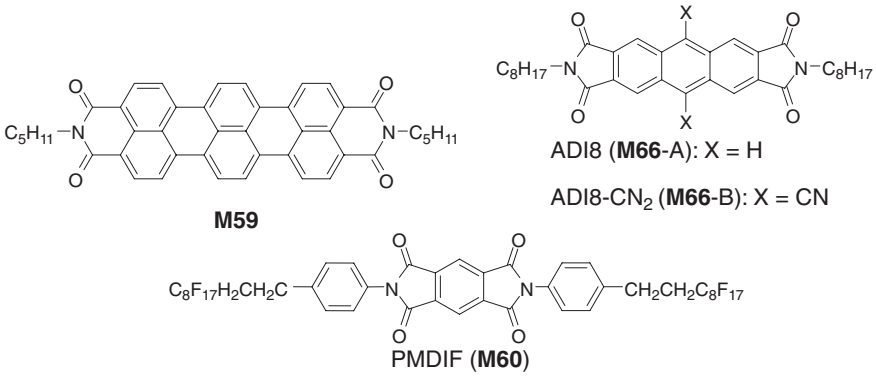

Figure 1.32 (*Continued*).

M55-B (or PDI8) with electron mobility of 0.6 $cm^2 V^{-1} s^{-1}$ under nitrogen, but with a high threshold voltage of +75 V, which was attributed to a large trap density. Later, Chesterfield *et al.* [201] demonstrated that devices with a maximum mobility of 1.7 $cm^2 V^{-1} s^{-1}$, an on/off current ratio of 10^7, and threshold voltages of 10 – 15 V can be obtained using **M55-B** by coating the SiO_2 gate dielectric with poly(α-methylstyrene). Coating of the dielectric with polymers also considerably improves the air stability of device operation for **M55-B**, presumably by passifying the acidic silanol groups on the SiO_2 surface which can act as electron traps [202]. Ichikawa *et al.* [203] demonstrated that the mobility of OFETs based on *N*,*N*′-bis-tridecyl **M55-C** can be increased 10^3 times to 2.1 $cm^2 V^{-1} s^{-1}$ by thermal annealing; the thermal treatments improve both the thin-film crystallinity and morphology. Bao, Würthner, and coworkers [204] reported that OFETs based on PDI **M56** exhibit mobilities as high as 0.72 $cm^2 V^{-1} s^{-1}$, which decrease only slightly after air exposure and remain stable for more than 50 days. As the partial fluorination has only a small effect on the redox potential (LUMO energy) relative to *N*,*N*′-di(alkyl) analogs, the stability was attributed to the hindrance of O_2 and H_2O diffusion by the dense packing of the cores and by the fluoroalkyl chains.

Core-cyanated PDIs (**M57**, Figure 1.32) were first synthesized by Wasielewski *et al.* [205]. These systems are significantly more readily reduced than their unsubstituted analogs (by about 0.36 V); the associated high electron affinity is believed to be a factor contributing to the high electron mobility (0.10 $cm^2 V^{-1} s^{-1}$) achieved in air for OFETs based on PDICy-CN_2. Combining partial fluorination of the N,N′ substituents and 1,7-dicyano substitution in PDIF-CN_2 affords a still higher electron mobility (0.64 $cm^2 V^{-1} s^{-1}$). The effects of PDIF-CN_2 film-growth conditions on n-channel OFET performance have also been investigated [43]; dramatic enhancements of the on/off current ratio and mobility are obtained with increased substrate temperature (T_s) during film growth, the increased mobility being correlated with higher levels of molecular ordering and with minimization of film-surface irregularities [206]. In addition, the effects modifying the SiO_2 surface of the gate dielectric with octadecyltrichlorosilane- or hexamethyldisilazane-derived monolayers, as well as with polystyrene, were

investigated for PDIF-CN_2 films deposited at $T_s = 130\,^{\circ}C$; the SiO_2 surface treatments substantially modulated the mobility and growth morphology of PDIF-CN_2 films. Recently, Morpurgo *et al.* [207] fabricated OFETs based on PDIF-CN_2 single crystals with PMMA as the gate dielectric, which exhibited electron mobilities approaching $6\,cm^2\,V^{-1}\,s^{-1}$, which is 10 times greater than those of the corresponding thin-film devices, both in air and in vacuum. Furthermore, these devices exhibit near-zero threshold voltage and subthreshold slopes and current on/off ratios ($10^3 - 10^4$) comparable to the very best p-channel single-crystal devices when the same gate dielectric is employed.

Weitz *et al.* [208] reported air-stable n-channel OFETs based on five dicyano PDIs with fluorinated linear and cyclic N,N′-substituents (mobilities up to $0.1\,cm^2\,V^{-1}\,s^{-1}$) and investigated the relationships between molecular structure, thin-film morphology, substrate temperature, device performance, and air stability. Interestingly, the mobility degradation rate in air was found to be similar for all compounds and at all substrate temperatures, raising the question of whether air stability can always be explained on the basis of kinetic barriers to O_2/H_2O diffusion formed by densely packed fluorine substituents. In addition to core cyanation, core halogenation is an effective way to functionalize the perylene "bay" positions. Würthner *et al.* studied a series of core-halogenated *N*,*N*′-bis(heptafluorobutyl) PDIs. While the introduction of halogens in the "bay" positions facilitates reduction, with 1,6,7,12-tetrahalo derivatives being slightly more readily reduced than their 1,7-dihalo analogs, the more highly substituted examples tend to exhibit lower mobilities; this can be attributed to the disruption of core planarity and, therefore, of effective $\pi-\pi$ overlap due to steric interactions [209]. Thus, both the difluoro compound **M58-A** (Figure 1.32) and the parent **M56** (Figure 1.32) exhibit densely π-stacked, more-or-less planar PDI units (torsion angles of 3.0° and 1.5°, respectively, between the two constituent naphthalene units according to X-ray crystal structures), with the FET electron mobility of **M58-A** being around half that of **M56**. On the other hand, the perylene core of **M58-B** (Figure 1.32) is distinctly nonplanar because of F–F steric interactions (torsion angles 20° – 25°), leading to less dense and less regular packing and to mobility that is an order of magnitude lower than that of **M58-A**. The tetrabromo derivative **M58-F** (Figure 1.32) also exhibits about 10 times lower mobility than its dibromo analog, **M58-E** (Figure 1.32). Furthermore, 1,6,7,12-tetrachloro and bromo derivatives **M58-C** (Figure 1.32) and **M58-F** (Figure 1.32) exhibit mobilities 10^3 times lower than that of their tetrafluoro counterpart, **M58-B**, presumably due to the increased bulk of the substituents leading to significantly increased torsion angles and reduced intermolecular $\pi-\pi$ interactions. Interestingly, replacing the *N*,*N*′-fluoroalkyl substituents of the 1,6,7,12-tetrachloro **M58-C** (Figure 1.32) by an *N*,*N*′-pentafluorophenyl groups in **M58-D** (Figure 1.32) led to $\sim 10^4$ times increase in the mobility. Müllen *et al.* [210] have pioneered the synthesis of higher rylene diimide dyes and other species based on extended PDI cores, investigating in detail their thermotropic behavior and optical properties as well as the details of their microstructure. However, exploitation of higher rylene diimides in organic electronics is limited to a report

by Petit *et al.* [211] on the FET properties of vapor-deposited films of *N*,*N*′-dipentylterrylene-3,4:11,12-tetracarboxylic diimide derivative **M59** (Figure 1.32) on Si/SiO_2 substrates; a maximum electron mobility of ~0.07 $cm^2 V^{-1} s^{-1}$ and an on/off current ratio in excess of 10^4 were obtained.

Katz *et al.* [212] reported the only example of an OFET based on a PyDI (**M60**, Figure 1.32). The synthesis of PyDI derivatives involves one simple conventional reaction between amines and pyromellitic dianhydride in dimethylformamide (DMF) at 110 °C. Single crystals of **M60** were obtained by slowly cooling hot, saturated DMF solutions. The unit cell of the single crystal is monoclinic with $a = 10.24$ Å, $b = 11.53$ Å, and $c = 9.28$ Å, with the crystal packing exhibiting a close π–π packing between the side-chain benzene ring and the PyDI core. **M60** exhibited a mobility of 0.054 $cm^2 V^{-1} s^{-1}$ in air and very high on/off current ratios.

The first OFET based on a rylene diimide was fabricated using the unsubstituted NDI, **M61-A** (Figure 1.32), and yielded electron mobilities of ~10^{-4} $cm^2 V^{-1} s^{-1}$ [213]. Later, Katz *et al.* demonstrated that the OFET performance could be greatly improved by functionalizing the NDI core at the nitrogen positions with *n*-octyl groups. The compound **M61-B** (or NDI-8, Figure 1.32) exhibits electron mobilities of ~0.16 $cm^2 V^{-1} s^{-1}$ in vacuum, although almost no FET activity was measurable in air [214]. It was found that N,N′ substitution with *n*-$CH_2C_7F_{15}$ groups in **M61-C** (Figure 1.32) significantly improved the device air stability, with mobilities of 0.05–0.1 $cm^2 V^{-1} s^{-1}$ in air [215]. Replacing the methyl substituents on the *N*,*N*′ benzyl groups of **M62-A** (Figure 1.32) with CF_3 groups in NDI-E led to 10^5 times enhancement of the mobility in air. Elongating CF_3 to *n*-$CH_2CH_2C_8F_{17}$ further enhances the mobility from 0.12 $cm^2 V^{-1} s^{-1}$ (**M62-B**, Figure 1.32) to 0.57 $cm^2 V^{-1} s^{-1}$ (**M62-C**, Figure 1.32) [25]. Strikingly, inserting an ethylene bridge between the nitrogen atoms and the perfluorophenyl substituents of **M63** (Figure 1.32) to give **M64-A** (Figure 1.32) led to a crystalline rather than an amorphous material and increased the mobility from $<10^{-6}$ to 0.31 $cm^2 V^{-1} s^{-1}$ [216]. Shukla *et al.* [217] reported that, compared to linear *n*-hexyl chains, cyclohexyl substituents assist in directing intermolecular π–π stacking, affording a dramatic increase in mobility from 0.70 (**M64-C**, Figure 1.32) to 6.2 $cm^2 V^{-1} s^{-1}$ (**M64-B**, Figure 1.32) in vacuum.

The studies described above show the great potential of core-unsubstituted NDIs. Wasielewski *et al.* [218] reported two new core-cyanated NDI semiconductors, NDI8-CN (**M65-A**, Figure 1.32) and NDI8-CN_2 (**M65-B**, Figure 1.32), which are air-stable, high-mobility, transparent organic n-type semiconductors. The syntheses of NDI8-CN and NDI8-CN_2 were achieved via a new NDI core bromination–cyanation sequence. The electronic structures of NDI8-CN and NDI8-CN_2 were examined by cyclic voltammetry, optical spectroscopy, and photoluminescence. Electrochemical reduction potentials in dichloromethane versus SCE were −0.22 V for NDI8-CN and +0.08 V for NDI8-CN_2, consistent with systematic LUMO energy depression with increasing cyanation. Importantly, NDI8-CN_2 has a reduction potential similar to that of *N*,*N*-dialkylsubstituted core-cyanated perylenes (PDI, see above) (−0.07 V vs SCE);

therefore, the LUMO/charge-carrier energies in the NDI and PDI materials should be similar. Optical and photoluminescence spectroscopy of these NDI derivatives reveals a band gap of >3 eV, reflecting the smaller conjugated core dimensions. Thus, thin films of these NDIs are transparent in the visible region. OFET measurements performed in vacuum ($<10^{-6}$ Torr) reveal optimal average electron mobilities for NDI8-CN and NDI8-CN_2 films of 4.7×10^{-3} and 0.15 $cm^2\,V^{-1}\,s^{-1}$, for films vapor-deposited at 130 and 110 °C, respectively. Interestingly, OFET operation in ambient atmosphere reveals that NDI8-CN devices undergo severe $I-V$ curve degradation, whereas the NDI-8CN2 devices exhibit stable operation with only a slightly lower maximum average mobility of 0.11 $cm^2\,V^{-1}\,s^{-1}$. The current on/off ratios (I_{on}:I_{off}) can be as high as $\sim 10^5$ for NDI-8CN and $\sim 10^3$ for NDI8-CN_2 thin films. The lower I_{on}/I_{off} ratio of NDI8-CN_2 was ascribed to a high I_{off}, which is likely due to dopants in the NDI8-CN_2 thin films from contacts or donor sites in the dielectric. Top-contact, bottom-gate, transparent, channel-flexible n-type OFETs were fabricated with NDI8-CN_2 to demonstrate its unique material properties. Thin NDI8-CN_2 films (50 nm) were vapor-deposited onto overhead transparency film coated with a spin-cast poly(3,4-ethylenedioxythiophene):polystyrene sulfonate (PEDOT:PSS) polymeric gate, a P-UV-013 (Polyera Corporation) polymer dielectric, and Au contacts. This air-stable, flexible, transparent OFET exhibited a mobility of 0.03 $cm^2\,V^{-1}\,s^{-1}$ in ambient atmosphere. An analogous rigid device fabricated on an ultrasmooth ITO (indium tin oxide)/glass substrate as gate gave a mobility value of $\sim$0.08 $cm^2\,V^{-1}\,s^{-1}$ in ambient atmosphere.

Marks *et al.* [219] reported the only examples of OFETs based on anthracene-2,3:6,7-tetracarboxylic diimides. Devices based on ADI8 (**M66-A**, Figure 1.32) exhibited a mobility of 0.02 $cm^2\,V^{-1}\,s^{-1}$ in vacuum, which is 10 times lower than its NDI counterpart. However, OFETs based on ADI8 cannot be operated in air because of the material's relatively low electron affinity. Also, in this case, the introduction of cyano groups in the 9,10 positions of the anthracene ring significantly increases the electron affinity and, therefore, affords improved air stability; devices based on ADI8-CN_2 (**M66-B**, Figure 1.32) exhibit a mobility of 0.02 $cm^2\,V^{-1}\,s^{-1}$ but very high current on/off ratios ($>10^7$).

In the last few years, several unconventional structures have been designed and synthesized as n-channel semiconductor candidates. Figure 1.33 collects the chemical structures of these derivatives. Yamashita *et al.* [220] have developed several molecular materials, such as functionalized anthracenes exhibiting electron mobilities up to $\sim 5 \times 10^{-3}$ $cm^2\,V^{-1}\,s^{-1}$, trifluoromethylphenyl-subtituted thiazole (**M67**) and thiazolothiazole (**M73**) oligomers enabling electron mobilities up to $\sim$2 $cm^2\,V^{-1}\,s^{-1}$, and tetrathiafulvalene (**M68** and **M69**) derivatives with electron mobilities up to $\sim$0.1 $cm^2\,V^{-1}\,s^{-1}$. Interesting are the performances of indenofluorenedione (**M74**)- and diindenopyrazinedione-based TFTs, which exhibit electron mobilities approaching 0.2 $cm^2\,V^{-1}\,s^{-1}$. Tetracene (**M72**) and perylene BF_2 complexes are also very interesting new electron-deficient arene semiconductors. Perfluoropentacene (**M70**) was developed by Sakamoto *et al.* [221] and exhibits the highest electron mobility of 0.11 $cm^2\,V^{-1}\,s^{-1}$.

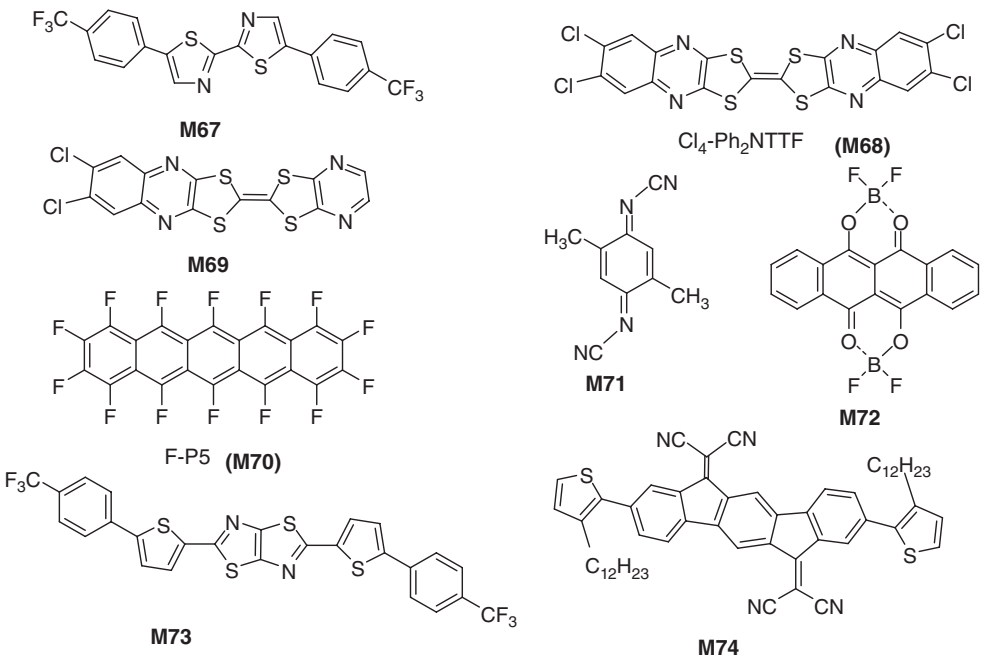

Figure 1.33 Chemical structure of n-channel small-molecule semiconductors **M67–M74**.

The same group also demonstrated the first CMOS circuit using pentacene as the p-channel counterpart. Particularly interesting are two new trifluoromethyltriphenodioxazine derivatives, the devices of which exhibit electron mobilities approaching 0.1 $cm^2 V^{-1} s^{-1}$ in ambient conditions [222]. Recently, dimethyldicyanoquinonediimine (**M71**, Figure 1.32) was developed as an n-channel semiconductor to achieve ambient-stable TFTs with electron mobilities of ~0.01 $cm^2 V^{-1} s^{-1}$ [223].

Dicyanomethylene-substituted quinoidal π-conjugated small molecules are excellent electron acceptors with high structural coplanarity and low-lying LUMO energy levels. Recently, they have been extensively studied as n-channel semiconductors for applications in OFETs, and some of them exhibited high charge-carrier mobilities of $\geq$0.5 $cm^2 V^{-1} s^{-1}$. In one of their papers, Zhu and coworkers [224] reported the design, synthesis, and characterization of a novel series of DPP-containing quinoidal small-molecule semiconductors with branched alkyl substituents. **M75** and **M76** were the first demonstration of DPP-based small molecules offering unipolar electron transport in OFET devices (Figure 1.34). Ambient-stable electron mobilities as high as 0.55 and 0.35 $cm^2 V^{-1} s^{-1}$ ($I_{on}/I_{off} = 10^5 - 10^6$) were obtained for vapor-deposited films of **M75** and solution-processed films of **M76**, respectively. These results showed that incorporation of a DPP unit to construct a quinoidal semiconductor architecture was an effective design strategy to enhance the charge-transport characteristics.

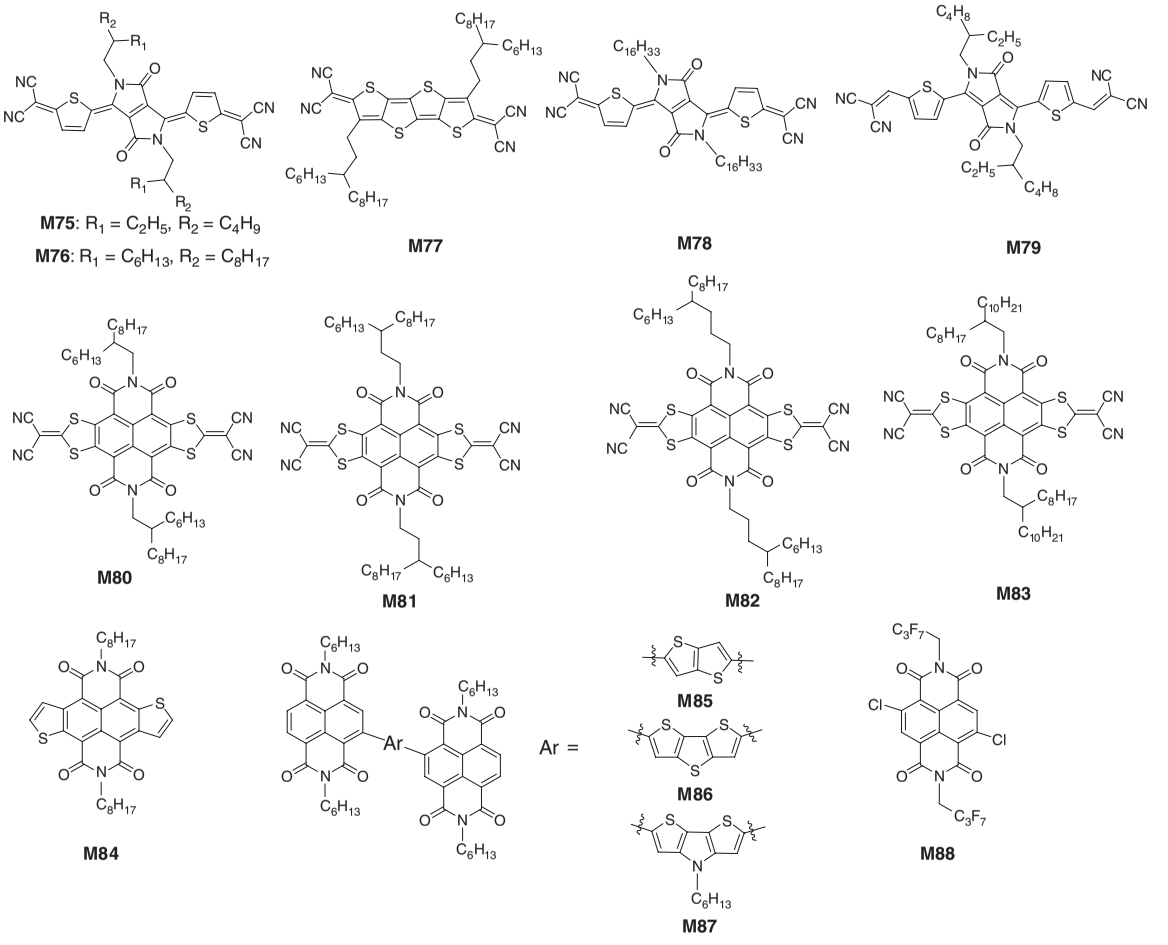

Figure 1.34 Chemical structure of n-channel small-molecule semiconductors **M75–M88**.

The same group recently reported another quinoidal semiconductor **M77** (Figure 1.34), which is a dicyanomethylene-substituted fused tetrathienoquinoid molecule with branched alkyl substituents [225]. OFET devices fabricated with solution-cast films of **M77**, without any post treatment, displayed good ambient stability and exceptionally high n-channel performance with an electron mobility of up to 0.9 $cm^2 V^{-1} s^{-1}$. In a parallel study, Heeney and coworkers [226] developed another DPP-based semiconductor **M78** (Figure 1.34), which has the same π backbone as **M75** and **M76** but with a linear alkyl chain ($C_{16}H_{33}$). Solution-processed thin films of **M78** were prepared with an insulating polymer binder (PαMS), and the resulting top-gate OFET devices yielded maximum electron mobilities of 0.5 $cm^2 V^{-1} s^{-1}$ and I_{on}/I_{off} ratios of $10^2 - 10^3$. **M78**-based devices showed excellent operating stability when exposed to ambient air for a prolonged period owing to their low-lying LUMO levels (−4.2 eV). Detailed thin-film analysis indicated that blended films of **M78** and the polymer binder exhibited strong vertical phase separation, with the DPP molecules diffusing and crystallizing on the surface of the composite film.

In another study, a new dicyanovinyl-substituted DPP-based molecule **M79** (Figure 1.34) was developed as a potential n-channel semiconductor by Park *et al.* [227]. The strong electron-withdrawing dicyanovinyl functionalities stabilize the LUMO level while conserving the aromaticity of the DPP-thiophene core. The authors claimed that the solubility and thin-film crystallinity of **M79** were slightly higher than those of dicyanomethylene-substituted quinoidal molecules **M75** and **M76**. Exceptionally high electron mobilities of up to 0.96 $cm^2 V^{-1} s^{-1}$ were obtained with solution-processed single-crystal OFET devices, which is one of the highest achieved to date for DPP-based small molecules. Polycrystalline OFETs prepared via vapor deposition of **M79** also showed great promise with electron mobilities up to 0.64 $cm^2 V^{-1} s^{-1}$. The remarkable crystallinity of **M79** in the solid state displaying uniform terraces along with the well-defined lamellar microstructure contributed to this high OFET performance.

New promising classes of rylene diimide-based small molecule n-channel semiconductors have recently been reported by several research groups. One example of this family is the core-expanded NDI derivatives bearing two 2-(1,3-dithiol-2-ylidene)malonitrile moieties at the central naphthalene core (**M80**–**M83**, Figure 1.34). These molecules were recently reported by Zhu *et al.* [228, 229] with varied *N*-alkyl chain lengths and different branching points. This study indicated that, although the *N*-alkyl substituent length has a moderate influence on thin-film microstructure and OFET performances, the position of branching point results in significant improvements in molecular packing and charge-transport characteristics. With this new core-expanded NDI structure, ambient-stable electron mobilities ranging from ~0.001 to 3.5 $cm^2 V^{-1} s^{-1}$ were observed depending on the nature of side-chain substituent (Figure 1.35). The highest electron mobility was achieved with the semiconductor **M81** which includes three-branched *N*-alkyl chains. Thin films of **M81** exhibit large grain sizes with efficient in-plane packing, which enables achieving large electron

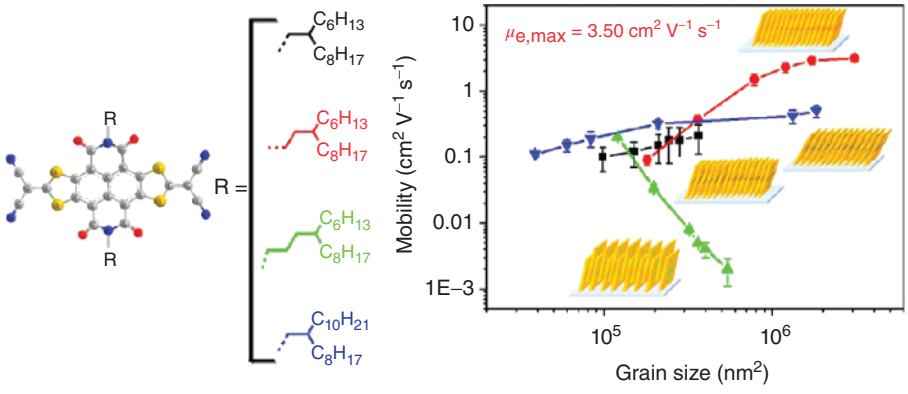

Figure 1.35 Charge-carrier mobilities as a function of grain size for OTFTs based on semiconductors **M80–M83** with different branching alkyl chains. The inset images are the schematic molecular packing demonstrating different grain sizes [229]. (Reproduced with permission. Copyright © 2013, American Chemical Society.)

mobilities of up to 3.5 $cm^2 V^{-1} s^{-1}$. This value of the mobility is currently a world record for ambient-stable, solution-processed, small-molecule n-channel OTFTs. Furthermore, an n-channel transistor array was fabricated by inkjet-printing **M83** on flexible substrates, which showed high mobility of up to 0.45 $cm^2 V^{-1} s^{-1}$ along with good saturation and sharp turn-on characteristics (Figure 1.36) [230].

Another promising family of core-expanded NDI small molecules was developed by fusing heterocyclic rings such as thiophene, indole, pyrrole, pyrazine, and thiazole to the NDI core [231]. Among such semiconductors, the thiophene-fused NDI derivative **M84** (Figure 1.34) was recently designed and synthesized by Takimiya and coworkers [232] as an attractive structure for the development of functional π-conjugated materials. Single-crystal X-ray analysis showed that **M84** had a highly planar core with relatively close π–π stacking (~3.43 Å). Electrochemical and optical studies demonstrated that the compound had a low-lying LUMO energy level (−4.0 eV) and a small HOMO–LUMO gap (2.1 eV). Electron mobility as high as 0.05 $cm^2 V^{-1} s^{-1}$ was achieved under vacuum, which is comparable to those of related core-expanded NDIs such as indole-fused NDI (~0.03 $cm^2 V^{-1} s^{-1}$) and thiazole-fused NDIs (~0.15 $cm^2 V^{-1} s^{-1}$). Another rylene diimide-based semiconductor family, which was recently reported by Marder *et al.* [233], includes bis(NDI) derivatives with conjugated bridging groups based on heterocyclic ring systems (**M85–M87**, Figure 1.34). Solution-processed thin films of **M87** exhibited electron mobility values of up to 1.5 $cm^2 V^{-1} s^{-1}$. It is noteworthy that, because of the presence of a strong donor unit in **M87**, these devices show slight ambipolar behavior with low hole mobilities ($\mu_h = 9.8 \times 10^{-3}$ $cm^2 V^{-1} s^{-1}$). On the other hand, OFETs based on **M85** and **M86** showed unipolar n-channel charge transports with

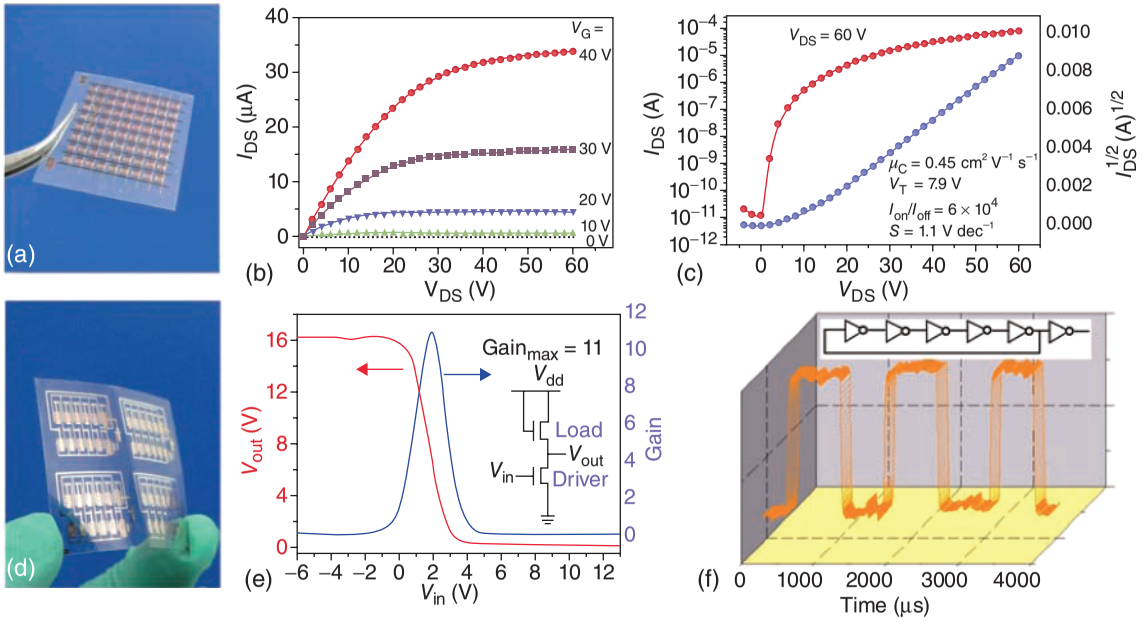

Figure 1.36 (a) Optical images, (b) output characteristics, and (c) transfer characteristics of all-solution-processed flexible OTFTs based on **M83**. (d) Optical images of a flexible five-stage organic oscillator. Electrical characteristics of (e) an organic inverter and (f) an organic oscillator [230]. (Reproduced with permission. Copyright © 2011, John Wiley & Sons, Inc.)

appreciable electron mobilities of 0.14 $cm^2 V^{-1} s^{-1}$ as a result of the decreased donor strength of the bridging unit. Finally, more recently, Würthner *et al.* [234] reported the preparation of high-quality thin films based on the dichlorinated NDI derivative **M88** (Figure 1.34) on bare SiO_2 via a solution shearing method. The OFET devices with these active layers exhibited electron mobilities of up to 0.95 $cm^2 V^{-1} s^{-1}$ in air. In this study, the authors optimized the device's processing parameters to enable the directional growth of large crystalline domains with high anisotropy. Remarkably, a reversible up to fourfold increase in charge-carrier mobility ($\mu_e = 4.26\ cm^2 V^{-1} s^{-1}$) was observed under positive bias stress.

1.6 Ambipolar Semiconductors

The vast majority of known organic semiconductors are either hole (p-channel) or electron (n-channel) transporting materials. However, very recently, ambipolar organic semiconductors have been attracting attention for their potential use in numerous technologically relevant applications [235]. The discovery of ambipolarity as a general characteristic of several semiconducting polymers was made possible by the understanding of the crucial role played by traps of electrons on the surface of several dielectrics, such as hydroxyl, silanol, and carbonyl groups. Representative technological examples include the area of organic microelectronics where patterning of p- and n-channel semiconductors is one of the major hurdles for the implementation of organic complementary logic. In this context, the use of ambipolar materials should enable the fabrication of complementary-like circuits through the use of a single semiconductor that functions both as p- and/or n-channel, thereby significantly reducing fabrication complexity [236]. The latest application of ambipolar organic semiconductors is in bifunctional TFTs such as light-sensing organic organic thin-film transistors (LS-OTFTs) and organic light-emitting transistors (OLETs) [237]. These types of OTFTs can combine electrical switching with additional functionalities such as light sensing or light emission in a single device, making them attractive for various optoelectronic applications including nanoscale light sources and image-sensor arrays. Ambipolar OFETs based on a number of different materials have been reported. These include thermally evaporated small molecules, spin-coated poly(9,9-dioctylfluorene-*alt*-benzothiadiazole) (F8BT), single crystals of copper and iron phthalocyanines, solution-processed nickel dithiolenes, and spin-cast squaraines. One of the common features in several ambipolar polymers is the lower bandgap (<2 eV) compared to the corresponding unipolar semiconductors. This is the result of the typical (but not essential) donor–acceptor-like structure characterized by copolymerization of electron-rich and electron-poor heteroaromatic units. However, despite intensive research on ambipolar organic semiconductors and OFETs, the key material and device properties that enable ambipolar charge transport have been investigated to a much less extent than for unipolar charge transport.

1.6.1 Polymers

Sirringhaus *et al.* [238] reported the general observation of ambipolar charge transport in a series of regioregular polyselenophene-based polymers. The HOMO of polythiophenes has little contribution from the sulfur heteroatom, whereas the LUMO has significant electron density on the heteroatom [239]. Polyselenophenes were initially developed as promising alternatives to polythiophenes for OPV cell applications, mainly because of their reduced optical bandgaps. The regioregular polyselenophenes investigated in that work were poly(3-octyl)selenophene (**P93**, Figure 1.37) and poly(3,3″-di-*n*-alkylterselenophene) (**P94**, Figure 1.37). Two-dimensional, grazing-incidence wide-angle X-ray scattering (GIWAXS) indicated that the films were polycrystalline with the side-chain stacking mainly along the out-of-plane direction (perpendicular to the substrate) and π–π stacking in the in-plane direction. TG–BC TFT configurations with gold source–drain electrodes were employed for all polymers. Polymer **P94**

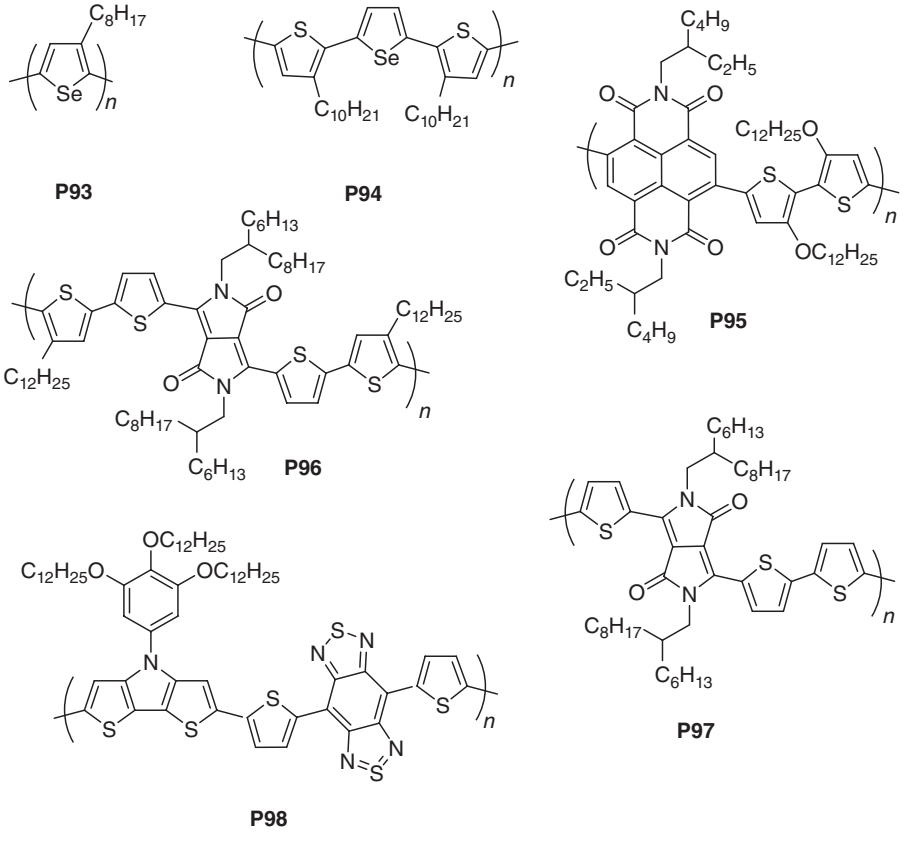

Figure 1.37 Chemical structure of ambipolar polymer semiconductors **P93–P98**.

showed clean ambipolar transport characteristics with similar hole and electron saturation and linear mobilities of >0.01 $cm^2 V^{-1} s^{-1}$ (PMMA as gate dielectric). While the saturation mobility values for holes and electrons were similar, some reversible hysteresis was systematically observed in the transfer characteristics in the electron transport regime but not in the hole transport regime, thus indicating the presence of a larger number of shallow traps for electrons than for holes. Using the same device configuration, TFTs based on **P93** exhibited ambipolar properties in as-spun films, with hole mobilities of ~0.02–0.09 $cm^2 V^{-1} s^{-1}$ and electron mobilities of ~0.004–0.009 $cm^2 V^{-1} s^{-1}$. Using **P94**, complementary-like inverters based on two identical TG–BC ambipolar transistors with a common gate as input and a common drain as output were fabricated, eliminating the need for semiconductor patterning. Despite the general fact that none of these TFTs cannot be fully switched off in such an inverter, the authors obtained very high gain in switching (absolute value as high as 86), much higher than the previously reported gain values in inverters composed of ambipolar OFETs [240].

Watson and Jenekhe *et al.* [241] reported a new naphthalenebiscarboximide-bithiophene copolymer semiconductor, **P95** (Figure 1.37), with an alternating donor–acceptor architecture consisting of electron-donating dialkoxybithiophene and electron-accepting naphthalene bisimide. High-mobility ambipolar transistors and high-gain complementary-like inverters were fabricated, which exhibited electron and hole mobilities as high as 0.04 and 0.003 $cm^2 V^{-1} s^{-1}$, respectively, and output voltage gains as high as 30. **P95**-based devices showed typical ambipolar features, such as a diode-like current increase with current saturation at high gate voltage in output curves and V-shaped transfer curves with a narrow off-state. However, the film annealing temperature (T_a = 100–250 °C) had notable effects on the ambipolar **P95** transistors. Figure 1.38a shows the

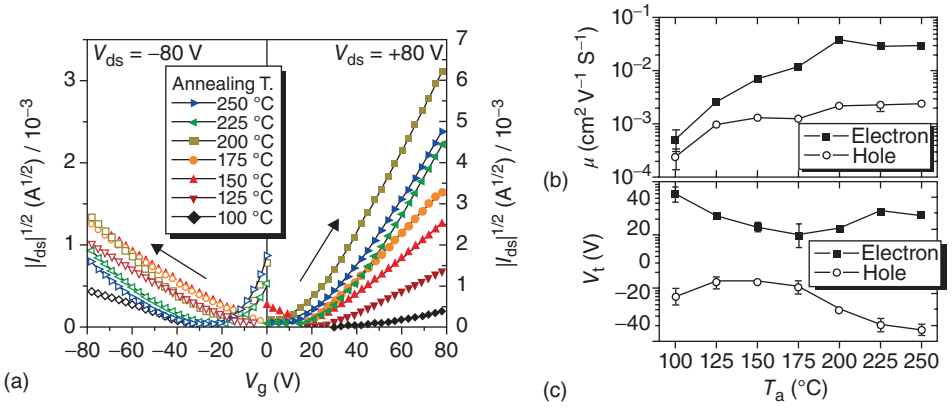

Figure 1.38 Ambipolar characteristics of **P95**. (a) Square-root of source–drain current versus gate voltage curves at various annealing temperatures (T_a). (b) Saturation mobility and (c) threshold voltage as a function of the annealing temperature [241]. (Reproduced with permission. Copyright © 2010, John Wiley & Sons, Inc.)

transfer curves of the ambipolar TFTs, $I_{SD}^{1/2}$ versus V_G, as a function of the annealing temperature T_a. The saturation electron and hole mobilities extracted from these transfer curves are shown in Figure 1.38b as a function of T_a. As T_a was increased from 100 to 200 °C, the mobility increased monotonically from $\sim 5 \times 10^{-4}$ to $\sim 0.03 - 0.04\,cm^2\,V^{-1}\,s^{-1}$ for electrons and from $\sim 2 \times 10^{-4}$ to $\sim 0.002 - 0.003\,cm^2\,V^{-1}\,s^{-1}$ for holes. About two orders of magnitude improvement in electron mobility was observed, while the hole mobility improved by 10 times. No significant change in the charge-carrier mobilities was observed for $T_a > 200$ °C. Unlike the carrier mobility and threshold voltage (Figure 1.38c), the current on/off ratios for the p- and n-channel operation were not affected by the annealing temperature.

Winnewisser *et al.* [74] reported on a new low-bandgap DPP-based polymer semiconductor (**P96**, Figure 1.37) with marked ambipolar charge-transport properties. Solution-processed devices using polymeric insulators (PVP (poly(vinyl pyrrolidone)) or PMMA) and an inorganic gate dielectric (octyltrichlorosilane-treated SiO_2) showed ambipolar behavior. The latter insulator resulted in the highest field-effect mobilities, reaching ~ 0.1 and up to $\sim 0.09\,cm^2\,V^{-1}\,s^{-1}$ for holes and electrons, respectively. These values are larger by an order of magnitude than the highest ones previously reported for solution-processed ambipolar transistors. Ambipolarity in this material is not limited to one particular transistor architecture but has been observed in five different configurations including transistors with solution-processed gate dielectrics in bottom-gate as well as top-gate structures. When driven under appropriate bias conditions, the ambipolar **P96** transistors emit near-infrared light. This was the first time that NIR light emission was reported for organic transistors with polymer gate dielectrics as well as for top-gate transistors (Figure 1.39). A similar structure, **P97** (Figure 1.37), was reported by Janssen *et al.* [242], which exhibited ambipolar transport with balanced electron and hole mobilities in the range of $\sim 0.01\,cm^2\,V^{-1}\,s^{-1}$, making it an interesting candidate for CMOS-like circuits.

To enable ambipolarity and simultaneously produce soluble low-bandgap polymers, Reynolds *et al.* [243] utilized the strong donor dithieno[3,2-*b*:2′,3′-*d*]pyrrole (DTP) functionalized with a trialkoxyphenyl group, combined with a strong acceptor based on benzo[1,2-*c*;4,5-*c*′]bis[1,2,5]thiadiazole (BBT) to produce the interesting polymer **P98** (Figure 1.37). This strategy provides a high-lying HOMO, planarity for π stacking, and solubility in the polymers due to the long-chain alkoxy substituents. This polymer is spray-processable and shows an optical bandgap of only 0.5 – 0.6 eV, which is the lowest value reported for a soluble polymer. In electrochemical cells, four differently colored redox states of the polymer can be accessed at moderate potentials and have good stability. This polymer also shows potential for use in ambipolar OFETs, with respectable mobilities of 1.2×10^{-3} and $5.8 \times 10^{-4}\,cm^2\,V^{-1}\,s^{-1}$ measured for p-channel and n-channel operation, respectively.

In a recent report by Pei *et al.* [244], ambipolar charge-transport behavior was observed for the first time in isoindigo-based donor – acceptor π-conjugated

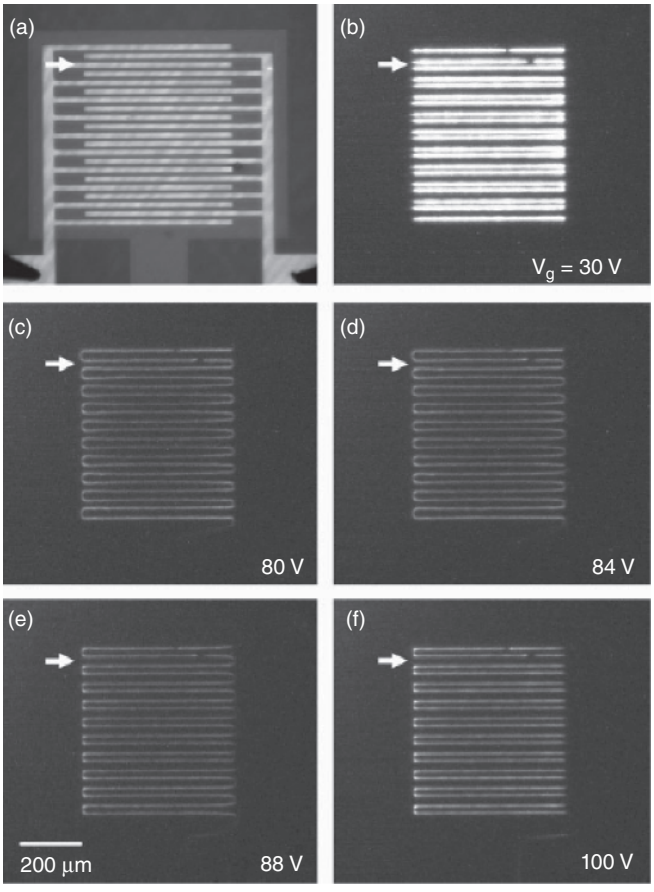

Figure 1.39 Microscopy images of an operating light-emitting bottom-gate FET. (a) Transistor with interdigitated source–drain electrodes under external illumination. The electrode fingers are 20 mm wide and the distance between them (i.e., the channel length *L*) is 10 mm. (b–f) NIR light emitted by the transistor when driven with $V_d = 140$ V (the drain electrode is the one contacted from the right side) and $V_g = 30$, 80, 84, 88, and 100 V, respectively. The camera settings were not changed during this series. The white arrow marks the position of the second source finger from the top [74]. (Reproduced with permission. Copyright © 2008, John Wiley & Sons, Inc.)

polymers. The new polymer **P99** (Figure 1.40) was synthesized with alternating fluorinated isoindigo and bithiophene units. As a result of fluorination, **P99** had an effectively lowered LUMO level (ΔLUMO = −0.2 eV), and the electron mobility increased from 10^{-2} to 0.43 $cm^2 V^{-1} s^{-1}$ in ambient compared to the non-fluorinated isoindigo-based polymers. The most impressive feature of **P99** is that it still maintains a high hole mobility of up to 1.85 $cm^2 V^{-1} s^{-1}$ in ambient (Figure 1.41). This polymer represents the first ambipolar polymer based on an isoindigo building block. GIXD and AFM studies indicated that the introduction

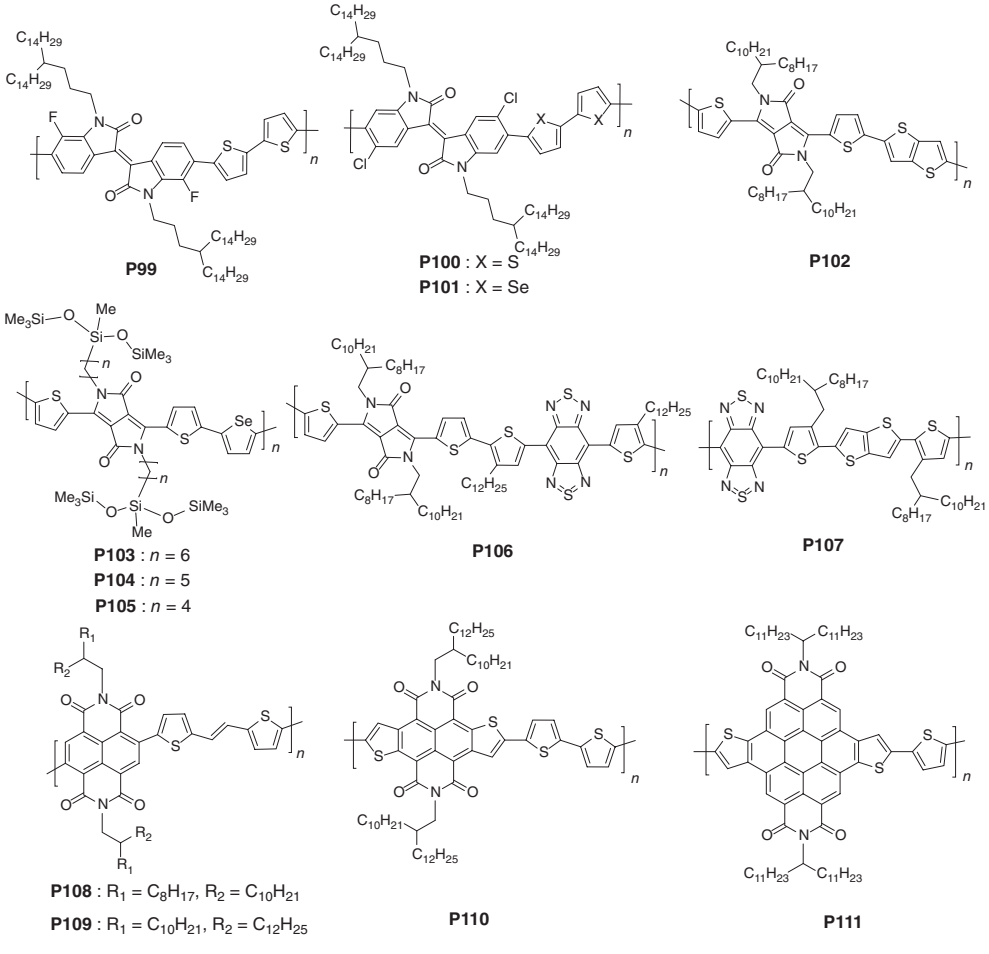

Figure 1.40 Chemical structure of ambipolar polymer semiconductors **P99–P111**.

of fluorine in an electron-deficient isoindigo core led to enhanced crystallinity with a different molecular packing. The structural influence of fluorine is based on the planarizing interaction of the fluorine on the isoindigo with the β-hydrogen on the bithiophene. The authors also believe that the strong crystallinity and dense, ordered packing of **P99** contributes to its improved ambient stability. The same group recently extended the halogenation strategy to chlorine atoms as well by developing an efficient chlorination reaction to engineer the isoindigo-based polymers [245]. Two new copolymers **P100** and **P101** containing a dichlorinated isoindigo unit as acceptor and bithiophene and biselenophene building blocks as donor were realized (Figure 1.40). Polymer FETs fabricated with the new ambipolar polymers in a TG–BC configuration showed high hole mobilities of up to 1.05 $cm^2 V^{-1} s^{-1}$ and balanced electron mobilities of up to 0.72 $cm^2 V^{-1} s^{-1}$. In addition, complementary-like inverters based on **P100** and **P101** showed

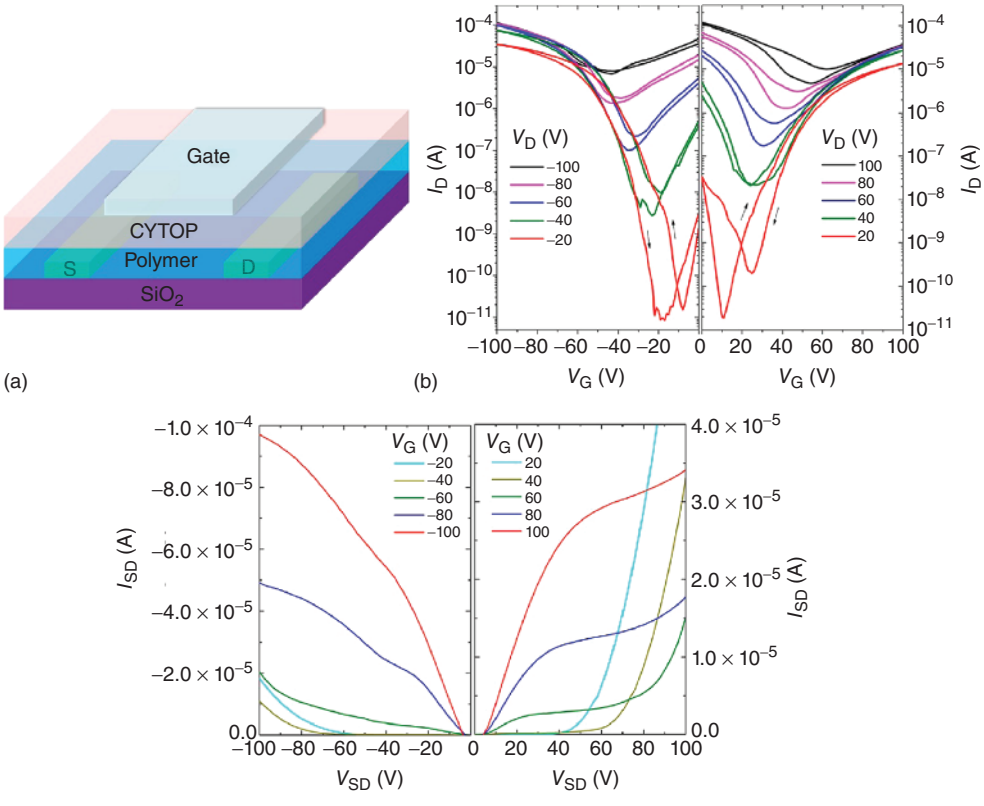

Figure 1.41 (a) Schematic diagram of a TG–BC OFET device structure based on **P99**. (b) The transfer and (c) output characteristics of **P99**-based devices fabricated in ambient. OFET devices ($L = 50\,\mu m$, $W = 1000\,\mu m$) were fabricated with CYTOP (500 nm thickness, $C_i = 3.7\,nF\,cm^{-2}$) [244]. (Reproduced with permission. Copyright © 2012, American Chemical Society.)

sharp signal-switching with high gains of up to 48. This report is the first study demonstrating that chlorination is an effective design strategy to tune the optoelectronic properties of semiconducting polymers and improve their device performances.

DPP-based donor–acceptor polymers have recently become very promising to demonstrate balanced and high ambipolar charge-transport characteristics. Ambipolarity of DPP-containing copolymers is attributed to their optimized molecular orbital architectures and energy levels, which enables donor and acceptor orbital hybridization and extends HOMO and LUMO distributions along the π backbone. Although the first DPP-based ambipolar polymer was reported with mobilities of 0.1 and $0.09\,cm^2\,V^{-1}\,s^{-1}$ for holes and electrons, respectively, much higher mobilities ($\geq 1\,cm^2\,V^{-1}\,s^{-1}$) were recently achieved with modified chemical structures [246]. In one of these reports, a DPP-based conjugated polymer, **P102** (Figure 1.40), was synthesized by Sirringhaus and

McCulloch *et al.* [247] with thiophene and thienothiophene comonomers. This polymer possesses proper HOMO (−5.33 eV) and LUMO (−4.07 eV) energy levels with a low bandgap of 1.26 eV, which enables efficient and balanced ambipolar charge injection and transport. As a result, ambipolar OFETs with high, balanced hole and electron mobilities of 1.4 – 1.6 $cm^2 V^{-1} s^{-1}$ were achieved upon careful optimization of the device architecture, charge injection, and polymer processing. In another recent study, Yang and coworkers developed a new polymer **P103** based on dithienyl-diketopyrrolopyrrole (TDPP) and selenophene building blocks with siloxane-terminated solubilizing groups (Figure 1.40) [248]. Extraordinarily high hole and electron mobilities of 3.97 and 2.20 $cm^2 V^{-1} s^{-1}$ with relatively well-balanced polarities were achieved for solution-sheared OFET devices made from **P103**. This ambipolar behavior is attributed to the synergistic combination of rational polymer backbone design, side-chain dynamics, and favorable solution processing. Additionally, in this study, CMOS-like inverters based on two identical ambipolar transistors of **P103** were fabricated, which yielded a gain of 18.0. Following this initial report, the same group demonstrated further improvement of charge-carrier mobilities based on **P103** π backbone via hybrid side-chain engineering [249]. In this study, two additional polymers (**P104** and **P105**) were synthesized with different alkyl spacer lengths to systematically study its effect on the ambipolar performance (Figure 1.40). The main goal was to induce denser molecular packing in polymer thin film and to facilitate charge transport through 3D conduction channels. Thin films of **P104** with pentyl spacers were found to exhibit the most optimized three-dimensional charge transport, yielding exceptionally high hole and electron mobilities of 8.84 and 4.34 $cm^2 V^{-1} s^{-1}$, respectively. In this study, it was found by GIXD characterizations that shorter alkyl spacer groups induced smaller lamellar spacing with a close π – π stacking distance compared to the longer chains, which led to enhanced charge transport in the as-prepared films (Figure 1.42). Additionally, the solution-shearing method resulted in dramatically improved performances compared to drop-casting technique as a result of improved alignment of the polymer grains. Charge-carrier mobility of **P104** currently represents the best ambipolar OFET performance reported to date with relatively well-balanced polarities.

Another promising acceptor building block, which was only recently incorporated into donor – acceptor polymers, is benzobisthiadiazole (BBT). BBT is a 14π electron system with a tetravalent sulfur atom. This core has a high electron affinity asbecause it generates a more stable Kekulé-type thiadiazole moiety upon accepting an electron. In the past few years, Wudl and Heeger *et al.* [250, 251] reported a family of BBT-based polymers with various donor spacers. The general observation was that ambipolar behavior is universal for these polymers owing to their very low band gaps and proper HOMO/LUMO energy levels. One of these polymers, **P106** (Figure 1.40), consists of two coupled acceptor units, that is, BBT and DPP, along with a thiophene-based donor moiety. This polymer exhibited excellent ambipolar transistor performance with mobilities exceeding 1 $cm^2 V^{-1} s^{-1}$ for both electrons and holes. In this polymer, the BBT moiety was

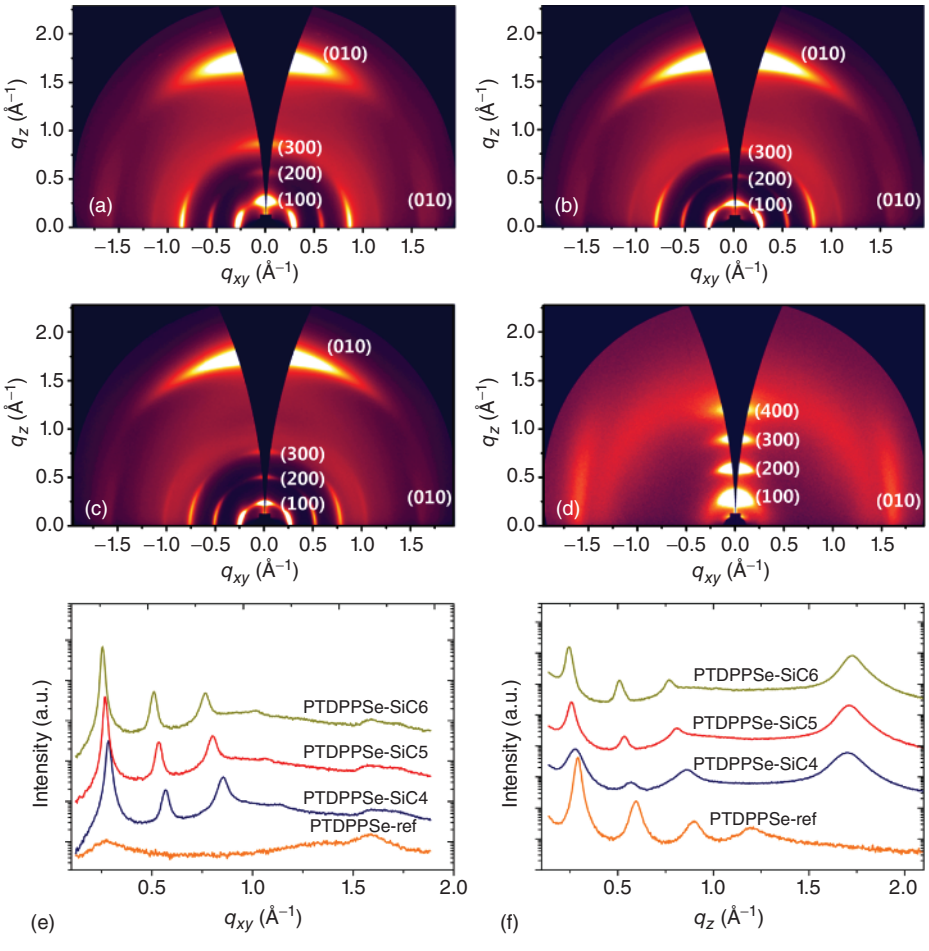

Figure 1.42 GIXD images of drop-cast TDPPSe-based copolymer films annealed at 220 °C. (a) **P105** (PTDPPSe-SiC4), (b) **P104** (PTDPPSe-SiC5), (c) **P103** (PTDPPSe-SiC6), and (d) TDPPSe-based copolymer containing 2-octyldodecyl chains (PTDPPSe-ref). The corresponding GIXD diffractogram profiles. (e) In-plane and (f) out-of-plane GIXD patterns [249]. (Reproduced with permission. Copyright © 2013, American Chemical Society.)

found to strengthen the interchain interactions providing higher thermal stability and higher OFET performance, compared to the reference polymers with no BBT unit. **P107** (Figure 1.40) is another recently synthesized ambipolar polymer containing a bi(thiophen-2-yl)-thieno[3,2-*b*]thiophene donor alternating with a BBT acceptor in the polymer backbone. This polymer exhibited an ultralow bandgap of 0.56 eV with HOMO and LUMO energy levels located at −4.36 and −3.80 eV, respectively, as a result of enhanced interactions between strong acceptor and strong donor units. This semiconducting polymer exhibited nearly balanced

electron and hole mobilities as high as 0.7 and 1.0 $cm^2 V^{-1} s^{-1}$, respectively, under an inert atmosphere. Inverters fabricated with only **P107**-based transistors exhibited a high gain of 35, which is much higher than values usually obtained for unipolar logic.

NDI is a well-known electron-deficient core with favorable optoelectronic properties, which has been successfully applied to high-performance n-channel polymer semiconductors. Nonetheless, there have been only a limited number of reports on its ambipolar behavior, especially in polymers with both electron and hole mobilities exceeding 0.1 $cm^2 V^{-1} s^{-1}$. Recently, Noh and Facchetti *et al.* [252] demonstrated that hole transport and injection for the well-known n-channel polymer P(NDI2OD-T2) could be significantly enhanced by using a fluorinated high-*k* dielectric (Figure 1.43). Balanced hole and electron mobilities of ~0.1 $cm^2 V^{-1} s^{-1}$ were obtained in the TG–BC device configuration. The observed hole mobility increase was attributed to the dielectric surface C–F dipoles and not to the bulk effects. In a parallel study, Liu and coworkers [253] reported the synthesis of two novel donor–acceptor copolymers **P108** and **P109** based on (NDI) acceptor and (*E*)-2-(2-(thiophen-2-yl)vinyl)thiophene (TVT) donor (Figure 1.40). The incorporation of a TVT unit into polymer backbone effectively promoted intermolecular π–π stacking and enhanced charge transport. Additionally, the HOMO level increased from −5.82 to −5.61 eV while the energy level of LUMO was maintained at −3.90 eV, thus facilitating both hole and electron injection/transport. TG–BC FETs fabricated with these polymers yielded high hole and electron mobilities of 0.30 and 1.57 $cm^2 V^{-1} s^{-1}$, respectively. This is among the best ambipolar performance reported to date in NDI-based polymers. Additionally, ambipolar inverters fabricated with **P108** exhibited a sharp signal switching with a high gain of 155 in ambient.

Recently, two new thiophene-fused, core-extended, diimide-based building blocks were reported in ambipolar semiconducting polymers [232, 254]. In these polymers **P110** and P111 (Figure 1.40), the acceptor units are thiophene-fused NDI and coronenediimide cores, respectively, while the donor units are based on electron-rich thiophene. These polymers showed small optical bandgaps (1.9–2.1 eV) with favorable HOMO and LUMO energy levels located at −5.6 and −3.7 to −4.4 eV, respectively. Solution-processed ambipolar OFETs have been demonstrated, yielding charge-carrier mobilities up to 0.30 $cm^2 V^{-1} s^{-1}$ (electron) and 0.1 $cm^2 V^{-1} s^{-1}$ (hole) for **P110**, and 0.30 $cm^2 V^{-1} s^{-1}$ (electron) and 0.04 $cm^2 V^{-1} s^{-1}$ (hole) for **P111**. Although these results are not among the best, it indicates that through rational design and synthesis, core-extended, π-conjugated, diimide-based building blocks are promising for ambipolar OFETs.

1.6.2 Small Molecules

Bao *et al.* reported the acene-based semiconductors **M89–M91** (Figure 1.44). Compound **M89** exhibited balanced ambipolar performance with a hole mobility of ~0.1 $cm^2 V^{-1} s^{-1}$ and electron mobility of 0.133 $cm^2 V^{-1} s^{-1}$ in nitrogen [255].

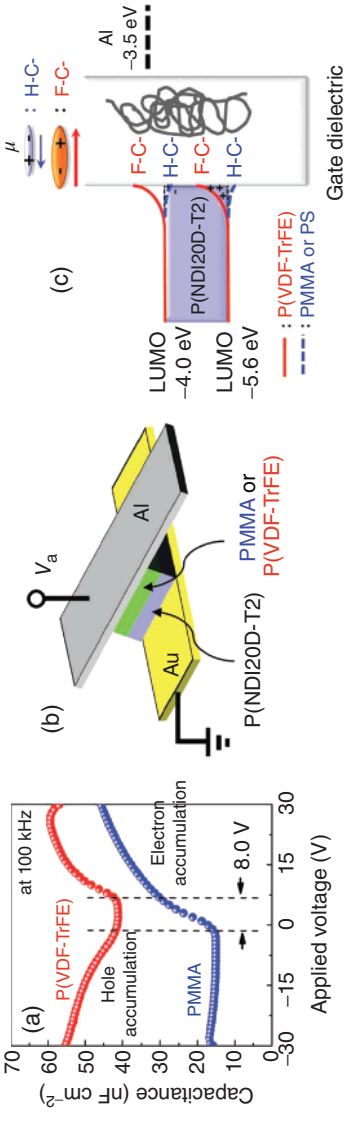

Figure 1.43 Capacitance versus voltage ($C-V$) characteristics at 100 kHz frequency for P(NDI2OD-T2)/PMMA and P(NDI2OD-T2)/P(VDF-TrFE) capacitors of the structure reported in (b). (c) Schematic description of the energy band diagram in the gate-to-channel direction from the source to the drain electrodes [252]. (Reproduced with permission. Copyright © 2012, John Wiley & Sons, Inc.)

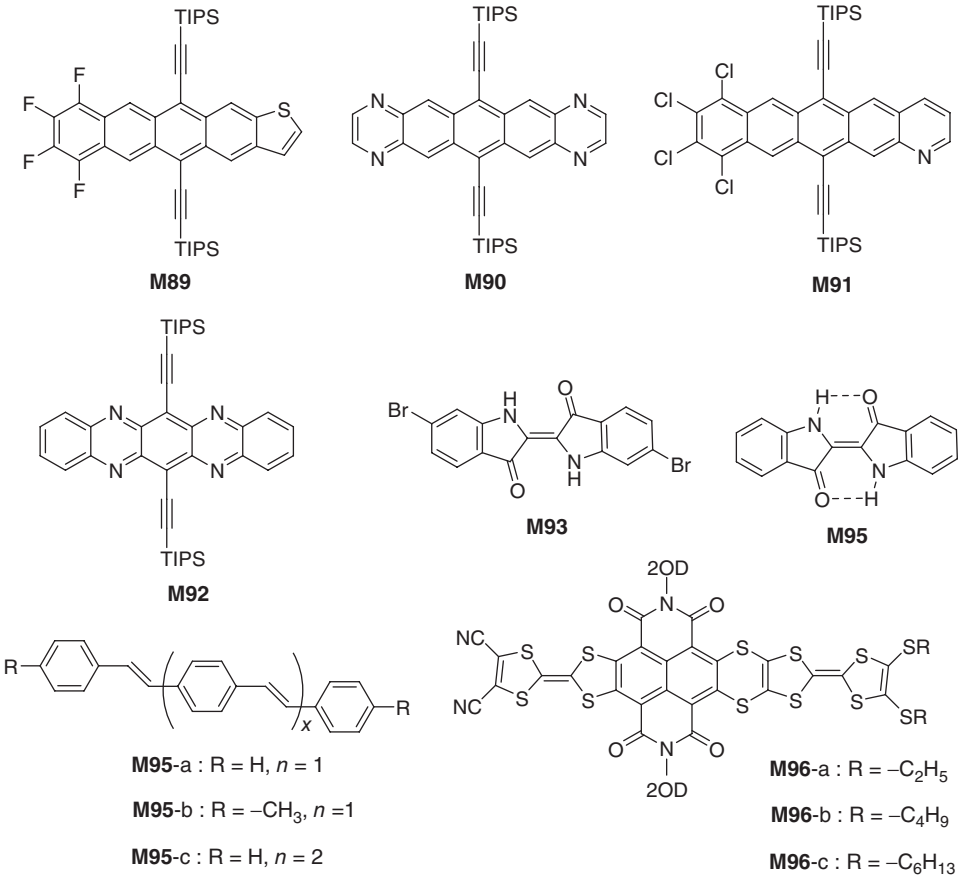

Figure 1.44 Chemical structure of ambipolar small-molecule semiconductors **M89**–**M96**.

M90 was reported as the constitutional isomer of **M92** with only a different position of the N atom [256]. **M92** (Figure 1.44) showed only high electron mobility while **M90** exhibited ambipolar performance with a hole mobility of $0.22\,cm^2\,V^{-1}\,s^{-1}$ and an electron mobility of $1.1\,cm^2\,V^{-1}\,s^{-1}$. Note that the high electron performance could only be obtained in vacuum, and when tested in ambient air, the electron mobility decreased to the range of $10^{-3}\,cm^2\,V^{-1}\,s^{-1}$ because of the electron trapping of oxygen or water. **M91** OFETs showed performance similar to that of **M89** [257]; An **M90**-based CMOS-like inverter with high gain up to 180 was also reported [258]. All these three acene-based semiconductors showed ambipolar performance only in vacuum or inert atmosphere because of their relatively high LUMO level. **M93** and **M94** were reported with similar chemical structures by the same group (Figure 1.44). They are a kind of natural material for ambipolar OFETs and circuits. **M93**- and **M94**-based OFET devices were fabricated on the natural resin shellac substrates, and Al was employed as gate electrode and AlO_x/tetratetracontane for dielectric layer.

Ambipolar performance was observed in vacuum, but after extensive exposure to air, n-channel performance showed deterioration in both **M93** and **M94** OFETs [259]. One interesting thing is that, apart from tetratetracontane, only evaporated polyethylene films allowed the observation of ambipolar transport in **M94**-based OFETs. **M94** did not show any semiconductor behavior on other investigated dielectrics, that is, poly(vinyl alcohol), shellac, melamine, adenine, and guanine, as well as plain aluminum oxide. Complementary-like inverter circuits were fabricated with both **M93** and **M94**, and the highest gain of 255 was obtained, which is one of the highest reported for organic ambipolar devices.

Single-crystal OFETs based on highly luminescent oligo(*p*-phenylenevinylene) derivatives **M95a–M95c** (Figure 1.44) were reported by Nakanotani *et al.* [260]. All the OFETs based on **M95a–M95c** showed ambipolar behavior, in which **M95c**-based OFETs exhibited balanced hole and electron mobilities both higher than 0.1 $cm^2 V^{-1} s^{-1}$. Intense electroluminescence was also observed in the channel of **M95c** single-crystal-based OFETs. **M96a–M96c** (Figure 1.44) are recently reported tetrathiafulvalene-fused NDI derivatives with a low LUMO energy level of −4.3 eV. Ambipolar behaviors were obtained for all the **M96a–M96c**-based OFETs in ambient air because of their low LUMO level [261]. However, the mobility was relatively low (about 10^{-4} $cm^2 V^{-1} s^{-1}$) for **M96a–M96c** OFETs. The highest mobilities of up to 0.03 and 0.003 $cm^2 V^{-1} s^{-1}$ were observed for holes and electrons, respectively, for **M96c**-based devices.

Wang and coworkers developed an ambient-stable, ambipolar, DPP-based oligomer **M97** with cyano terminal functionalities (Figure 1.45). **M97** was found to exhibit a very low bandgap of 1.48 eV with HOMO and LUMO energies of −5.45 and −3.74 eV, respectively. Bottom-gate/top-contact OFETs fabricated by solution-processing of **M97** exhibited hole and electron mobilities of 0.07 and 0.03 $cm^2 V^{-1} s^{-1}$, respectively, under ambient conditions [262]. This performance is currently among the highest for solution-processable, ambipolar, small-molecule semiconductors measured under ambient conditions. The authors also synthesized a reference oligomer without cyano groups, which exhibited only p-channel behavior. The ambient ambipolar characteristic of **M97** was attributed to its relatively low-lying LUMO and dense intermolecular packing.

In a recent study by Nishinaga and Kunugi *et al.* [263], a new sulfur-bridged tetra[2,3-thienylene] semiconductor (**M98**, Figure 1.45) with (triisopropylsilyl)ethynyl groups was synthesized and characterized in single-crystal FET devices. **M98** has a narrow HOMO–LUMO gap of 1.9 eV because of the antiaromatic cyclooctatetraene core. OFET devices based on **M98** single crystals exhibited ambipolar characteristics with hole and electron mobilities of up to 0.40 and 0.18 $cm^2 V^{-1} s^{-1}$, respectively. Different from the previous donor–acceptor approaches, ambipolarity of a small-molecule semiconductor was achieved for the first time with antiaromaticity. This is a novel and effective strategy to realize high and balanced ambipolar charge transport, because it does not lead to HOMO and LUMO localization on separate donor and acceptor units. Another example of an antiaromatic, small-molecule, ambipolar semiconductor,

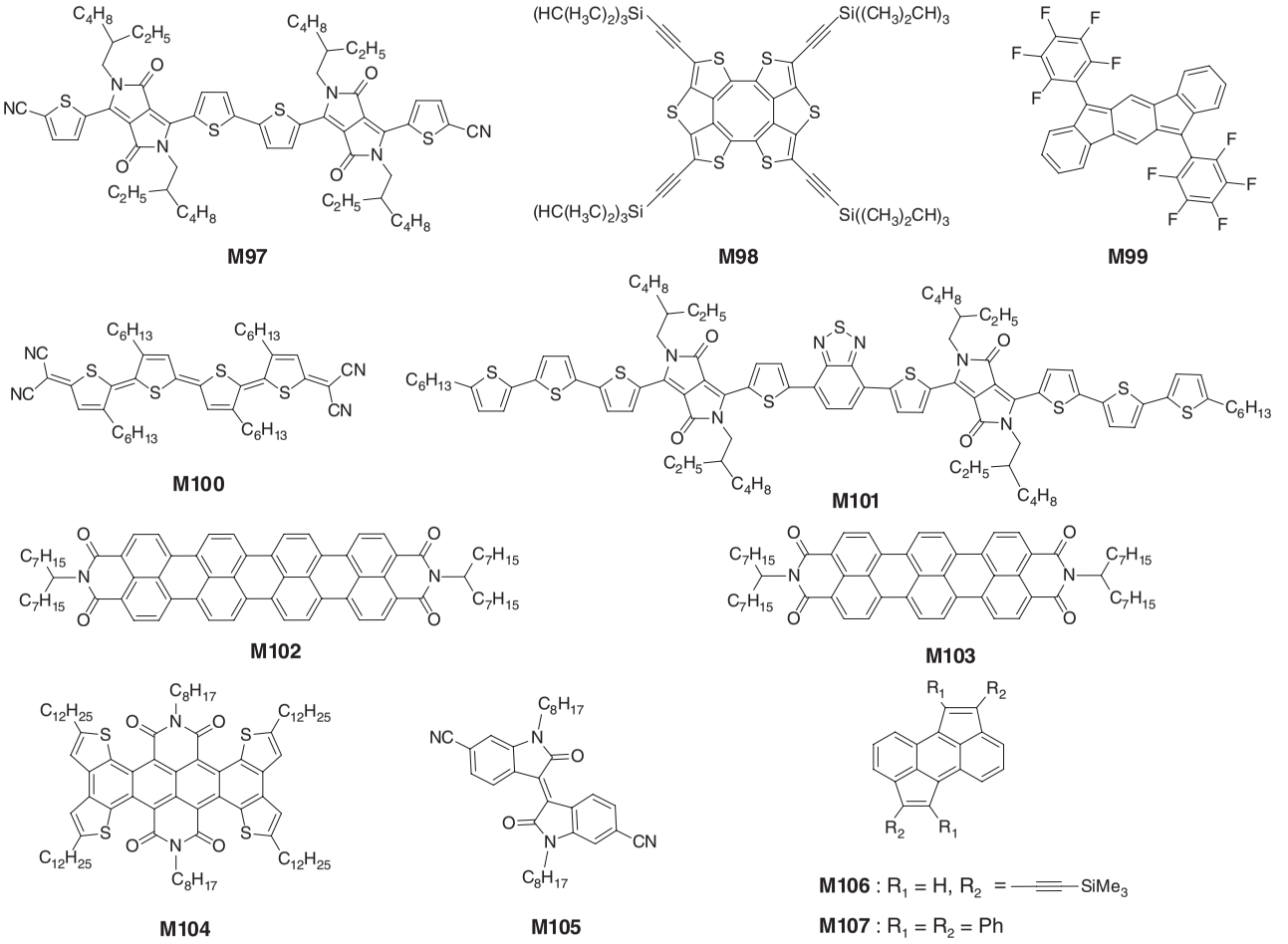

Figure 1.45 Chemical structure of ambipolar small-molecule semiconductors **M97**–**M107**.

which was recently reported by Haley and coworkers, is 6,12-diarylindeno[1,2-*b*]fluorene (IF). A single crystal of the pentafluorophenyl-substituted IF derivative **M99** (Figure 1.45) yielded ambipolar OFET devices with hole and electron mobilities of 7×10^{-4} and 3×10^{-3} $cm^2\ V^{-1}\ s^{-1}$, respectively [264].

Quinoidal oligothiophene derivatives have shown great promise for the realization of ambipolar OFETs. Aoyama *et al.* [265] reported high-performance, air-stable, solution-processed ambipolar **M100** (Figure 1.45) with hole and electron mobilities of 0.1 and 0.006 $cm^2\ V^{-1}\ s^{-1}$, respectively. This semiconductor exhibits an extremely low bandgap of ~0.9 eV in the solid state, which enables efficient injection of both charge-carrier types. The same group recently reported more optimized device structures with **M100**, which yielded more balanced hole and electron mobilities of 0.08 and 0.015 $cm^2\ V^{-1}\ s^{-1}$, respectively [266]. In this study, the relationship between OFET performance and semiconductor film thickness was explained on the basis of the effects of grain boundaries and contact resistances.

In another study by Nguyen *et al.* [267], ambipolar charge transport in a solution-processed thin film of newly synthesized bis-DPP compound, **M101** (Figure 1.45), was investigated with a low-work-function ($\Phi_m = 2.7$ eV) Ba electrode. **M101** includes two electron-accepting units, DPP and benzothiadiazole, along with thiophene-based donor units. Ambipolar OFETs fabricated with **M101** showed hole and electron mobilities of up to 0.016 and 0.015 $cm^2\ V^{-1}\ s^{-1}$, respectively. Thermal annealing at 150 °C was found to be critical to enhance field-effect mobilities of **M101** due to the formation of continuous grain boundaries with low surface roughness (Figure 1.46). Larger crystalline domain formation at 240 °C leads to discontinuous grain boundaries, which deteriorates charge-transport characteristics. Additionally, in **M101**-based OFET devices, electron injection was greatly enhanced by using low-work-function Ba contacts, leading to an improvement of electron current at the saturation regime.

Müllen *et al.* [268] utilized a discotic dye **M102** (Figure 1.45) as an ambipolar semiconductor in solution-processed OFETs. **M102** includes a quaterrylenediimide π backbone with swallow tails, and the design rationale was that the conjugation of perylenediimides was extended along the long axis to effectively increase the HOMO energy level without effecting the LUMO level. Hole and electron mobilities of ~10^{-3} $cm^2\ V^{-1}\ s^{-1}$ were obtained in solution-processed bottom-gate/bottom-contact OFETs. For this semiconductor, ambipolarity was found to be lost after a thermal treatment, which was attributed to a change in morphology. Another solution-processable, rylenediimide-based, ambipolar semiconductor, terrylenediimide **M103** (Figure 1.45), was developed by Müllen and Sirringhaus *et al.* [269]. When applied in a TG–BC OFET structure with a polycyclohexylethylene-based gate dielectric, **M103**-based devices exhibited ambipolar transport with electron and hole mobilities of 7.2×10^{-3} and 2.2×10^{-3} $cm^2\ V^{-1}\ s^{-1}$, respectively. Spin-coated, annealed **M103** films indicated a terraced crystalline microstructure with an "edge-on" molecular orientation, a favorable packing arrangement for charge transport in the plane of the film.

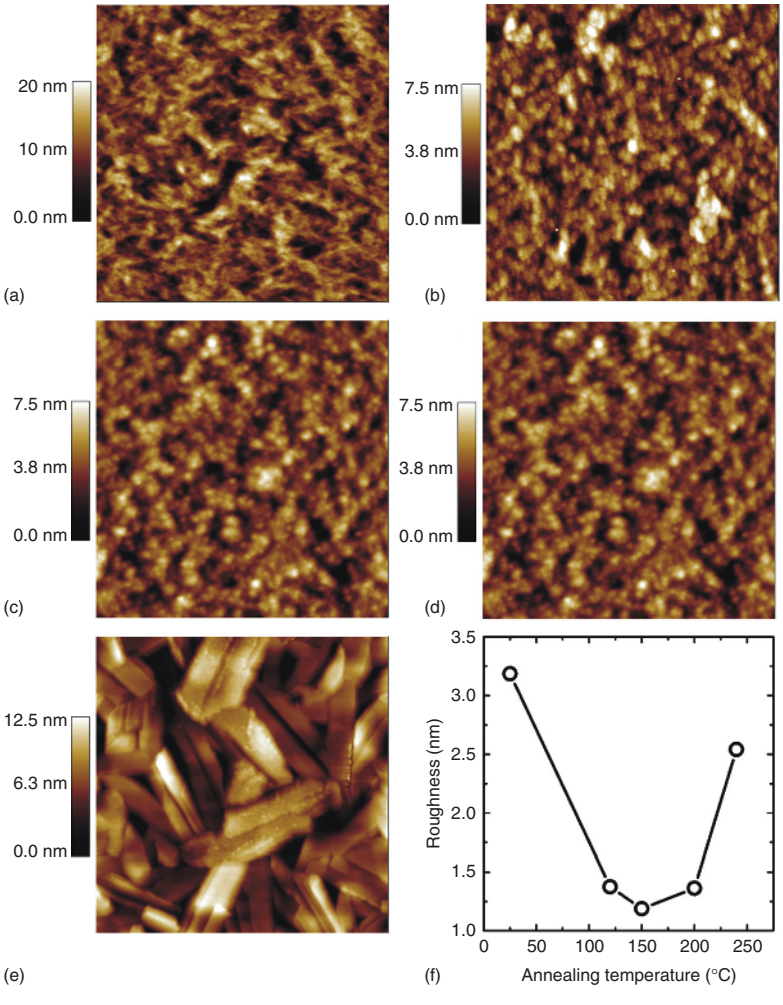

Figure 1.46 2 μm × 2 μm AFM topographic images of **M101** films prepared at different conditions. (a) As cast, and annealed at (b) 120 °C, (c) 150 °C, (d) 200 °C, and (e) 240 °C. (f) root-mean-square (RMS) film roughness versus the annealing temperature [267]. (Reproduced with permission. Copyright © 2012, John Wiley & Sons, Inc.)

The first successful synthesis of a tetrathienyl-fused tetracene diimide **M104** (Figure 1.45) was reported by Chi *et al.* [270] via a $FeCl_3$-mediated oxidative cyclodehydrogenation reaction. The design strategy was to make a core expansion from a smaller NDI building block with the aim of obtaining a low bandgap (1.52 eV) as a result of strong intramolecular donor–acceptor interactions. **M104** showed a liquid-crystalline behavior and ambipolar charge transport in thin-film FETs. The devices exhibited typical ambipolar behavior in ambient, with hole and electron mobilities approaching 10^{-3} cm^2 V^{-1} s^{-1} and I_{on}/I_{off} ratios of 10^3–10^4. It

is noteworthy that the hole transport of **M104** could only be obtained when the devices were measured in ambient, which indicated that it was most likely due to doping by molecular oxygen.

Solution-processed, small-molecule, bulk heterojunction (BHJ), ambipolar OTFTs were very recently reported by Chu *et al.* [271] based on a combination of two heteroacene-based p-channel small molecules and C_{60}. An optimized blending of two p-channel semiconductors with the n-channel semiconductor C_{60} results in an efficient charge-transport network with balanced hole and electron mobilities of 0.03 and 0.02 $cm^2\,V^{-1}\,s^{-1}$, respectively. Complementary-like inverter with a large transfer gain of 115 was achieved by using these blend-based ambipolar transistors.

Würthner and coworkers [272] recently reported a new core-cyanated isoindigo derivative **M105** (Figure 1.45) with a decreased LUMO level of −3.88 eV. The synthesis was achieved via palladium-catalyzed cyanation of a core-brominated isoindigo compound. As shown in Figure 1.47, the crystal structure of **M105** reveals a highly planar core adopting a favorable packing with face-to-face π−π contacts with a minimum interplanar spacing of 3.22 Å and hydrogen bonding between cyano and CH units (Figure 1.47c). OFET devices fabricated via vacuum deposition on pentadecylfluorooctadecylphosphonic acid (FOPA)-modified substrates exhibit ambipolar behavior with very good I_{on}/I_{off} ratios of 10^5-10^6 and electron and hole mobilities of 0.11 and 0.045 $cm^2\,V^{-1}\,s^{-1}$, respectively. However, only n-channel transport was observed with other self-assembled monolayers such as *n*-tetradecylphosphonic acid, which is most likely due to the absence of polarization of the active layer by the electronegative fluorine substituents of the FOPA.

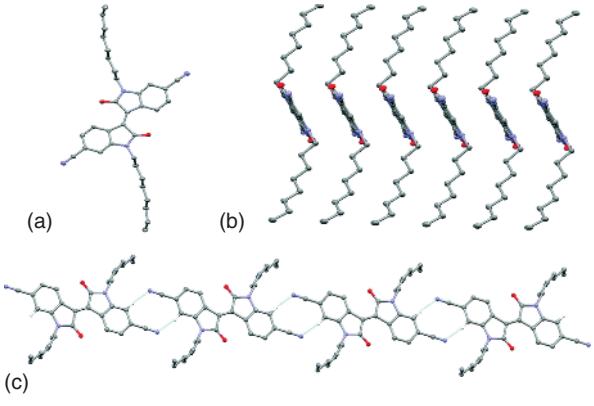

Figure 1.47 Molecular structure of **M105** (a) and solid-state packing (b,c). In (b), the one-dimensional face-to-face π−π stacking and in (c) the hydrogen bonding between cyano and CH groups are shown (the details for the C–H···N H-bonding are as follows: H···N 2.40 Å, C···N 3.3339(15) Å, and C–H···N 168°). Hydrogen atoms are partially omitted for clarity [272]. (Reproduced with permission. Copyright © 2014, The Royal Society of Chemistry.)

A new family of cyclopent[*hi*]aceanthrylene derivatives, which have a cyclopentadiene moiety to accept electrons, was synthesized by Miao *et al.* [273] as potential ambipolar semiconductors. Similar to fullerenes, cyclopenta-fused polycyclic aromatic hydrocarbons exhibit low LUMO energy levels because the five-membered ring tends to form aromatic cyclopentadienide structure (6π-electrons) by accepting one additional electron. **M106** and **M107** (Figure 1.45) are two examples of this family with low LUMO energy levels of about −3.6 eV and balanced HOMO levels of about −5.4 eV. OFET devices with thermally evaporated films of **M106** and **M107** as semiconductor layers exhibited ambipolar characteristics, and hole and electron mobilities as high as 0.21 and 0.10 $cm^2 V^{-1} s^{-1}$, respectively, were achieved. This study demonstrates that the incorporation of a cyclopentadiene unit into π-conjugated cores is an effective strategy to realize ambipolar charge transport.

1.7 Conclusions

In this chapter, we reviewed several first-generation and recently reported molecular and polymeric semiconductors for TFTs. It is now clear that during the last 2–3 years impressive performance, now approaching that of polycrystalline silicon, have been achieved. p-Channel semiconductors based on small molecules now achieve field-effect mobilities of ∼30 $cm^2 V^{-1} s^{-1}$, also when processed from solution. Polymeric p-channel TFTs have reached new heights, with hole mobilities unthinkable only few years back and surpassing 10 $cm^2 V^{-1} s^{-1}$. Implemented into a commercially relevant process, these materials could be useful in fabricating unipolar backplane arrays for electrophoretic as well as LCD and possibly OLED displays. The performance of n-channel semiconductors continues to lag behind that of p-channel devices, but small molecules have now demonstrated electron mobilities as high as 7 $cm^2 V^{-1} s^{-1}$ whereas polymers as high as ∼1 $cm^2 V^{-1} s^{-1}$. These results are encouraging for enabling the design of complementary circuits. Ambipolar semiconductors, where both hole and electron transport is promoted by the sign of the gate bias, have also experienced dramatic performance improvements, with balanced ambipolar mobilities surpassing 1 $cm^2 V^{-1} s^{-1}$. However, the stability and reproducibility of this performance remains an issue for practical application in, for example, CMOS and light-emitting transistors. All these results combined clearly demonstrate that electronics based on organic semiconductors will be part of a new generation of widely employed products.

References

1. (a) Farchioni, R. and Grosso, G. (eds) (2001) *Organic Electronic Materials: Conjugated Polymers and Low Molecular Weight Organic Solids*, Springer, Berlin; (b) Miller, L.S. and Mullin, J.B. (eds) (1991) *Electronic Materials: From Silicon to Organics*, Plenum Press, New York.

2. (a) Nalwa, H.S. (ed.) (1997) *Handbook of Organic Conductive Molecules and Polymers*, vol. 1-4, John Wiley & Sons, Ltd, Chichester; (b) Müllen, K. and Wegner, G. (eds) (1998) *Electronic Materials: The Oligomer Approach*, John Wiley & Sons, Inc, New York.
3. (a) Coughlin, J.E., Henson, Z.B., Welch, G.C., and Bazan, G.C. (2014) *Acc. Chem. Res.*, **47**, 257; (b) Heeger, A.J. (2014) *Adv. Mater.*, **26**, 10; (c) Dang, M.T., Hirsch, L., Wantz, G., and Wuest, J.D. (2013) *Chem. Rev.*, **113**, 3734; (d) Di, C.-A., Zhang, F., and Zhu, D. (2013) *Adv. Mater.*, **25**, 313; (e) Lee, S.S., Loth, M.A., Anthony, J.E., and Loo, Y.-L. (2012) *J. Am. Chem. Soc.*, **134**, 5436; (f) Natali, D. and Caironi, M. (2012) *Adv. Mater.*, **24**, 1357; (g) Baeg, K.-J., Khim, D., Kim, J., Yang, B.-D., Kang, M., Jung, S.-W., You, I.-K., Kim, D.-Y., and Noh, Y.-Y. (2012) *Adv. Funct. Mater.*, **22**, 2881; (h) Usta, H., Facchetti, A., and Marks, T.J. (2011) *Acc. Chem. Res.*, **44**, 501; (i) Beaujuge, P.M. and Fréchet, J.M.J. (2011) *J. Am. Chem. Soc.*, **133**, 20009; (j) Kelley, T.W., Baude, P.F., Gerlach, C., Ender, D.E., Muyres, D., Haase, M.A., Vogel, D.E., and Theiss, S.D. (2004) *Chem. Mater.*, **16**, 4413; (k) Forrest, S.R. (2004) *Nature*, **428**, 911; (l) Tsutsui, T. and Fujita, K. (2002) *Adv. Mater.*, **14**, 949; (m) Shaw, J.M. and Seidler, P.F. (2001) *IBM J. Res. Dev.*, **45**, 3.
4. (a) Cornil, J., Verlaak, S., Martinelli, N., Mityashin, A., Olivier, Y., Van Regemorter, T., D'Avino, G., Muccioli, L., Zannoni, C., Castet, F., Beljonne, D., and Heremans, P. (2013) *Acc. Chem. Res.*, **46**, 434; (b) Wang, C., Dong, H., Hu, W., Liu, Y., and Zhu, D. (2012) *Chem. Rev.*, **112**, 2208; (c) Rivnay, J., Mannsfeld, S.C.B., Miller, C.E., Salleo, A., and Toney, M.F. (2012) *Chem. Rev.*, **112**, 5488; (d) Saeki, A., Koizumi, Y., Aida, T., and Seki, S. (2012) *Acc. Chem. Res.*, **45**, 1193; (e) Figueira-Duarte, T.M. and Müllen, K. (2011) *Chem. Rev.*, **111**, 7260; (f) Mas-Torrent, M. and Rovira, C. (2011) *Chem. Rev.*, **111**, 4833; (g) Pingel, P., Zhu, L.P., Kue, S., Vogel, J.-O., Janietz, S., Kim, E.-G., Rabe, J.P., Bredas, J.-L., and Koch, N. (2010) *J. Phys. Chem. Lett.*, **1**, 2037; (h) Chang, H.-C., Ruden, P.P., Liang, Y., and Frisbie, C.D. (2010) *J. Appl. Phys.*, **107**, 104502/1; (i) Gutierrez Lezama, I. and Morpurgo, A.F. (2009) *Phys. Rev. Lett.*, **103**, 066803/1; (j) Bredas, J.-L., Norton, J.E., Cornil, J., and Coropceanu, V. (2009) *Acc. Chem. Res.*, **42**, 1691; (k) Troisi, A. (2010) *Adv. Polym. Sci.*, **223**, 259; (l) Choi, S.H., Risko, C., Ruiz Delgado, M.C., Kim, B.S., Bredas, J.-L., and Frisbie, C.D. (2010) *J. Am. Chem. Soc.*, **132**, 4358; (m) Liu, C. and Sirringhaus, H. (2010) *Org. Electron.*, **11**, 558.
5. (a) Sekitani, T. and Someya, T. (2010) *Adv. Mater.*, **22**, 2228; (b) Ma, H., Yip, H.-L., Huang, F., and Jen, A.K.-Y. (2010) *Adv. Funct. Mater.*, **20**, 1371; (c) Wu, W., Liu, Y., and Zhu, D. (2010) *Chem. Soc. Rev.*, **39**, 1489; (d) Ortiz, R.P., Yan, H., Facchetti, A., and Marks, T. (2010) *J. Mater.*, **3**, 1533; (e) Wen, Y. and Liu, Y. (2010) *Adv. Mater.*, **22**, 1331; (f) Lee, W.H., Cho, J.H., and Cho, K. (2010) *J. Mater. Chem.*, **20**, 2549; (g) Miozzo, L., Yassar, A., and Horowitz, G. (2010) *J. Mater. Chem.*, **20**, 2513; (h) Smith, J., Hamilton, R., McCulloch, I., Stingelin-Stutzmann, N., Heeney, M., Bradley, D.D.C., and Anthopoulos, T.D. (2010) *J. Mater. Chem.*, **20**, 2562; (i) Singh, M., Haverinen, H.M., Dhagat, P., and Jabbour, G.E. (2010) *Adv. Mater.*, **22**, 673; (j) Hoppe, A., Balster, T., Muck, T., and Wagner, V. (2009) in *Organic Electronics: Structural and Electronic Properties of OFETs* (ed. C., Wöll), Wiley-VCH Verlag GmbH & Co. KGaA, Weinheim, pp. 469–497, ISBN: 9783527408108; (k) Hamilton, R., Heeney, M., Anthopoulos, T., and McCulloch, I. (2010) Development of Polymer Semiconductors for Field-Effect Transistor Devices in *Organic Electronics: Materials, Processing, Devices and Applications*, (ed. So, F.) CRC Press, Boca Raton, FL, p. 393; (l) Kaake, L.G., Barbara, P.F., and Zhu, X.-Y. (2010) *J. Phys. Chem. Lett.*, **1**, 628; (m) Sirringhaus, H. (2009) *Adv. Mater.*, **21**, 3859; (n) Ortiz, R.P., Facchetti, A., and Marks, T. (2010) *J. Chem. Rev.*,

110, 205; (o) Yamashita, Y. (2009) *Chem. Lett.*, **38**, 870; (p) Ohshita, J. (2009) *Macromol. Chem. Phys.*, **210**, 1360; (q) Katz, H.E. and Huang, J. (2009) *Annu. Rev. Mater. Res.*, **39**, 71; (r) Di, C.-A., Liu, Y., Yu, G., and Zhu, D. (2009) *Acc. Chem. Res.*, **42**, 1573; (s) Roberts, M.E., Sokolov, A.N., and Bao, Z. (2009) *J. Mater. Chem.*, **19**, 3351; (t) DiBenedetto, S.A., Facchetti, A., Ratner, M.A., and Marks, T. (2009) *J. Adv. Mater.*, **21**, 1407; (u) Braga, D. and Horowitz, G. (2009) *Adv. Mater.*, **21**, 1473; (v) McCulloch, I., Heeney, M., Chabinyc, M.L., De Longchamp, D., Kline, R.J., Colle, M., Duffy, W., Fischer, D., Gundlach, D., Hamadani, B., Hamilton, R., Richter, L., Salleo, A., Shkunov, M., Sparrowe, D., Tierney, S., and Zhang, W. (2009) *Adv. Mater.*, **21**, 1091; (w) Zhan, X., Barlow, S., and Marder, S.R. (2009) *Chem. Commun.*, 1948; (x) Panzer, M.J. and Frisbie, C.D. (2008) *Adv. Mater.*, **20**, 3177; (y) de Boer, B. and Facchetti, A. (2008) *Polym. Rev.*, **48**, 423.

6. (a) Watanabe, M., Chen, K.-Y., Chang, Y.J., and Chow, T.J. (2013) *Acc. Chem. Res.*, **46**, 1606; (b) Bujak, P., Kulszewicz-Bajer, I., Zagorska, M., Maurel, V., Wielgus, I., and Pron, A. (2013) *Chem. Soc. Rev.*, **42**, 8895; (c) Jiang, W., Li, Y., and Wang, Z. (2013) *Chem. Soc. Rev.*, **42**, 6113; (d) Dong, H., Fu, X., Liu, J., Wang, Z., and Hu, W. (2013) *Adv. Mater.*, **25**, 6158; (e) Baeg, K.-J., Caironi, M., and Noh, Y.-Y. (2013) *Adv. Mater.*, **25**, 4210; (f) Zhao, Y., Guo, Y., and Liu, Y. (2013) *Adv. Mater.*, **25**, 5372; (g) Lin, Y., Fan, H., Li, Y., and Zhan, X. (2012) *Adv. Mater.*, **24**, 3087; (h) Lin, Y., Li, Y., and Zhan, X. (2012) *Chem. Soc. Rev.*, **41**, 4245; (i) Gaudiana, R. (2010) *J. Phys. Chem. Lett.*, **1**, 1288; (j) Giridharagopal, R. and Ginger, D.S. (2010) *J. Phys. Chem. Lett.*, **1**, 1160; (k) Steim, R., Kogler, F.R., and Brabec, C.J. (2010) *J. Mater. Chem.*, **20**, 2499; (l) Bredas, J.-L. and Durrant, J.R. (2009) *Acc. Chem. Res.*, **42**, 1689; (m) Nelson, J., Kwiatkowski, J.J., Kirkpatrick, J., and Frost, J.M. (2009) *Acc. Chem. Res.*, **42**, 1768; (n) Cheng, Y.-J., Yang, S.-H., and Hsu, C.-S. (2009) *Chem. Rev.*, **109**, 5868; (o) Heremans, P., Cheyns, D., and Rand, B.P. (2009) *Acc. Chem. Res.*, **42**, 1740; (p) Potscavage, W.J. Jr., Sharma, A., and Kippelen, B. (2009) *Acc. Chem. Res.*, **42**, 1758; (q) Roncali, J. (2009) *Acc. Chem. Res.*, **42**, 1719; (r) Chen, J. and Cao, Y. (2009) *Acc. Chem. Res.*, **42**, 1709; (s) Dennler, G., Scharber, M.C., and Brabec, C. (2009) *Adv. Mater.*, **21**, 1323; (t) Pagliaro, M., Ciriminna, R., and Palmisano, G. (2008) *ChemSusChem*, **1**, 880.
7. (a) *Organic Semiconductors and Devices* (Ed. G. Malliaras), John Wiley & Sons, Inc., Hoboken, NJ 2003; (b) Karl, N. (2003) *Synth. Met.*, **133–134**, 649.
8. (a) Sirringhaus, H. (2003) *Nat. Mater.*, **2**, 641; (b) Pron, A. and Rannou, P. (2002) *Prog. Polym. Sci.*, **27**, 135; (c) Cacialli, F. (2000) *Philos. Trans. R. Soc. London, Ser. A*, **358**, 173; (d) Kowalsky, W., Becker, E., Benstem, T., Johannes, H.-H., Metzdorf, D., Neuner, H., and Schobel, J. (2000) *Adv. Solid State Phys.*, **40**, 795; (e) Horowitz, G. (1990) *Adv. Mater.*, **2**, 287.
9. (a) Katz, H.E. (2004) *Chem. Mater.*, **16**, 4748; (b) Allard, S., Forster, M., Souharce, B., Thiem, H., and Scherf, U. (2008) *Angew. Chem. Int. Ed.*, **47**, 4070.
10. Hamilton, R., Bailey, C., Duffy, W., Heeney, M., Shkunov, M., Sparrowe, D., Tierney, S., McCulloch, I., Kline, R.J., DeLongchamp, D.M., and Chabinyc, M. (2006) *Proc. SPIE-Int. Soc. Opt. Eng.*, **6336**, 158.
11. (a) Klauk, H. (ed.) (2006) *Organic Electronics: Materials, Manufacturing, and Applications*, Wiley-VCH Verlag GmbH , Weinheim; (b) Crawford, G.P. (ed.) (2005) *Flexible Flat Panel Display*, John Wiley & Sons, Inc., New York; (c) Gamota, D., Brazis, P., Kalyanasumdaram, K., and Zhang, J. (eds) (2004) *Printed Organic and Molecular Electronics*, Kluwer Academic Publishers, Boston, MA.
12. Perepichka, I.F., Perepichka, D.F., Meng, H., and Wudl, F. (2005) *Adv. Mater.*, **17**, 2281.
13. Kline, R.J., McGehee, M.D., Kadnikova, E.N., Liu, J., Frechet, J.M.J., and Toney, M.F. (2005) *Macromolecules*, **38**, 3312.

14. Zen, A., Saphiannikova, M., Neher, D., Grenzer, J., Grigorian, S., Pietsch, U., Asawapirom, U., Janietz, S., Scherf, U., Lieberwirth, I., and Wegner, G. (2006) *Macromolecules*, **39**, 2162.
15. Zhang, R., Li, B., Iovu, M.C., Jeffries-EL, M., Sauve, G., Cooper, J., Jia, S., Tristram-Nagle, S., Smilgies, D.M., Lambeth, D.N., McCullough, R.D., and Kowalewski, T. (2006) *J. Am. Chem. Soc.*, **128**, 3480.
16. Chang, J.-F., Sun, B., Breiby, D.W., Nielsen, M.M., Soelling, T.I., Giles, M., McCulloch, I., and Sirringhaus, H. (2004) *Chem. Mater.*, **16**, 4772.
17. Majewski, L.A., Kingsley, J.W., Balocco, C., and Song, A.M. (2006) *Appl. Phys. Lett.*, **88**, 222108/1.
18. Surin, M., Leclere, P., Lazzaroni, R., Yuen, J.D., Wang, G., Moses, D., Heeger, A.J., Cho, S., and Lee, K. (2006) *J. Appl. Phys.*, **100**, 033712.
19. Jia, H., Gowrisanker, S., Pant, G.K., Wallace, R.M., and Gnade, B.E. (2006) *J. Vac. Sci. Technol., A*, **24**, 1228.
20. Kim, D.H., Jang, Y., Park, Y.D., and Cho, K. (2006) *J. Phys. Chem. B*, **110**, 15763.
21. Hoshino, S. *et al.* (2004) *J. Appl. Phys.*, **95**, 5088.
22. Park, Y.D., Kim, D.H., Jang, Y., Cho, J.H., Hwang, M., Lee, H.S., Lim, J.A., and Cho, K. (2006) *Org. Electron.*, **7**, 514.
23. Bao, Z., Feng, Y., Dodabalapur, A., Raju, V.R., and Lovinger, A.J. (1997) *Chem. Mater.*, **9**, 1299.
24. Ong, B.S., Wu, Y., Liu, P., and Gardner, S. (2004) *J. Am. Chem. Soc.*, **126**, 3378.
25. Chabinyc, M.L., Endicott, F., Vogt, B.D., DeLongchamp, D.M., Lin, E.K., Wu, Y., Liu, P., and Ong, B.S. (2006) *Appl. Phys. Lett.*, **88**, 113514/1.
26. Heeney, M., Bailey, C., Genevicius, K., Shkunov, M., Sparrowe, D., Tierney, S., and McCulloch, I. (2005) *J. Am. Chem. Soc.*, **127**, 1078.
27. McCulloch, I., Heeney, M., Bailey, C., Genevicius, K., MacDonald, I., Shkunov, M., Sparrowe, D., Tierney, S., Wagner, R., Zhang, W., Chabinyc, M.L., Kline, R.J., McGehee, M.D., and Toney, M.F. (2006) *Nat. Mater.*, **5**, 328.
28. DeLongchamp, D.M., Kline, R.J., Lin, E.K., Fischer, D.A., Richter, L.J., Lucas, L.A., Heeney, M., McCulloch, I., and Northrup, J.E. (2007) *Adv. Mater.*, **19**, 833.
29. Chua, L.-L., Ho, P.K.H., Sirringhaus, H., Friend, R.H. *et al.* (2004) *Adv. Mater.*, **16**, 1609.
30. Yan, H., Yoon, M.-H., Facchetti, A., and Marks, T.J. (2005) *Appl. Phys. Lett.*, **87**, 183501.
31. (a) Fielke, D., Huebler, A.C., Hahn, U., Brandt, N., Bartzsch, M., Fuegmann, U., Fischer, T., Veres, J., and Ogier, S. (2005) *Appl. Phys. Lett.*, **87**, 123508/1; (b) Veres, J., Ogier, S.D., Leeming, S.W., Cupertino, D.C., and Khaffaf, S.M. (2003) *Adv. Funct. Mater.*, **13**, 199.
32. Li, Y., Wu, Y., and Ong, B.S. (2006) *Macromolecules*, **39**, 6521.
33. Drolet, N., Morin, J.-F., Leclerc, N., Wakim, S., Tao, Y., and Leclerc, M. (2005) *Adv. Funct. Mater.*, **15**, 1671.
34. (a) Ogawa, K. and Rasmussen, S.C. (2003) *J. Org. Chem.*, **68**, 2921; (b) Ogawa, K., Stafford, J.A., Rothstein, S.D., Tallman, D.E., and Rasmussen, S.C. (2005) *Synth. Met.*, **152**, 137.
35. (a) Ogawa, K. and Rasmussen, S.C. (2006) *Macromolecules*, **39**, 1771; (b) Koeckelberghs, G. and Samyn, C. (2005) *Macromolecules*, **38**, 4545.
36. Liu, J., Zhang, R., Sauve, G., Kowalewski, T., and McCullough, R.D. (2008) *J. Am. Chem. Soc.*, **130**, 13167.
37. (a) Yamamoto, T., Kokubo, H., Kobashi, M., and Sakai, Y. (2004) *J. Mater. Chem.*, **16**, 4616; (b) Yamamoto, T., Arai, M., Kokubo, H., and Sasaki, S. (2003) *Macromolecules*, **36**, 7986; (c) Li, W., Katz, H., Lovinger, A., and Laquindanum, J. (1999) *Chem. Mater.*, **11**, 458.
38. Liu, J., Zhang, R., Osaka, I., Mishra, S., Javier, A.E., Smilgies, D., Kowalewski, T., and McCullough, R.D. (2009) *Adv. Funct. Mater.*, **19**, 3427.
39. (a) Fong, H.H., Pozdin, V.A., Amassian, A., Malliaras, G.G., Smilgies, D.-M., He, M., Gasper, S., Zhang, F., and Sorensen, M. (2008) *J. Am. Chem. Soc.*, **130**, 13202; (b) He, M., Li, J., Sorensen, M.L., Zhang, F., Hancock, R.R., Fong,

H.H., Pozdin, V.A., Smilgies, D.-M., and Malliaras, G.G. (2009) *J. Am. Chem. Soc.*, **131**, 11930.

40. He, M., Li, J., Tandia, A., Sorensen, M., Zhang, F., Fong, H.H., Pozdin, V.A., Smilgies, D., and Malliaras, G.G. (2010) *Chem. Mater.*, **22**, 2770.
41. Li, J., Qin, F., Li, C.M., Bao, Q., Chan-Park, M.B., Zhang, W., Qin, J., and Ong, B.S. (2008) *Chem. Mater.*, **20**, 2057.
42. Rieger, R., Beckmann, D., Pisula, W., Steffen, W., Kastler, M., and Mullen, K. (2010) *Adv. Mater.*, **22**, 83.
43. Prosa, T.J., Winokur, M.J., Moulton, J., Smith, P., and Heeger, A.J. (1992) *Macromolecules*, **25**, 4364.
44. Nakayama, J. and Fujimiri, T. (1991) *Heterocycles*, **32**, 991.
45. (a) Fu, Y., Cheng, H., and Elsenbaumer, R.L. (1997) *Chem. Mater.*, **9**, 1720; (b) Elandaloussi, E.H., Fre're, P., Richomme, P., Orduna, J., Garin, J., and Roncali, J. (1997) *J. Am. Chem. Soc.*, **119**, 10774.
46. (a) Payne, M., Parkin, S., Anthony, J., Kuo, C., and Jackson, T. (2005) *J. Am. Chem. Soc.*, **127**, 4986; (b) Stingelin-Stutzmann, N., Smits, E., Wondergem, H., Tanase, C., Blom, P., Smith, P., and de Leeuw, D.M. (2005) *Nat. Mater.*, **4**, 601; (c) Mathijssen, S.G.J., Cölle, M., Gomes, H., Smits, E.C.P., de Boer, B., McCulloch, I., Bobbert, P.A., and de Leeuw, D.M. (2007) *Adv. Mater.*, **19**, 2785; (d) Mathijssen, S.G.J., Kemerink, M., Sharma, A., Colle, M., Bobbert, P.A., Janssen, R.A.J., and de Leeuw, D.M. (2008) *Adv. Mater.*, **20**, 975; (e) Street, R.A., Chabinyc, M.L., Endicott, F., and Ong, B. (2006) *J. Appl. Phys.*, **100**, 114518; (f) Street, R.A., Salleo, A., and Chabinyc, M. (2003) *Phys. Rev. B*, **68**, 085316; (g) Salleo, A. and Street, R.A. (2004) *Phys. Rev. B*, **70**, 235324; (h) Salleo, A., Endicott, F., and Street, R.A. (2005) *Appl. Phys. Lett.*, **86**, 263505.
47. Tsukada, T. (2000) in *Technology and Applications of Amorphous Silicon*, vol. 37 (ed. R.A. Street), Springer-Verlag, Heidelberg, p. 49.
48. Kim, D.H., Lee, B., Moon, H., Kang, H.M., Jeong, E.J., Park, J., Han, K., Lee, S., Yoo, B.W., Koo, B.W., Kim, J.Y., Lee, W.H., Cho, K., Becerril, H.A., and Bao, Z. (2009) *J. Am. Chem. Soc.*, **131**, 6124.
49. (a) Yamamoto, T., Kokudo, H., Kobashi, M., and Sakai, Y. (2004) *Chem. Mater.*, **16**, 4616; (b) Kokudo, H., Sato, T., and Yamamoto, T. (2006) *Macromolecules*, **39**, 3959.
50. Osaka, I., Zhang, R., Sauve, G., Smilgies, D., Kowalewski, T., and McCullough, R.D. (2009) *J. Am. Chem. Soc.*, **131**, 2521.
51. (a) Jenekhe, S.A. and Osaheni, J.A. (1994) *Science*, **265**, 765; (b) Osaheni, J.A. and Jenekhe, S.A. (1995) *J. Am. Chem. Soc.*, **117**, 7389; (c) So, Y.-H., Zaleski, J.M., Murlick, C., and Ellaboudy, A. (1996) *Macromolecules*, **29**, 2783; (d) Mike, J.F., Makowski, A.J., and Jeffries-EL, M. (2008) *Org. Lett.*, **10**, 4915.
52. (a) Wolfe, J.F., Loo, B.H., and Arnold, F.E. (1981) *Macromolecules*, **14**, 915; (b) Choe, E.W. and Kim, S.N. (1981) *Macromolecules*, **14**, 920; (c) Roberts, M.F. and Jenekhe, S.A. (1993) *Chem. Mater.*, **5**, 1744; (d) Osaheni, J.A. and Jenekhe, S.A. (1995) *Chem. Mater.*, **7**, 672; (e) Osaheni, J.A. and Jenekhe, S.A. (1993) *Macromolecules*, **26**, 4726; (f) Alam, M.M. and Jenekhe, S.A. (2002) *Chem. Mater.*, **14**, 4775; (g) Jenekhe, S.A., Osaheni, J.A., Meth, J.S., and Vanherzeele, H. (1992) *Chem. Mater.*, **4**, 683; (h) Osaheni, J.A. and Jenekhe, S.A. (1992) *Chem. Mater.*, **4**, 1282; (i) Dotrong, M., Mehta, R., Balchin, G.A., Tomlinson, R.C., Sinsky, M., Lee, C.Y.C., and Evers, R.C.J. (1993) *Polym. Sci., Part A*, **31**, 723.
53. (a) Babel, A. and Jenekhe, S.A. (2002) *J. Phys. Chem. B*, **106**, 6129; (b) Babel, A. and Jenekhe, S.A. (2003) *J. Am. Chem. Soc.*, **125**, 13656.
54. (a) Pang, H., Vilela, F., Skabara, P.J., McDouall, J.J.W., Crouch, D.J., Anthopoulos, T.D., Bradley, D.D.C., de Leeuw, D., Horton, P.N., and Hursthouse, M.B. (2007) *Adv. Mater.*, **19**, 4438; (b) Mamada, M., Nishida, J.-I., Tokito, S., and Yamashita, Y. (2008) *Chem. Lett.*, **37**, 766.
55. Zhang, W., Smith, J., Hamilton, R., Heeney, M., Kirkpatrick, J., Song, K., Watkins, S.E., Anthopoulos, T., and

McCulloch, I. (2009) *J. Am. Chem. Soc.*, **131**, 10814.

56. Zhang, W., Smith, J., Watkins, S.W., Gysel, R., McGehee, M., Salleo, A., Kirkpatrick, J., Ashraf, S., Anthopoulos, T., Heeney, M., and McCulloch, I. (2010) *J. Am. Chem. Soc.*, **132**, 11437.
57. (a) Usta, H., Lu, G., Facchetti, A., and Marks, T.J. (2006) *J. Am. Chem. Soc.*, **128**, 9034–9035; (b) Usta, H., Facchetti, A., and Marks, T.J. (2008) *J. Am. Chem. Soc.*, **130**, 8580–8581.
58. Beaujuge, P.M., Tsao, H.N., Hansen, M.R., Amb, C.M., Risko, C., Subbiah, J., Choudhury, K.R., Mavrinskiy, A., Pisula, W., Brédas, J.-L., So, F., Müllen, K., and Reynolds, J.R. (2012) *J. Am. Chem. Soc.*, **134**, 8944–8957.
59. Mondal, R., Miyaki, N., Becerril, H.A., Norton, J.E., Parmer, J., Mayer, A.C., Tang, M.L., Bredas, J.-L., McGehee, M.D., and Bao, Z. (2009) *Chem. Mater.*, **21**, 3618.
60. (a) Takimiya, K., Ebata, H., Sakamoto, K., Izawa, T., Otsubo, T., and Kunugi, Y. (2006) *J. Am. Chem. Soc.*, **128**, 12604; (b) Ebata, H., Izawa, T., Miyazaki, E., Takimiya, K., Ikeda, M., Kuwabara, H., and Yui, T. (2007) *J. Am. Chem. Soc.*, **129**, 15732.
61. Osaka, I., Abe, T., Shinamura, S., Miyazaki, E., and Takimiya, K. (2010) *J. Am. Chem. Soc.*, **132**, 5000.
62. Shinamura, S., Miyazaki, E., and Takimiya, K. (2010) *J. Org. Chem.*, **75**, 1228.
63. Yang, C., Cho, S., Chiechi, R.C., Walker, W., Coates, N.E., Moses, D., Heeger, A.J., and Wudl, F. (2008) *J. Am. Chem. Soc.*, **130**, 16524.
64. Guo, X., Kim, F.S., Jenekhe, S.A., and Watson, M.D. (2009) *J. Am. Chem. Soc.*, **131**, 7206–7207.
65. (a) Bleiholder, C., Gleiter, R., Werz, D.B., and Koeppel, H. (2007) *Inorg. Chem.*, **46**, 2249; (b) Pomerantz, M. (2003) *Tetrahedron Lett.*, **44**, 1563; (c) Irvin, J.A., Schwendeman, I., Lee, Y., Abboud, K.A., and Reynolds, J.R. (2001) *J. Polym. Sci. A: Polym. Chem.*, **39**, 2164; (d) Cloutier, R. and Leclerc, M. (1991) *J. Chem. Soc., Chem. Commun.*, 1194; (e) Vangheluwe, M., Verbiest, T., and Koeckelberghs, G. (2008) *Macromolecules*, **41**, 1041.
66. (a) Thompson, B.C., Kim, Y.G., McCarley, T.D., and Reynolds, J.R. (2006) *J. Am. Chem. Soc.*, **128**, 12714; (b) Roncali, J. (1997) *Chem. Rev.*, **97**, 173.
67. FitzHugh, E.W. (ed.) (1997) *Artists' Pigments: A Handbook of Their History and Characteristics*, vol. 3, Oxford University Press, New York.
68. Stalder, R., Mei, J., and Reynolds, J.R. (2010) *Macromolecules*, **43**, 8348.
69. Wang, E., Ma, Z., Zhang, Z., Vandewal, K., Henriksson, P., Inganäs, O., Zhang, F., and Andersson, M.R. (2011) *J. Am. Chem. Soc.*, **133**, 14244.
70. Lei, T., Cao, Y., Fan, Y., Liu, C.-J., Yuan, S.-C., and Pei, J. (2011) *J. Am. Chem. Soc.*, **133**, 6099.
71. Mei, J., Kim, D.H., Ayzner, A.L., Toney, M.F., and Bao, Z. (2011) *J. Am. Chem. Soc.*, **133**, 20130.
72. Holliday, S., Donaghey, J.E., and McCulloch, I. (2014) *Chem. Mater.*, **26**, 647.
73. Lei, T., Dou, J.-H., and Pei, J. (2012) *Adv. Mater.*, **24**, 6457.
74. Burgi, L., Turbiez, M., Pfeiffer, R., Bienewald, F., Kirner, H.-J., and Winnewisser, C. (2008) *Adv. Mater.*, **20**, 2217.
75. (a) Li, Y., Sonar, P., Singh, S.P., Soh, M.S., Meurs, M.v., and Tan, J. (2011) *J. Am. Chem. Soc.*, **133**, 2198; (b) Zhang, X., Richter, L.J., DeLongchamp, D.M., Kline, R.J., Hammond, M.R., McCulloch, I., Heeney, M., Ashraf, R.S., Smith, J.N., Anthopoulos, T.D., Schroeder, B., Geerts, Y.H., Fischer, D.A., and Toney, M.F. (2011) *J. Am. Chem. Soc.*, **133**, 15073; (c) Ha, J.S., Kim, K.H., and Choi, D.H. (2011) *J. Am. Chem. Soc.*, **133**, 10364; (d) Bronstein, H., Chen, Z., Ashraf, R.S., Zhang, W., Du, J., Durrant, J.R., Tuladhar, P.S., Song, K., Watkins, S.E., Geerts, Y., Wienk, M.M., Janssen, R.A.J., Anthopoulos, T., Sirringhaus, H., Heeney, M., and McCulloch, I. (2011) *J. Am. Chem. Soc.*, **133**, 3272.
76. Li, J., Zhao, Y., Tan, H.S., Guo, Y., Di, C.-A., Yu, G., Liu, Y., Lin, M., Lim,

S.H., Zhou, Y., Su, H., and Ong, B.S. (2012) *Sci. Rep.*, **2**, 754.

77. Kang, I., Yun, H.-J., Chung, D.S., Kwon, S.-K., and Kim, Y.-H. (2013) *J. Am. Chem. Soc.*, **135**, 14896.
78. Li, Y., Sonar, P., Murphy, L., and Hong, W. (2013) *Energy Environ. Sci.*, **6**, 1684.
79. Li, Y., Sonar, P., Singh, S.P., Zeng, W., and Soh, M.S. (2011) *J. Mater. Chem.*, **21**, 10829.
80. Nielsen, C.B., Turbiez, M., and McCulloch, I. (2013) *Adv. Mater.*, **25**, 1859.
81. Yi, Z., Ma, L., Chen, B., Chen, D., Chen, X., Qin, J., Zhan, X., Liu, Y., Ong, W.J., and Li, J. (2013) *Chem. Mater.*, **25**, 4290.
82. Zhang, M., Tsao, H.N., Pisula, W., Yang, C., Mishra, A.K., and Müllen, K. (2007) *J. Am. Chem. Soc.*, **129**, 3472.
83. Tsao, H.N., Cho, D.M., Park, I., Hansen, M.R., Mavrinskiy, A., Yoon, D.Y., Graf, R., Pisula, W., Spiess, H.W., and Müllen, K. (2011) *J. Am. Chem. Soc.*, **133**, 2605.
84. Fan, J., Yuen, J.D., Cui, W., Seifter, J., Mohebbi, A.R., Wang, M., Zhou, H., Heeger, A., and Wudl, F. (2012) *Adv. Mater.*, **24**, 6164.
85. Wu, Q., Wang, M., Qiao, X., Xiong, Y., Huang, Y., Gao, X., and Li, H. (2013) *Macromolecules*, **46**, 3887.
86. Kim, J., Lim, B., Baeg, K.-J., Noh, Y.-Y., Khim, D., Jeong, H.-G., Yun, J.-M., and Kim, D.-Y. (2011) *Chem. Mater.*, **23**, 4663.
87. Hajlaoui, R., Horowitz, G., Garnier, F., Arce-Brouchet, A., Laigre, L., El Kassmi, A., Demanze, F., and Kouki, F. (1997) *Adv. Mater.*, **9**, 389.
88. Dodabalapur, A., Torsi, L., and Katz, H.E. (1995) *Science*, **268**, 270.
89. Hajlaoui, R., Fichou, D., Horowitz, G., Nessakh, B., Constant, M., and Garnier, F. (1997) *Adv. Mater.*, **9**, 557.
90. (a) Garnier, F., Horowitz, G., Fichou, D., and Yassar, A. (1996) *Synth. Met.*, **81**, 163; (b) Fichou, D., Horowitz, G., and Garnier, F. (1992) *Mol. Cryst. Liq. Cryst. Sci. Technol., Sect. A*, **217**, 193.
91. (a) Lovinger, A.J., Davis, D.D., Dodabalapur, A., and Katz, H.E. (1996) *Chem. Mater.*, **8**, 2836; (b) Lovinger, A.J., Davis, D.D., Dodabalapur, A., Katz, H.E., and Torsi, L. (1996) *Macromolecules*, **29**, 4952.
92. (a) Katz, H.E., Bao, Z., and Gilat, S.L. (2001) *Acc. Chem. Res.*, **34**, 359; (b) Fichou, D., Teulade-Fichou, M.P., Horowitz, G., and Demanze, F. (1997) *Adv. Mater.*, **9**, 75; (c) Horowitz, G., Garnier, F., Yassar, A., Hajlaoui, R., and Kouki, F. (1996) *Adv. Mater.*, **8**, 52; (d) Katz, H.E., Torsi, L., and Dodabalapur, A. (1995) *Chem. Mater.*, **7**, 2235.
93. (a) Nagamatsu, S., Kaneto, K., Azumi, R., Matsumoto, M., Yoshida, Y., and Yase, K. (2005) *J. Phys. Chem. B*, **109**, 9374; (b) Horowitz, G., Peng, X.Z., Fichou, D., and Garnier, F. (1991) *J. Mol. Electron.*, **7**, 85.
94. Ostoja, P., Maccagnani, P., Gazzano, M., Cavallini, M., Kengne, J.C., Kshirsagar, R., Biscarini, F., Melucci, M., Zambianchi, M., and Barbarella, G. (2004) *Synth. Met.*, **146**, 243.
95. Hajlaoui, M.E., Garnier, F., Hassine, L., Kouki, F., and Bouchriha, H. (2002) *Synth. Met.*, **129**, 215.
96. Loi, M.A., Da Como, E., Dinelli, F., Murgia, M., Zamboni, R., Biscarini, F., and Muccini, M. (2005) *Nat. Mater.*, **4**, 81.
97. Dinelli, F., Murgia, M., Levy, P., Cavallini, M., Biscarini, F., and de Leeuw, D.M. (2004) *Phys. Rev. Lett.*, **92**, 116802/1.
98. (a) Waragai, K., Akimichi, H., Hotta, S., Kano, H., and Sakaki, H. (1993) *Synth. Met.*, **57**, 4053; (b) Waragai, K., Akimichi, H., Hotta, S., Kano, H., and Sakaki, H. (1995) *Phys. Rev. B*, **52**, 1786.
99. (a) Garnier, F., Hajlaoui, R., El Kassmi, A., Horowitz, G., Laigre, L., Porzio, W., Armanini, M., and Provasoli, F. (1998) *Chem. Mater.*, **10**, 3334; (b) Katz, H.E., Lovinger, A.J., and Laquindanum, J.G. (1998) *Chem. Mater.*, **10**, 457.
100. Li, W., Katz, H.E., Lovinger, A.J., and Laquindanum, J.G. (1999) *Chem. Mater.*, **11**, 458.127.
101. (a) Facchetti, A., Yoon, M.-H., Hutchison, G.R., Stern, C.L., Ratner, M.A., and Marks, T.J. (2004) *J. Am. Chem. Soc.*, **126**, 13480–13501; (b) Facchetti, A., Mushrush, M., Yoon, M.-H., Hutchison, G.R., Ratner, M.A., and

Marks, T.J. (2004) *J. Am. Chem. Soc.*, **126**, 13859–13874.

102. (a) Katz, H.E., Dodabalapur, A., Torsi, L., and Elder, D. (1995) *Chem. Mater.*, **7**, 2238; (b) Horowitz, G., Deloffre, F., Garnier, F., Hajlaoui, R., Hmyene, M., and Yassar, A. (1993) *Synth. Met.*, **54**, 435; (c) Garnier, F., Hajlaoui, R., Yassar, A., and Srivastava, P. (1994) *Science*, **265**, 1684.
103. Dimitrakopoulos, C.D., Furman, B.K., Graham, T., Hegde, S., and Purushothaman, S. (1998) *Synth. Met.*, **92**, 47.
104. (a) Hotta, S. and Lee, S.A. (1999) *Synth. Met.*, **101**, 551; (b) Dingemans, T.J., Bacher, C.J., Thelakkat, M., Pederson, L.G., Samulski, E.T., and Schimidt, H.-W. (1999) *Synth. Met.*, **105**, 171.
105. (a) Mohapatra, S., Holmes, B.T., Newman, C.R., Prendergast, C.F., Frisbie, C.D., and Ward, M.D. (2004) *Adv. Funct. Mater.*, **14**, 605; (b) Yanagi, H., Araki, Y., Ohara, T., Hotta, S., Ichikawa, M., and Taniguchi, Y. (2003) *Adv. Funct. Mater.*, **13**, 767; (c) Casado, J., Ruiz Delgado, M.C., Shirota, Y., Hernandez, V., and Lopez Navarrete, J.T. (2003) *J. Phys. Chem. B*, **107**, 2637; (d) Ichikawa, M., Yanagi, H., Shimizu, Y., Hotta, S., Suganuma, N., Koyama, T., and Taniguchi, Y. (2002) *Adv. Mater.*, **14**, 1272; (e) Apperloo, J.J., Groenendaal, L.B., Verheyen, H., Jayakannan, M., Janssen, R.A.J., Dkhissi, A., Beljonne, D., Lazzaroni, R., and Bredas, J.-L. (2002) *Chemistry*, **8**, 2384; (f) Moreno Castro, C., Ruiz Delgado, M.C., Hernandez, V., Hotta, S., Casado, J., and Lopez Navarrete, J.T. (2002) *J. Phys. Chem. B*, **116**, 10419; (g) Lee, S.A., Yoshida, Y., Fukuyama, M., and Hotta, S. (1999) *Synth. Met.*, **106**, 39.
106. (a) Hotta, S. and Katagiri, T. (2003) *J. Heterocycl. Chem.*, **40**, 845; (b) Hotta, S., Kimura, H., Lee, S.A., and Tamaki, T. (2000) *J. Heterocycl. Chem.*, **37**, 281; (c) Hotta, S., Lee, S.A., and Tamaki, T. (2000) *J. Heterocycl. Chem.*, **37**, 25.
107. (a) Yanagi, H., Yoshiki, A., Hotta, S., and Kobayashi, S. (2004) *J. Appl. Phys.*, **96**, 4240; (b) Ichikawa, M., Hibino, R., Inoue, M., Haritani, T., Hotta, S., Koyama, T., and Taniguchi, Y. (2003) *Adv. Mater.*, **15**, 213; (c) Nagawa, M., Hibino, R., Hotta, S., Yanagi, H., Ichikawa, M., Koyama, T., and Taniguchi, Y. (2002) *Appl. Phys. Lett.*, **80**, 544; (d) Kim, Y.C., Lee, T.-W., Park, O.O., Kim, C.Y., and Cho, H.N. (2001) *Adv. Mater.*, **13**, 646.
108. Ponomarenko, S.A., Kirchmeyer, S., Halik, M., Klauk, H., Zschieschang, U., Schmid, G., Karbach, A., Drechsler, D., and Alpatova, N.M. (2005) *Synth. Met.*, **149**, 231.
109. Hong, X.M., Katz, H.E., Lovinger, A.J., Wang, B.C., and Raghavachari, K. (2001) *Chem. Mater.*, **13**, 4686.
110. Ponomarenko, S.A., Kirchmeyer, S., Elschner, A., Alpatova, N.M., Halik, M., Klauk, H., Zschieschang, U., and Schmid, G. (2006) *Chem. Mater.*, **18**, 579.
111. Sung, A., Ling, M.M., Tang, M.L., Bao, Z., and Locklin, J. (2007) *Chem. Mater.*, **19**, 2342.
112. Laquindanum, J.G., Katz, H.E., Lovinger, A.J., and Dodabalapur, A. (1997) *Adv. Mater.*, **9**, 36.
113. Takimiya, K., Shinamura, S., Osaka, I., and Miyazaki, E. (2011) *Adv. Mater.*, **23**, 4347.
114. (a) Wang, C., Dong, H., Hu, W., Liu, Y., and Zhu, D. (2011) *Chem. Rev.*, **112**, 2208; (b) Dong, H., Wang, C., and Hu, W. (2010) *Chem. Commun.*, **46**, 5211; (c) Takimiya, K., Kunugi, Y., and Otsubo, T. (2007) *Chem. Lett.*, **36**, 578; (d) Shinamura, S., Osaka, I., Miyazaki, E., Nakao, A., Yamagishi, M., Takeya, J., and Takimiya, K. (2011) *J. Am. Chem. Soc.*, **133**, 5024.
115. Sirringhaus, H., Friend, R.H., Wang, C., Leuninger, J., and Mullen, K. (1999) *J. Mater. Chem.*, **9**, 2095.
116. (a) Sirringhaus, H., Friend, R.H., Li, X.C., Moratti, S.C., Holmes, A.B., and Feeder, N. (1997) *Appl. Phys. Lett.*, **71**, 3871; (b) Li, X.C., Sirringhaus, H., Garnier, F., Holmes, A.B., Moratti, S.C., Feeder, N., Clegg, W., Teat, S.J., and Friend, R.H. (1998) *J. Am. Chem. Soc.*, **120**, 2206.
117. Iosip, M.D., Destri, S., Pasini, M., Porzio, W., Pernstich, K.P., and Batlogg, B. (2004) *Synth. Met.*, **146**, 251.

118. (a) Zhang, X., Cote, A.P., and Matzger, A.J. (2005) *J. Am. Chem. Soc.*, **127**, 10502; (b) Zhang, X. and Matzger, A.J. (2003) *J. Org. Chem.*, **68**, 9813.

119. Xiao, K., Liu, Y., Qi, T., Zhang, W., Wang, F., Gao, J., Qiu, W., Ma, Y., Cui, G., Chen, S., Zhan, X., Yu, G., Qin, J., Hu, W., and Zhu, D. (2005) *J. Am. Chem. Soc.*, **127**, 13281.

120. Nenajdenko, V.G., Sumerin, V.V., Chernichenko, K.Y., and Balenkova, E.S. (2004) *Org. Lett.*, **6**, 3437.

121. Takimiya, K., Kunugi, Y., Konda, Y., Niihara, N., and Otsubo, T. (2004) *J. Am. Chem. Soc.*, **126**, 5084.

122. Laquindanum, J.G., Katz, H.E., and Lovinger, A.J. (1998) *J. Am. Chem. Soc.*, **120**, 664.

123. Dickey, K.C., Anthony, J.E., and Loo, Y.-L. (2006) *Adv. Mater.*, **18**, 1721.

124. Valiyev, F., Hu, W.-S., Chen, H.-Y., Kuo, M.-Y., Chao, I., and Tao, Y.-T. (2007) *Chem. Mater.*, **19**, 3018.

125. Gao, P., Beckmann, D., Tsao, H.N., Feng, X., Enkelmann, V., Baumgarten, M., Pisula, W., and Müllen, K. (2009) *Adv. Mater.*, **21**, 213.

126. Uemura, T., Hirose, Y., Uno, M., Takimiya, K., and Takeya, J. (2009) *Appl. Phys. Express*, **2**, 111501.

127. Minemawari, H., Yamada, T., Matsui, H., Tsutsumi, J., Haas, S., Chiba, R., Kumai, R., and Hasegawa, T. (2011) *Nature*, **475**, 364.

128. Yamamoto, T. and Takimiya, K. (2007) *J. Am. Chem. Soc.*, **129**, 2224.

129. Kang, M.J., Doi, I., Mori, H., Miyazaki, E., Takimiya, K., Ikeda, M., and Kuwabara, H. (2011) *Adv. Mater.*, **23**, 1222.

130. (a) Inokuchi, H., Imaeda, K., Enoki, T., Mori, T., Maruyama, Y., Saito, G., Okada, N., Yamochi, H., Seki, K., Higuchi, Y., and Yasuoka, N. (1987) *Nature*, **329**, 39; (b) Inokuchi, H., Saito, G., Wu, P., Seki, K., Tang, T.B., Mori, T., Imaeda, K., Enoki, T., Higuchi, Y., Inaka, K., and Yasuoka, N. (1986) *Chem. Lett.*, 1263.

131. Nakayama, K., Hirose, Y., Soeda, J., Yoshizumi, M., Uemura, T., Uno, M., Li, W., Kang, M.J., Yamagishi, M., Okada, Y., Miyazaki, E., Nakazawa, Y., Nakao, A., Takimiya, K., and Takeya, J. (2011) *Adv. Mater.*, **23**, 1626.

132. Kang, M.J., Yamamoto, T., Shinamura, S., Miyazaki, E., and Takimiya, K. (2010) *Chem. Sci.*, **1**, 179.

133. Niimi, K., Shinamura, S., Osaka, I., Miyazaki, E., and Takimiya, K. (2011) *J. Am. Chem. Soc.*, **133**, 8732.

134. Okamoto, T., Mitsui, C., Yamagishi, M., Nakahara, K., Soeda, J., Hirose, Y., Miwa, K., Sato, H., Yamano, A., Matsushita, T., Uemura, T., and Takeya, J. (2013) *Adv. Mater.*, **25**, 6392.

135. Cho, H., Lee, S., Cho, N.S., Jabbour, G.E., Kwak, J., Hwang, D.-H., and Lee, C. (2013) *ACS Appl. Mater. Interfaces*, **5**, 3855.

136. Dadvand, A., Moiseev, A.G., Sawabe, K., Sun, W.-H., Djukic, B., Chung, I., Takenobu, T., Rosei, F., and Perepichka, D.F. (2012) *Angew. Chem. Int. Ed.*, **51**, 3837.

137. (a) Yoon, M.-Y., Kim, C.S., Facchetti, A., and Marks, T.J. (2006) *J. Am. Chem. Soc.*, **128**, 12851; (b) Chua, L.L., Zaumseil, J., Chang, J.F., Ou, E.C.W., Ho, P.K.H., Sirringhaus, H., and Friend, R.H. (2005) *Nature*, **434**, 194.

138. Briseno, A.L., Mannsfeld, S.C.B., Shamberger, P.J., Ohuchi, F.S., Bao, Z., Jenekhe, S.A., and Xia, Y. (2008) *Chem. Mater.*, **20** (14), 4712.

139. Letizia, J., Salata, M., Tribout, C., Facchetti, A., Ratner, M.A., and Marks, T.J. (2008) *J. Am. Chem. Soc.*, **130**, 9679.

140. Zhan, X., Tan, Z., Domercq, B., An, Z., Zhang, X., Barlow, S., Li, Y., Zhu, D., Kippelen, B., and Marder, S.R. (2007) *J. Am. Chem. Soc.*, **129**, 7246.

141. Zhan, X., Tan, Z., Zhou, E., Li, Y., Misra, R., Grant, A., Domercq, B., Zhang, X., An, Z., Zhang, X., Barlow, S., Kippelen, B., and Marder, S.R. (2009) *J. Mater. Chem.*, **19**, 5794.

142. Hüttner, S., Sommer, M., and Thelakkat, M. (2008) *Appl. Phys. Lett.*, **92**, 093302.

143. Lang, A.S., Muth, M.-A., Heinrich, C.D., Carassco-Orozco, M., and Thelakkat, M. (2013) *J. Polym. Sci. Pol. Phys.*, **51**, 1480.

144. Chen, Z., Zheng, Y., Yan, H., and Facchetti, A. (2009) *J. Am. Chem. Soc.*, **131**, 8.
145. Facchetti, A. (2010) Presented at the 9th International Symposium on Functional π-Electron Systems, "*Semiconducting Polymers for Printed Transistors and Circuits*", Atlanta, GA.
146. Yan, H., Chen, Z., Zheng, Y., Newman, C.E., Quin, J., Dolz, F., Kastler, M., and Facchetti, A. (2009) *Nature*, **457**, 679.
147. Baeg, K.-J., Khim, D., Kim, D.-Y., Jung, S.-W., Koo, J.B., You, I.-K., Yan, H., Facchetti, A., and Noh, Y.-Y. (2011) *J. Poly. Sci. B: Polym. Phys.*, **49**, 62.
148. (a) Sirringhaus, H., Brown, P.J., Friend, R.H., Nielsen, M.M., Bechgaard, K., Langeveld-Voss, B.M.W., Spiering, A.J.H., Janssen, R.A.J., Meijer, E.W., Herwig, P., and de Leeuw, D.M. (1999) *Nature*, **401**, 685; (b) Kline, R.J., McGehee, M.D., and Toney, M.F. (2006) *Nat. Mater.*, **5**, 222; (c) Kim, D.H., Park, Y.D., Jang, Y., Yang, H., Kim, Y.H., Han, J.I., Moon, D.G., Park, S., Chang, T., Chang, C., Joo, M., Ryu, C.Y., and Cho, K. (2005) *Adv. Funct. Mater.*, **15**, 77; (d) Street, R.A., Northrup, J.E., and Salleo, A. (2005) *Phys. Rev. B*, **71**, 165202; (e) Tsao, H.N., Cho, D., Andreasen, J.W., Rouhanipour, A., Breiby, D.W., Pisula, W., and Müllen, K. (2009) *Adv. Mater.*, **21**, 209; (f) Yang, H., Shin, T.J., Yang, L., Cho, K., Ryu, C.Y., and Bao, Z. (2005) *Adv. Funct. Mater.*, **15**, 671.
149. (a) Kline, R.J., DeLongchamp, D.M., Fischer, D.A., Lin, E.K., Heeney, M., McCulloch, I., and Toney, M.F. (2007) *Appl. Phys. Lett.*, **90**, 062117; (b) Salleo, A. (2007) *Mater. Today*, **10**, 38.
150. Rivnay, J., Toney, M.F., Zhang, Y., Kauvar, I.V., Wagner, V., Facchetti, A., and Salleo, A. (2010) *Adv. Mater.*, **22**, 4359–4363.
151. Steyrleuthner, R., Schubert, M., Jaiser, F., Blakesley, J.C., Chen, Z., Facchetti, A., and Neher, D. (2010) *Adv. Mater.*, **22**, 2799.
152. (a) Mandoc, M.M., de Boer, B., and Blom, P.W.M. (2006) *Phys. Rev. B*, **73**, 155205; (b) Steyrleuthner, R., Bange, S., and Neher, D. (2009) *J. Appl. Phys.*, **105**, 8.
153. Hwang, Y.-J., Murari, N.M., and Jenekhe, S.A. (2013) *Polym. Chem.*, **4**, 3187.
154. Kim, Y., Hong, J., Oh, J.H., and Yang, C. (2013) *Chem. Mater.*, **25**, 3251.
155. Kim, R., Amegadz, P.S.K., Kang, I., Yun, H.-J., Noh, Y.-Y., Kwo, S.-K., and Kim, Y.-H. (2013) *Adv. Funct. Mater.*, **23**, 5719.
156. Lei, T., Dou, J.-H., Cao, X.-Y., Wang, J.-Y., and Pei, J. (2013) *J. Am. Chem. Soc.*, **135**, 12168.
157. Li, H., Kim, F.S., Ren, G., Hollenbeck, E.C., Subramaniyan, S., and Jenekhe, S.A. (2013) *Angew. Chem. Int. Ed.*, **52**, 5513.
158. Li, H., Kim, F.S., Ren, G., and Jenekhe, S.A. (2013) *J. Am. Chem. Soc.*, **135**, 14920.
159. Takeda, Y., Andrew, T.L., Lobez, J.M., Mork, A.J., and Swager, T.M. (2012) *Angew. Chem. Int. Ed.*, **51**, 9042.
160. Kanimozhi, C., Yaacobi-Gross, N., Chou, K.W., Amassian, A., Anthopoulos, T.D., and Patil, S. (2012) *J. Am. Chem. Soc.*, **134**, 16532.
161. Kola, S., Kim, J.H., Ireland, R., Yeh, M.-L., Smith, K., Guo, W., and Katz, H.E. (2013) *ACS Macro Lett.*, **2**, 664.
162. Zheng, Q., Huang, J., Sarjeant, A., and Katz, H.E. (2008) *J. Am. Chem. Soc.*, **130**, 14410.
163. Guillaud, G., Al Sadound, M., and Maitrot, M. (1990) *Chem. Phys. Lett.*, **67**, 503.
164. Bao, Z., Lovinger, A.J., and Brown, J. (1998) *J. Am. Chem. Soc.*, **120** (1), 207–208.
165. (a) Tang, Q., Jiang, L., Tong, Y., Li, H., Liu, Y., Wang, Z., Hu, W., Liu, Y., and Zhu, D. (2008) *Adv. Mater.*, **20**, 2497; (b) Reese, C. and Bao, Z. (2007) *Mater. Today*, **10** (3), 20; (c) de Boer, R.W.I., Gershenson, M.E., Morpurgo, A.F., and Podzorov, V. (2005) *Phys. Org. Semicond.*, 393.
166. (a) Tang, Q.X., Li, H.X., Song, Y.B., Xu, W., Hu, W.P., Jiang, L., Liu, Y., Wang, X., and Zhu, D.B. (2006) *Adv. Mater.*, **18**, 3010; (b) Tang, Q.X., Li, H.X., Liu, Y.L., and Hu, W.P. (2006) *J. Am. Chem. Soc.*, **128**, 4634; (c) Tang, Q., Jiang, L., Tong, Y., Li, H., Liu, Y., Wang, Z., Hu,

W., Liu, Y., and Zhu, D. (2008) *Adv. Mater.*, **20**, 2947–2951.
167. Ling, M.M., Bao, Z., and Erk, P. (2006) *Appl. Phys. Lett.*, **89**, 163516.
168. Wang, H., Zhu, F., Yang, J., Geng, Y., and Yan, D. (2007) *Adv. Mater.*, **19**, 2168.
169. Song, D., Wang, H., Zhu, F., Yang, J., Tian, H., Geng, Y., and Yan, D. (2008) *Adv. Mater.*, **20** (11), 2142.
170. (a) Facchetti, A., Mushrush, M., Yoon, M.-H., Hutchison, G.R., Ratner, M.A., and Marks, T.J. (2004) *J. Am. Chem. Soc.*, **126**, 13859; (b) Facchetti, A., Yoon, M.-H., Stern, C.L., Hutchison, G.R., Ratner, M.A., and Marks, T.J. (2004) *J. Am. Chem. Soc.*, **126**, 13480; (c) Facchetti, A., Mushrush, M., Katz, H.E., and Marks, T.J. (2003) *Adv. Mater.*, **15**, 33; (d) Facchetti, A., Deng, Y., Wang, A., Koide, Y., Sirringhaus, H., Marks, T.J., and Friend, R.H. (2000) *Angew. Chem. Int. Ed.*, **39**, 4547; (e) Casado, J., Ponce Ortíz, R., Hernández, V., López Navarrete, J.T., Facchetti, A., and Marks, T.J. (2005) *J. Am. Chem. Soc.*, **127**, 13364.
171. Bunn, C.W. and Howells, E.R. (1954) *Nature*, **174**, 549.
172. (a) Barbarella, G., Zambianchi, M., Bongini, A., and Antolini, L. (1992) *Adv. Mater.*, **4**, 282; (b) Herrema, J.K., Wildeman, J., van Bolhuis, F., and Hadziioannou, G. (1993) *Synth. Met.*, **60**, 239; (c) Dihexyl-α6T:Sato, T., Fujitsuka, M., Shiro, M., and Tanaka, K. (1998) *Synth. Met.*, **95**, 143.
173. (a) Yoon, M.H., Facchetti, A., Stern, C.F., and Marks, T.J. (2006) *J. Am. Chem. Soc.*, **128**, 5792; (b) Facchetti, A., Yoon, M.H., Stern, C.L., Katz, H.E., and Marks, T.J. (2003) *Angew. Chem. Int. Ed.*, **42**, 3900.
174. Koh, S.E., Delley, B., Medvedeva, J.E., Facchetti, A., Freeman, A.J., Marks, T.J., and Ratner, M.A. (2006) *J. Phys. Chem. B*, **110**, 24361.
175. (a) Yoon, M.H., DiBenedetto, S.A., Russell, M.T., Facchetti, A., and Marks, T.J. (2007) *Chem. Mater.*, **19**, 4864; (b) Yoon, M.-H., DiBenedetto, S., Facchetti, A., and Marks, T.J. (2005) *J. Am. Chem. Soc.*, **127**, 1348.
176. (a) Chiechi, R.C., Sonmez, G., and Wudl, F. (2005) *Adv. Funct. Mater.*, **15**, 427; (b) Donat-Bouillud, A., Mazerolle, L., Gagnon, P., Goldenberg, L., Petty, M.C., and Leclerc, M. (1997) *Chem. Mater.*, **9**, 2815.
177. Schols, S., Willigenburg, L.V., Müller, R., Bode, D., Debucquoy, M., Jonge, S.D., Genoe, J., Heremans, P., Lu, S., and Facchetti, A. (2008) *Appl. Phys. Lett.*, **93**, 263303.
178. Letizia, J.A., Facchetti, A., Stern, C.L., Ratner, M.A., and Marks, T.J. (2005) *J. Am. Chem. Soc.*, **127**, 13476.
179. Letizia, J.A., Rivnay, J., Facchetti, A., Ratner, M.A., and Marks, T.J. (2010) *Adv. Funct. Mater.*, **20**, 50.
180. Pappenfus, T.M., Chesterfield, R.J., Frisbie, C.D., Mann, K.R., Casado, J., Raff, J.D., and Miller, L.L. (2002) *J. Am. Chem. Soc.*, **124**, 4184.
181. Casado, J. *et al.* (2002) *J. Am. Chem. Soc.*, **124**, 12380.
182. Chesterfield, R.J. (2003) *Adv. Mater.*, **15**, 1278.
183. Handa, S., Miyazaki, E., Takimiya, K., and Kunugi, Y. (2007) *J. Am. Chem. Soc.*, **129**, 11684.
184. Kastner, J., Paloheimo, J., and Kuzmany, H. (1993) *Solid State Sciences*, Springer, New York.
185. Haddon, R.C., Perel, A.S., Morris, R.C., Palstra, T.T.M., Hebard, A.F., and Fleming, R.M. (1995) *Appl. Phys. Lett.*, **67** (1), 121.
186. Haddon, R.C. (1996) *J. Am. Chem. Soc.*, **118** (12), 3041.
187. Itaka, K., Yamashiro, M., Yamaguchi, J., Haemori, M., Yaginuma, S., Matsumoto, Y., Kondo, M., and Koinuma, H. (2006) *Adv. Mater.*, **18**, 1713.
188. Jang, J., Kim, J.W., Park, N., and Kim, J.J. (2008) *Org. Elctron.*, **9**, 481.
189. Anthopoulos, T.D., Singh, B., Marjanovic, N., Sarciftci, N.S., Montaigne, A., Sitter, H., Cölle, M., and de Leeuw, D.M. (2006) *Appl. Phys. Lett.*, **89**, 213504.
190. Zhang, X.H. and Kippelen, B. (2008) *Appl. Phys. Lett.*, **93**, 133305.
191. Chikamatsu, M., Nagamatsu, S., Yoshida, Y., Saito, K., Yase, K., and Kikuchi, K. (2005) *Appl. Phys. Lett.*, **87**, 203504.

192. Wöbkenberg, P.H., Ball, J., Bradley, D.D.C., Anthopoulos, T.D., Kooistra, F., Hummelen, J.C., and de Leeuw, D.M. (2008) *Appl. Phys. Lett.*, **92**, 143310.
193. Chikamatsu, M., Itakura, A., Yoshida, Y., Azumi, R., and Yase, K. (2008) *Chem. Mater.*, **20**, 7365.
194. Wobkenberg, P.H., Bradley, D.H., Kronholm, D., Hummelen, J.C., de Leeuw, D.M., Colle, M., and Anthopoulos, T.D. (2008) *Synth. Met.*, **158** (11), 468.
195. Yang, C., Cho, S., Heeger, A.J., and Wudl, F. (2009) *Angew. Chem. Int. Ed.*, **48** (9), 1592.
196. Kanbara, T., Shibata, K., Fujiki, S., Kubozono, Y., Kashino, S., Urisu, T., Sakai, M., Fujiwara, A., Kumashiro, R., and Tanigaki, K. (2003) *Chem. Phys. Lett.*, **379** (3,4), 223.
197. Kitamura, M. and Arakawa, Y. (2007) *Appl. Phys. Lett.*, **91** (5), 53505.
198. Zhang, X.-H., Potscavage, W.J. Jr., Choi, S., and Kippelen, B. (2009) *Appl. Phys. Lett.*, **94** (4), 43312.
199. Horowitz, G., Kouki, F., Spearman, P., Fichou, D., Nogues, C., Pan, X., and Garnier, F. (1996) *Adv. Mater.*, **8**, 242.
200. Malenfant, P.R.L., Dimitrakopoulos, C.D., Gelorme, J.D., Kosbar, L.L., Graham, T.O., Curioni, A., and Andreoni, W. (2002) *Appl. Phys. Lett.*, **80**, 2517.
201. Chesterfield, R.J., McKeen, J.C., Newman, C.R., Ewbank, P.C., da Silva Filho, D.A., Brédas, J.L., Miller, L.L., Mann, K.R., and Frisbie, C.D. (2004) *J. Phys. Chem. B*, **108**, 19281.
202. Chen, F.-C. and Liao, C.H. (2008) *Appl. Phys. Lett.*, **93**, 103310.
203. Tatemichi, S., Ichikawa, M., Koyama, T., and Taniguchi, Y. (2006) *Appl. Phys. Lett.*, **89**, 112108.
204. Oh, J.H., Liu, S., Bao, Z., Schmidt, R., and Würthner, F. (2007) *Appl. Phys. Lett.*, **91**, 212107.
205. Jones, B.A., Ahrens, M.J., Yoon, M.H., Facchetti, A., Marks, T.J., and Wasielewski, M.R. (2004) *Angew. Chem. Int. Ed.*, **43**, 6363.
206. Jones, B.A., Facchetti, A., Wasielewski, M.R., and Marks, T.J. (2008) *Adv. Funct. Mater.*, **18**, 1329.
207. Molinari, A.S., Alves, H., Chen, Z., Facchetti, A., and Morpurgo, A.F. (2009) *J. Am. Chem. Soc.*, **131**, 2462.
208. Weitz, R.T., Amsharov, K., Zschieschang, U., Villas, E.B., Goswami, D.K., Burghard, M., Dosch, H., Jansen, M., Kern, K., and Klauk, H. (2008) *J. Am. Chem. Soc.*, **130**, 4637.
209. Schmidt, R., Oh, J.H., Sun, Y.S., Deppisch, M., Krause, A.-M., Radacki, K., Braunschweig, H., Könemann, M., Erk, P., Bao, Z., and Würthner, F. (2009) *J. Am. Chem. Soc.*, **131**, 6215.
210. (a) Nolde, F., Pisula, W., Mueller, S., Kohl, C., and Müllen, K. (2006) *Chem. Mater.*, **18**, 3715; (b) Nolde, F., Qu, J., Kohl, C., Pschirer, N.G., Reuther, E., and Müllen, K. (2005) *Chemistry*, **11**, 3959.
211. Petit, M., Hayakawa, R., Shirai, Y., Wakayama, Y., Hill, J.P., Ariga, K., and Chikyow, T. (2008) *Appl. Phys. Lett.*, **92**, 163301.
212. Zheng, Q., Huang, J., Sarjeant, A., and Katz, H.E. (2008) *J. Am. Chem. Soc.*, **130**, 14410.
213. Laquindanum, J.G., Katz, H.E., Dodabalapur, A., and Lovinger, A.J. (1996) *J. Am. Chem. Soc.*, **118**, 11331.
214. Katz, H.E., Johnson, J., Lovinger, A.J., and Li, W. (2000) *J. Am. Chem. Soc.*, **122**, 7787.
215. Katz, H.E., Lovinger, A.J., Johnson, J., Kloc, C., Siegrist, T., Li, W., Lin, Y.-Y., and Dodabalapur, A. (2000) *Nature*, **404**, 478.
216. Jung, B.J., Sun, J., Lee, T., Sarjeant, A., and Katz, H.E. (2009) *Chem. Mater.*, **21**, 94.
217. Shukla, D., Nelson, S.F., Freeman, D.C., Rajeswaran, M., Ahearn, W.G., Meyer, D.M., and Carey, J.T. (2008) *Chem. Mater.*, **20**, 7486.
218. Jones, B.A., Facchetti, A., Marks, T.J., and Wasielewski, M.R. (2007) *Chem. Mater.*, **19**, 2703.
219. (a) Wang, Z., Kim, C., Facchetti, A., and Marks, T.J. (2007) *J. Am. Chem. Soc.*, **129**, 13362; (b) Usta, H., Wang, Z., Kim, C., Huang, H., Lu, S., Facchetti, A., and Marks, T.J. (2012) *J. Mater. Chem.*, **22**, 4459.
220. (a) Ando, S., Nishida, J.-I., Fujiwara, E., Tada, H., Inoue, Y., Tokito, S., and

Yamashita, Y. (2005) *Chem. Mater.*, **17**, 1261; (b) Ando, S., Nishida, J.-I., Fujiwara, E., Tada, H., Inoue, Y., Tokito, S., and Yamashita, Y. (2005) *J. Am. Chem. Soc.*, **127**, 5336; (c) Ando, S., Murakami, R., Nishida, J.-I., Fujiwara, E., Tada, H., Inoue, Y., Tokito, S., and Yamashita, Y. (2005) *J. Am. Chem. Soc.*, **127**, 14996; (d) Naraso, J.-I., Nishida, D., Kumaki, S., Tokito, S., and Yamashita, Y. (2006) *J. Am. Chem. Soc.*, **128**, 9598; (e) Nakagawa, T., Nishida, J.-I., Tokito, S., and Yamashita, Y. (2008) *Chem. Mater.*, **20**, 2015; (f) Ono, K., Yamaguchi, H., Taga, K., Saito, K., Nishida, J.-I., and Yamashita, Y. (2009) *Org. Lett.*, **11**, 149.

221. Sakamoto, Y., Suzuki, T., Kobayashi, M., Gao, Y., Fukai, Y., Inoue, Y., Sato, F., and Tokito, S. (2004) *J. Am. Chem. Soc.*, **126**, 8138.

222. Di, C.-A., Li, J., Yu, G., Xiao, Y., Guo, Y., Liu, Y., Qian, X., and Zhu, D. (2008) *Org. Lett.*, **10**, 3025.

223. Wada, H., Shibata, K., Bando, Y., and Mori, T. (2008) *J. Mater. Chem.*, **18**, 4165.

224. Qiao, Y., Guo, Y., Yu, C., Zhang, F., Xu, W., Liu, Y., and Zhu, D. (2012) *J. Am. Chem. Soc.*, **134**, 4084.

225. Wu, Q., Li, R., Hong, W., Li, H., Gao, X., and Zhu, D. (2011) *Chem. Mater.*, **23**, 3138.

226. Zhong, H., Smith, J., Rossbauer, S., White, A.J.P., Anthopoulos, T.D., and Heeney, M. (2012) *Adv. Mater.*, **24**, 3205.

227. Yoon, W.S., Park, S.K., Cho, I., Oh, J.-A., Kim, J.H., and Park, S.Y. (2013) *Adv. Funct. Mater.*, **23**, 3519.

228. Gao, X., Di, C.-A., Hu, Y., Yang, X., Fan, H., Zhang, F., Liu, Y., Li, H., and Zhu, D. (2010) *J. Am. Chem. Soc.*, **132**, 3697.

229. Zhang, F., Hu, Y., Schuettfort, T., Di, C.-A., Gao, X., McNeill, C.R., Thomsen, L., Mannsfeld, S.C.B., Yuan, W., Sirringhaus, H., and Zhu, D. (2013) *J. Am. Chem. Soc.*, **135**, 2338.

230. Zhao, Y., Di, C.-A., Gao, X., Hu, Y., Guo, Y., Zhang, L., Liu, Y., Wang, J., Hu, W., and Zhu, D. (2011) *Adv. Mater.*, **23**, 2448.

231. (a) Suraru, S.-L., Zschieschang, U., Klauk, H., and Würthner, F. (2011) *Chem. Commun.*, **47**, 11504; (b) Li, C., Xiao, C., Li, Y., and Wang, Z. (2013) *Org. Lett.*, **15**, 682; (c) Ye, Q., Chang, J., Huang, K.-W., Shi, X., Wu, J., and Chi, C. (2013) *Org. Lett.*, **15**, 1194; (d) Chen, X., Guo, Y., Tan, L., Yang, G., Li, Y., Zhang, G., Liu, Z., Xu, W., and Zhang, D. (2013) *J. Mater. Chem. C*, **1**, 1087.

232. Fukutomi, Y., Nakano, M., Hu, J.-Y., Osaka, I., and Takimiya, K. (2013) *J. Am. Chem. Soc.*, **135**, 11445.

233. Polander, L.E., Tiwari, S.P., Pandey, L., Seifried, B.M., Zhang, Q., Barlow, S., Risko, C., Bredas, J.-L., Kippelen, B., and Marder, S.R. (2011) *Chem. Mater.*, **23**, 3408.

234. Stolte, M., Gsänger, M., Hofmockel, R., Suraru, S.-L., and Würthner, F. (2012) *Phys. Chem. Chem. Phys.*, **14**, 14181.

235. (a) Shkunov, M., Simms, R., Heeney, M., Tierney, S., and McCulloch, I. (2005) *Adv. Mater.*, **17**, 2608; (b) Kang, S.-M. and Leblebici, Y. (1996) *CMOS Digital Integrated Circuits: Analysis and Design*, McGraw-Hill, New York.

236. (a) Anthopoulos, T.D., de Leeuw, D.M., Cantatore, E., Setayesh, S., Meijer, E.J., Tanase, C., Hummelen, J.C., and Blom, P.W.M. (2004) *Appl. Phys. Lett.*, **85**, 4205; (b) Anthopoulos, T.D., de Leeuw, D.M., Cantatore, E., van 't Hof, P., Alma, J., and Hummelen, J.C. (2005) *J. Appl. Phys.*, **98**, 6; (c) Anthopoulos, T.D., Setayesh, S., Smits, E., Cölle, M., Cantatore, E., de Boer, B., Blom, P.W.M., and de Leeuw, D.M. (2006) *Adv. Mater.*, **18**, 1900.

237. (a) Capelli, R., Toffanin, S., Generali, G., Usta, H., Facchetti, A., and Muccini, M. (2010) *Nat. Mater.*, **9**, 496; (b) Swensen, J.S., Soci, C., and Heeger, A.J. (2005) *Appl. Phys. Lett.*, **87**, 3; (c) Generali, G., Capelli, R., Toffanin, S., Facchetti, A., and Muccini, M. (2010) *Microelectron. Reliab.*, **50**, 1861; (d) Zaumseil, J., Friend, R.H., and Sirringhaus, H. (2006) *Nat. Mater.*, **5**, 69; (e) Muccini, M. (2006) *Nat. Mater.*, **5**, 605.

238. Chen, Z., Lemke, H., Albert-Seifried, S., Caironi, M., Nielsen, M.M., Heeney, M., Zhang, W., McCulloch, I., and

Sirringhaus, H. (2010) *Adv. Mater.*, **22**, 2371.

239. (a) Heeney, M., Zhang, W., Crouch, D.J., Chabinyc, M.L., Gordeyev, S., Hamilton, R., Higgins, S.J., McCulloch, I., Skabara, P.J., Sparrowe, D., and Tierney, S. (2007) *Chem. Commun.*, 5061; (b) Oyaizu, K., Iwasaki, T., Tsukahara, Y., and Tsuchida, E. (2004) *Macromolecules*, **37**, 1257.

240. Meijer, E.J., De Leeuw, D.M., Setayesh, S., Van Veenendaal, E., Huisman, B.H., Blom, P.W.M., Hummelen, J.C., Scherf, U., and Klapwijk, T.M. (2003) *Nat. Mater.*, **2**, 678.

241. Kim, F.S., Guo, X., Watson, M.D., and Jenekhe, S.A. (2010) *Adv. Mater.*, **22**, 478.

242. Bijleveld, J.C., Zoombelt, A.P., Mathijssen, S.G.J., Wienk, M.M., Turbiez, M., de Leeuw, D.M., and Janssen, R.A.J. (2009) *J. Am. Chem. Soc.*, **131**, 16616.

243. Steckler, T.T., Zhang, Z., Hwang, J., Honeyager, R., Ohira, S., Zhang, X., Grant, A., Ellinger, S., Odom, S.A., Sweat, D., Tanner, D.B., Rinzler, A.G., Barlow, S., Bredas, J.-L., Kippelen, B., Marder, S.R., and Reynolds, J.R. (2009) *J. Am. Chem. Soc.*, **131**, 2824.

244. Lei, T., Dou, J.-H., Ma, Z.-J., Yao, C.-H., Liu, C.-J., Wang, J.-Y., and Pei, J. (2012) *J. Am. Chem. Soc.*, **134**, 20025.

245. Lei, T., Dou, J.-H., Ma, Z.-J., Liu, C.-J., Wang, J.-Y., and Pei, J. (2013) *Chem. Sci.*, **4**, 2447.

246. Bürgi, L., Turbiez, M., Pfeiffer, R., Bienewald, F., Kirner, H.-J., and Winnewisser, C. (2008) *Adv. Mater.*, **20**, 2217.

247. Chen, Z., Lee, M.J., Ashraf, R.S., Gu, Y., Albert-Seifried, S., Nielsen, M.M., Schroeder, B., Anthopoulos, T.D., Heeney, M., McCulloch, I., and Sirringhaus, H. (2012) *Adv. Mater.*, **24**, 647.

248. Lee, J., Han, A.-R., Kim, J., Kim, Y., Oh, J.H., and Yang, C. (2012) *J. Am. Chem. Soc.*, **134**, 20713.

249. Lee, J., Han, A.-R., Yu, H., Shin, T.J., Yang, C., and Oh, J.H. (2013) *J. Am. Chem. Soc.*, **135**, 9540.

250. Fan, J., Yuen, J.D., Wang, M., Seifter, J., Seo, J.-H., Mohebbi, A.R., Zakhidov, D., Heeger, A., and Wudl, F. (2012) *Adv. Mater.*, **24**, 2186.

251. Yuen, J.D., Fan, J., Seifter, J., Lim, B., Hufschmid, R., Heeger, A.J., and Wudl, F. (2011) *J. Am. Chem. Soc.*, **133**, 20799.

252. Baeg, K.-J., Khim, D., Jung, S.-W., Kang, M., You, I.-K., Kim, D.-Y., Facchetti, A., and Noh, Y.-Y. (2012) *Adv. Mater.*, **24**, 5433.

253. Chen, H., Guo, Y., Mao, Z., Yu, G., Huang, J., Zhao, Y., and Liu, Y. (2013) *Chem. Mater.*, **25**, 3589.

254. Usta, H., Newman, C., Chen, Z., and Facchetti, A. (2012) *Adv. Mater.*, **24**, 3678.

255. Tang, M.L., Reichardt, A.D., Miyaki, N., Stoltenberg, R.M., and Bao, Z. (2008) *J. Am. Chem. Soc.*, **130**, 6064.

256. Liang, Z., Tang, Q., Mao, R., Liu, D., Xu, J., and Miao, Q. (2011) *Adv. Mater.*, **23**, 5514.

257. Song, C.L., Ma, C.B., Yang, F., Zeng, W.J., Zhang, H.L., and Gong, X. (2011) *Org. Lett.*, **13**, 2880.

258. Zeng, W.J., Zhou, X.Y., Pan, X.J., Song, C.L., and Zhang, H.L. (2013) *AIP Adv.*, **3**, 012101.

259. (a) Glowacki, E.D., Leonat, L., Voss, G., Bodea, M.A., Bozkurt, Z., Ramil, A.M., Irimia-Vladu, M., Bauer, S., and Sariciftci, N.S. (2011) *AIP Adv.*, **1**, 042132; (b) Irimia-Vladu, M., Glowacki, E.D., Troshin, P.A., Schwabegger, G., Leonat, L., Susarova, D.K., Krystal, O., Ullah, M., Kanbur, Y., Bodea, M.A., Razumov, V.F., Sitter, H., Bauer, S., and Sariciftci, N.S. (2011) *Adv. Mater.*, **24**, 375.

260. Nakanotani, H., Saito, M., Nakamura, H., and Adachi, C. (2009) *Appl. Phys. Lett.*, **95**, 033308.

261. Tan, L.X., Guo, Y.L., Yang, Y., Zhang, G.X., Zhang, D.Q., Yu, G., Xu, W., and Liu, Y.Q. (2012) *Chem. Sci.*, **3**, 2530.

262. Wang, L., Zhang, X., Tian, H., Lu, Y., Geng, Y., and Wang, F. (2013) *Chem. Commun.*, **49**, 11272.

263. Nishinaga, T., Ohmae, T., Aita, K., Takase, M., Iyoda, M., Arai, T., and Kunugi, Y. (2013) *Chem. Commun.*, **49**, 5354.

264. Chase, D.T., Fix, A.G., Kang, S.J., Rose, B.D., Weber, C.D., Zhong, Y., Zakharov,

L.N., Lonergan, M.C., Nuckolls, C., and Haley, M.M. (2012) *J. Am. Chem. Soc.*, **134**, 10349.

265. Ribierre, J.C., Watanabe, S., Matsumoto, M., Muto, T., and Aoyama, T. (2010) *Appl. Phys. Lett.*, **96**, 083303.

266. Ribierre, J.C., Watanabe, S., Matsumoto, M., Muto, T., Hashizume, D., and Aoyama, T. (2011) *J. Phys. Chem. C*, **115**, 20703.

267. Zhang, Y., Kim, C., Lin, J., and Nguyen, T.-Q. (2012) *Adv. Funct. Mater.*, **22**, 97.

268. Tsao, H.N., Pisula, W., Liu, Z.H., Osikowicz, W., Salaneck, W.R., and Müllen, K. (2008) *Adv. Mater.*, **20**, 2715.

269. Liu, C., Liu, Z., Lemke, H.T., Tsao, H.N., Naber, R.C.G., Li, Y., Banger, K., Müllen, K., Nielsen, M.M., and Sirringhaus, H. (2010) *Chem. Mater.*, **22**, 2120.

270. Ye, Q., Chang, J., Huang, K.-W., and Chi, C. (2011) *Org. Lett.*, **13**, 5960.

271. Cheng, S.-S., Huang, P.-Y., Ramesh, M., Chang, H.-C., Chen, L.-M., Yeh, C.-M., Fung, C.-L., Wu, M.C., Liu, C.-C., Kim, C., Lin, H.-C., Chen, M.-C., and Chu, C.-W. (2014) *Adv. Funct. Mater.*, **24**, 2057.

272. Yue, W., He, T., Stolte, M., Gsänger, M., and Würthner, F. (2014) *Chem. Commun.*, **50**, 545.

273. Xia, H., Liu, D., Xua, X., and Miao, Q. (2013) *Chem. Commun.*, **49**, 4301.